VOL 11
ISSUE 5
Sept 2026

eMetN METEOR JOURNAL

eJournal for meteor observers www.emetn.net

Stacked image for 12-13 August 2026 showing the perspective of the Perseid radiant very well recorded by UA000A installed west of Kyiv in Ukraine, part of UMON, Ukrainian Meteor Observational Network (Copyright Alex Aitov).

- New shower M2026-P1
- 26-Bootids confirmed
- psi-Phoenicids
- Sporadic meteors
- Ursids filament
- CARMELo reports
- Fireball report
- ACM 2026 report

ISSN 3041 - 4261

Contents

New meteor shower in Scorpius (M2026-P1)

Milan Kalina[1], Denis Vida[2,3], Damir Šegon[4,5], Paul Roggemans[6], James M. Scott[7], Jeff Wood[8]

[1] **Czech Astronomical Society, Ondřejov, Czech Republic**
kalina@astro.cz

[2] **Department of Physics and Astronomy, University of Western Ontario, Richmond Street, London, N6A 3K7, Ontario, Canada.**
[3] **Institute for Earth and Space Exploration, University of Western Ontario, Perth Drive, London, N6A 5B8, Ontario, Canada**
denis.vida@gmail.com

[4] **Astronomical Society Istra Pula, Park Monte Zaro 2, 52100 Pula, Croatia.**
[5] **Višnjan Observatory, Istarska 5, 52463 Višnjan, Croatia**

[6] **Pijnboomstraat 25, 2800 Mechelen, Belgium**

[7] **Department of Geoscience, Aarhus University, Høegh-Guldbergs Gade 2, DK-8000 Aarhus C, Denmark**

[8] **PO Box 162, Willetton, Western Australia 6955, Australia**

A new meteor shower from a Jupiter Family Comet type orbit ($T_J = 2.7$) was detected during July 14 – 16, 2026, by the Global Meteor Network. 43 meteors belonging to the new shower were observed between 111° < $\lambda_{\odot}$ < 118° from a radiant at R.A. = 263.2° and Decl.= –44.6° in the constellation of Scorpion, with a geocentric velocity of 14.3 km/s. The new meteor shower has been listed in the IAU MDC Working List of Meteor Showers under the temporary name-designation: M2026-P1.

1 Introduction

The GMN radiant maps for July 14 – 16, 2026, showed a clear radiant concentration in the constellation of Scorpius. The activity lasted for about 3 days with the best activity at $\lambda_{\odot}$ = 114.5° with the radiant visible on the radiant density maps (*Figures 1*). When the activity had completely ceased, 43 meteors of this new meteor shower had been registered by the Global Meteor Network low-light video cameras. The shower was independently observed by 114 cameras in Australia, Bosnia and Herzegovina, Brazil, Croatia and New Zealand.

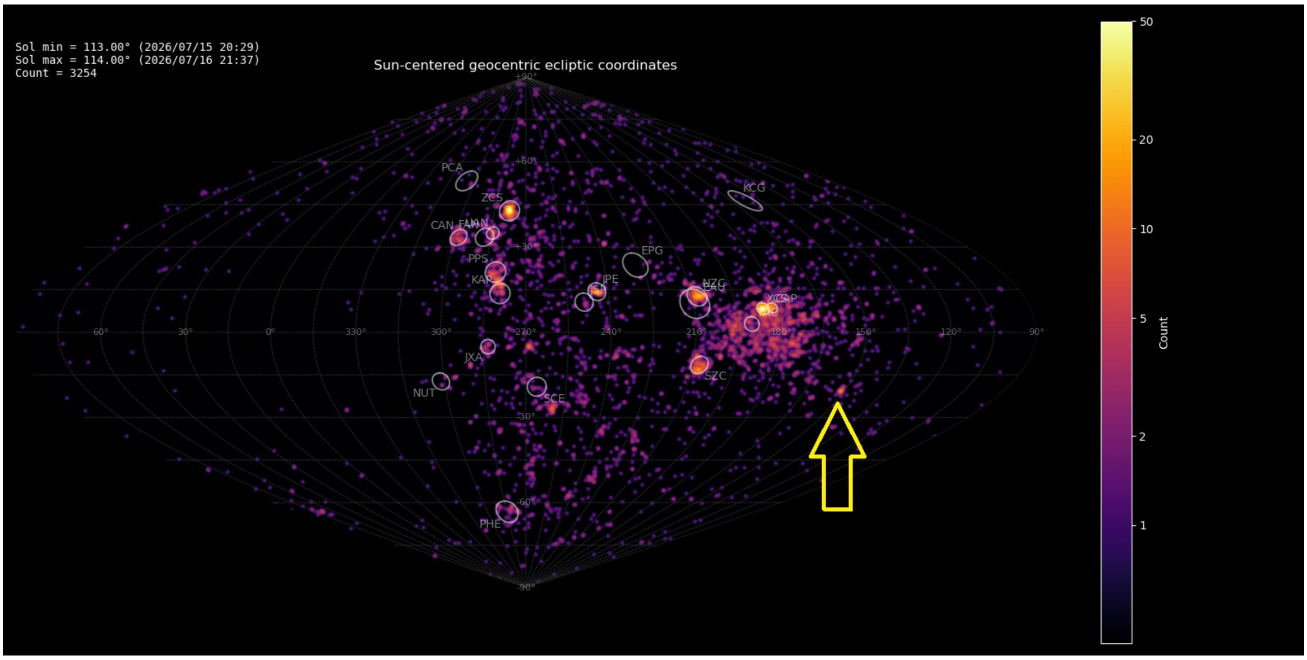

Figure 1 – Radiant density map in sinusoidal projection with 3254 radiants obtained by the Global Meteor Network during July 15 – 16, 2026. A distinct concentration is visible in Sun-centered geocentric ecliptic coordinates which was identified as a new meteor shower with the temporary identification M2026-P1. Activity from this new source was detected during several days.

2 Shower classification based on radiants

The GMN shower association criteria assume that meteors within 1° in solar longitude, within 1.5° in radiant in this case, and within 10% in geocentric velocity of a shower reference location are members of that shower. Further details about the shower association are explained in Moorhead et al. (2020). Initially 67 possible shower members were selected and after removal of outliers, 43 members remained for final analysis. The shower parameters as obtained by the GMN method are listed in *Table 1*.

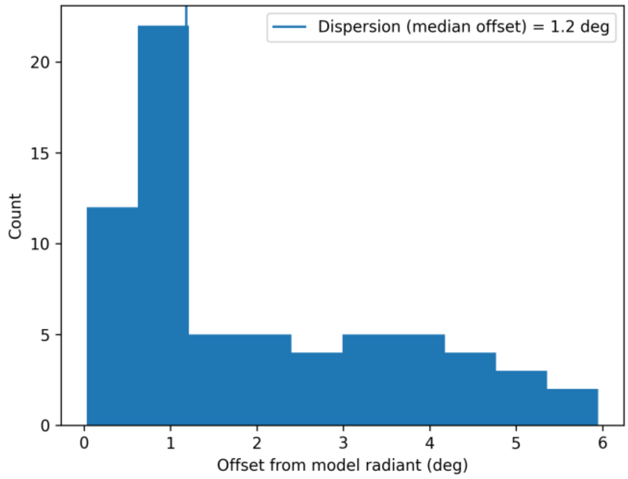

Figure 2 – Dispersion median offset on the radiant position.

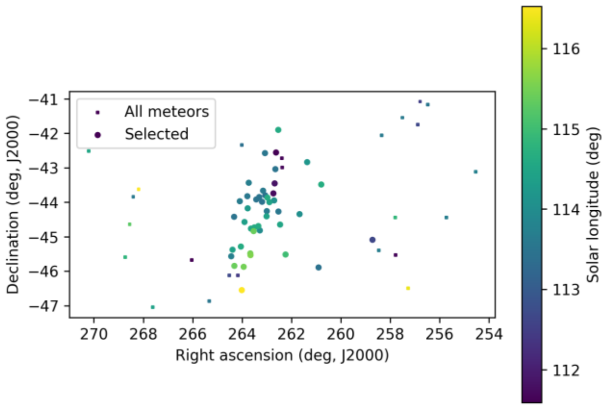

Figure 3 – The radiant distribution during the solar-longitude interval 111.5° – 116.5° in equatorial coordinates.

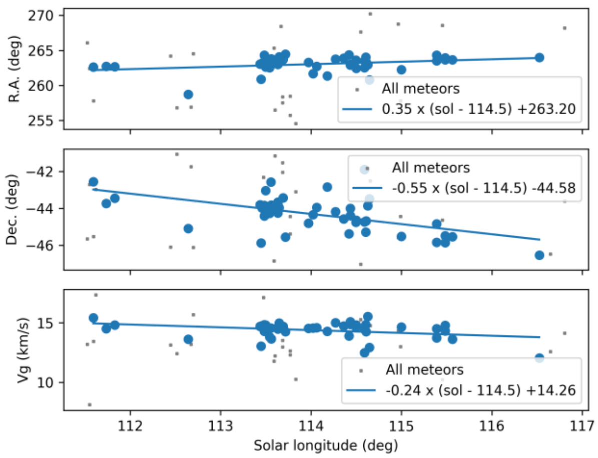

Figure 4 – The radiant drift.

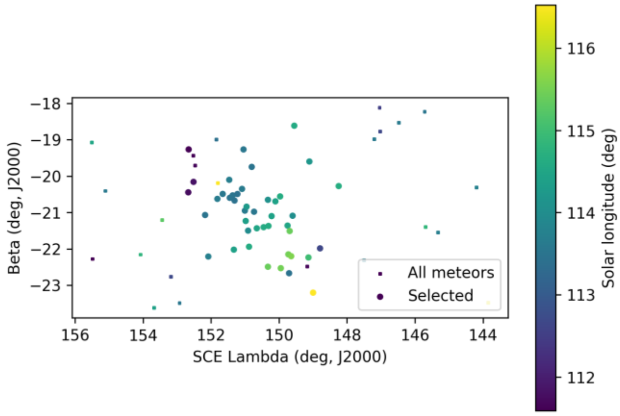

Figure 5 – The radiant distribution during the solar-longitude interval 111.5° – 116.5° in Sun centered geocentric ecliptic coordinates.

3 Shower classification based on orbits

A complete independent meteoroid stream search has been applied to orbit data obtained between solar longitude 111° and 116° during 2026. The method has been described in detail in a separate publication (Roggemans et al., 2026a). 20524 orbits were available within this time interval and a final mean orbit has been computed by the method of Jopek et al. (2006) for the thresholds $D_{SH} < 0.075$ and $D_D < 0.03$ and $D_J < 0.075$ (Southworth and Hawkins, 1963; Drummond, 1981; Jopek, 1993). The Rayleigh fit in *Figure 6* indicates a larger cutoff value, but this type of low inclination short period orbits requires great care to exclude spurious associations. The resulting mean orbit based upon 38 meteors for 2026 is listed in *Table 1*.

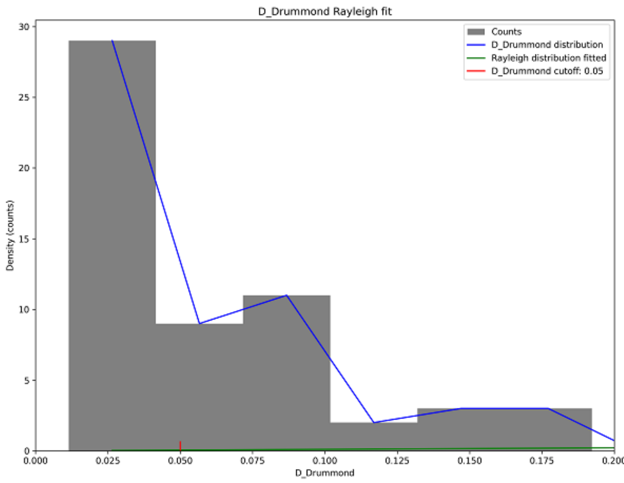

Figure 6 – Rayleigh fit on the Drummond criterion for the new shower, 2026 data results in a cutoff value od $D_D = 0.05$.

The radiant is very compact in geocentric equatorial coordinates (*Figure 7*). Most higher threshold points appear as outliers among the sporadic background. The compactness of the radiant is also clear in the geocentric Sun-centered ecliptic coordinates (*Figure 8*). The number of shower meteors as a percentage relative to the total number of meteors recorded from camera stations south of 40° latitude results in the profile plotted in *Figure 9*. Best rates occurred at $\lambda_O = 114.5 \pm 0.5°$ and the total activity duration took about 3 days. Other possible shower members outside this activity interval are most likely sporadic meteors that fit the similarity criteria by chance. The results obtained by the radiant based classification method and the orbit method are in good agreement.

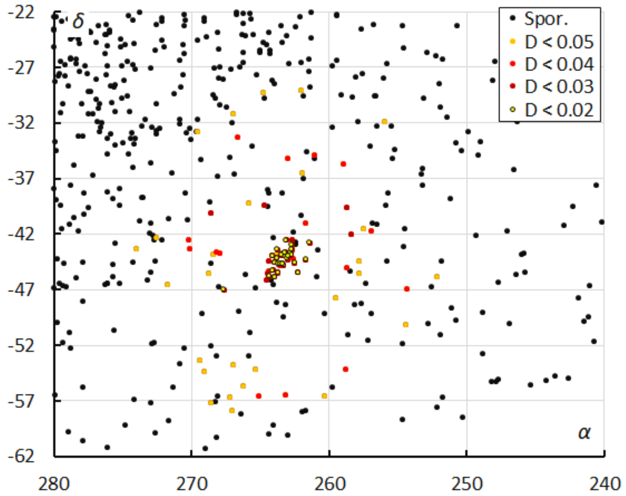

Figure 7 – The radiant distribution during the solar-longitude interval 111.5° – 116.5° in equatorial coordinates, color-coded for different threshold values of the combined similarity criteria.

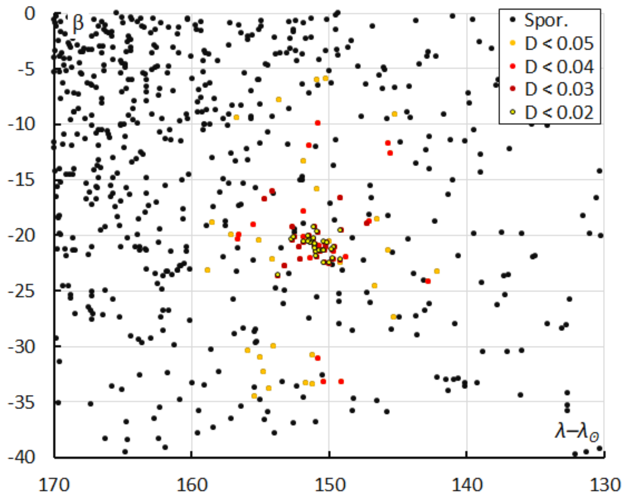

Figure 8 – The radiant distribution during the solar-longitude interval 111.5° – 116.5° in Sun-centered geocentric ecliptic coordinates, color-coded for different threshold values of the combined similarity criteria.

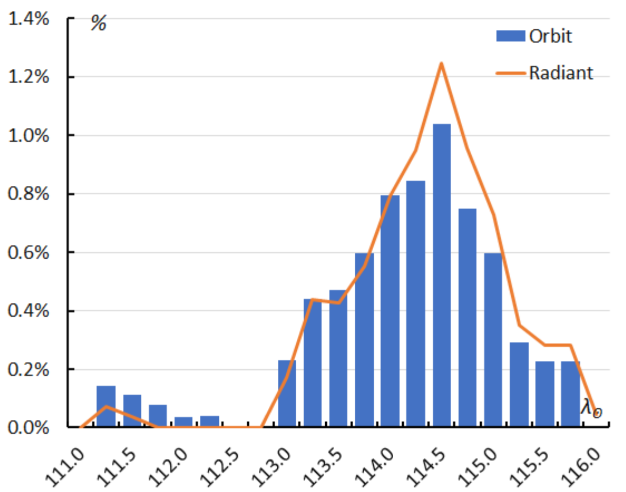

Figure 9 – The percentage of shower meteors relative to the total number of meteors recorded south of 40° Northern latitude.

32 meteors were identified in common by the two methods, six were identified by the orbit method but failed for the radiant method. The radiant method associated 11 meteors that failed to fit the orbit similarity threshold with $D_{SH} < 0.075$ and $D_D < 0.03$ and $D_J < 0.075$. Both methods result in a slightly different solution which are both representative for the new meteor shower.

4 Orbit and parent body

The diagram of the inclination *i* versus the longitude of perihelion *Π* shows a clear concentration (*Figure 10*). The eccentricity *e* versus the longitude of perihelion *Π* also appears concentrated in *e* versus *Π* (*Figure 11*), *e* versus *i* (*Figure 12*) and *q* versus *i* (*Figure 13*). In *Figure 12* we see a large concentration with inclination between 6° and 10° and eccentricity between 0.75 and 0.85. This is caused by the xi2-Capricornids (XCS#623) which are also visible in *Figure 13* at a perihelion distance of 0.50 to 0.55 AU. Some of these meteors were identified as alpha-Capricornids (CAP#1).

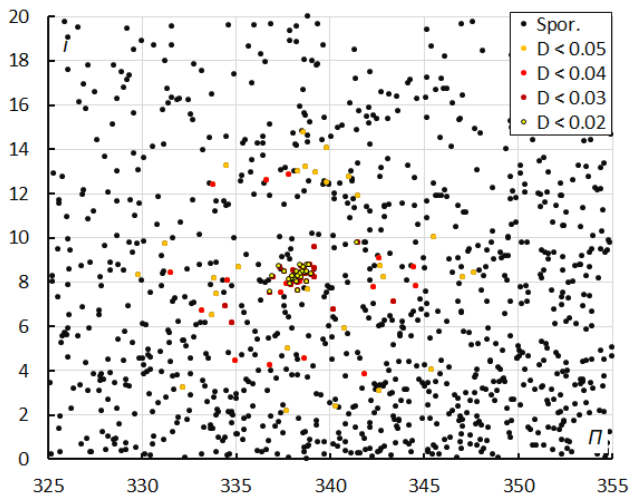

Figure 10 – Inclination *i* versus the longitude of perihelion *Π* color-coded for different classes of D-criteria thresholds, for $\lambda_{\odot}$ between 111.5° – 116.5°. Spor. = sporadics.

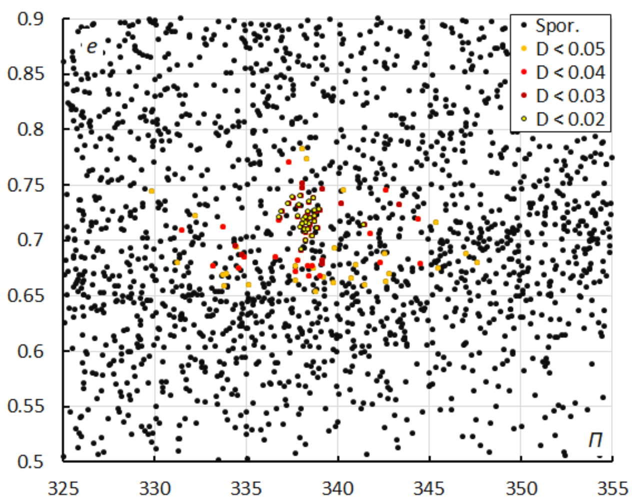

Figure 11 – Eccentricity *e* versus the longitude of perihelion *Π* color-coded for different classes of D-criteria thresholds, for $\lambda_{\odot}$ between 111.5° – 116.5°. Spor. = sporadics.

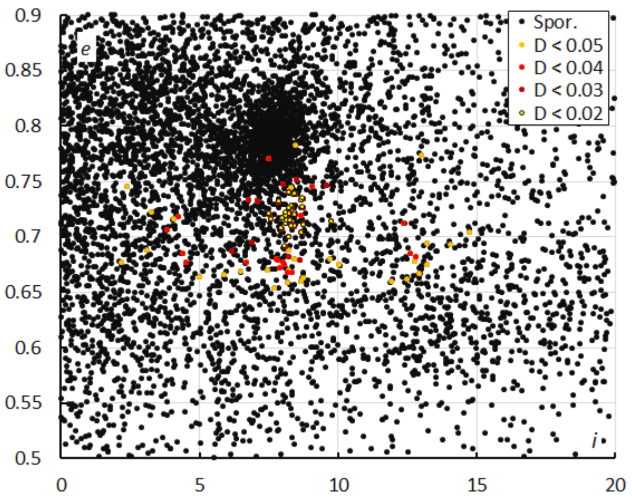

Figure 12 – Eccentricity *e* versus the inclination *i* color-coded for different classes of D-criteria thresholds, for $\lambda_\odot$ between 111.5° – 116.5°. Spor. = sporadics.

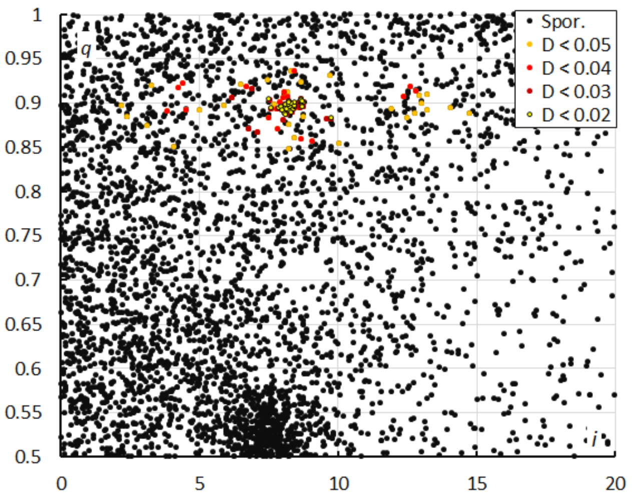

Figure 13 – Perihelion distance *q* versus the inclination *i* color-coded for different classes of D-criteria thresholds, for $\lambda_\odot$ between 111.5° – 116.5°. Spor. = sporadics.

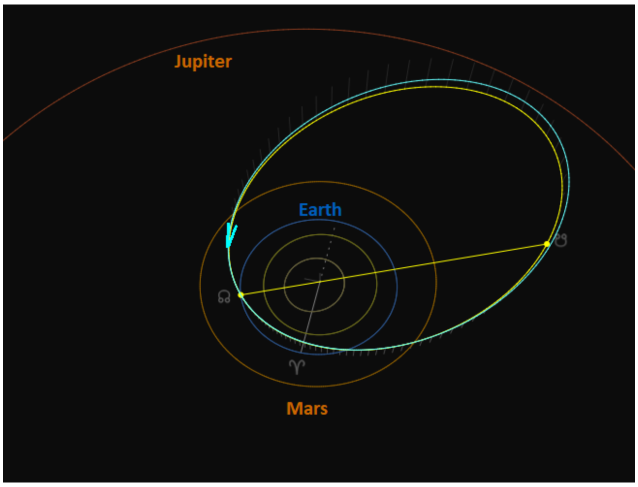

Figure 14 – Comparing the radiant determined new shower solution for 2026 (yellow) with the orbit determined solution for 2026 (blue). (Plotted with the Orbit visualization app provided by Pető Zsolt).

With a Tisserand value of about 2.7 relative to Jupiter, this is a typical Jupiter Family Comet orbit. A search for possible parent bodies yields one possible candidate 2023 VN9 (*Table 2*). The median ablation height of these meteors is rather deep in the atmosphere which is uncommon for fragile cometary particles and suggests a possible asteroidal origin.

Table 1 – Comparing solutions derived by two different methods, GMN-method based on radiant positions and orbit association for $D_D < 0.03$ and $D_D < 0.02$.

	Radiant method	$D_D < 0.03$	$D_D < 0.02$
$\lambda_\odot$ (°)	114.5	114.5	114.1
$\lambda_{\odot b}$ (°)	111.1	111.6	111.7
$\lambda_{\odot e}$ (°)	117.8	115.5	115.5
α_g (°)	263.2	263.3	263.3
δ_g (°)	–44.6	–44.1	–44.2
$\Delta\alpha_g$ (°)	0.35	0.40	0.34
$\Delta\delta_g$ (°)	–0.55	–0.95	–0.75
v_g (km/s)	14.3	14.7	14.7
H_b (km)	88.8	88.9	88.8
H_e (km)	76.0	75.9	75.8
H_p (km)	80.7	80.7	80.6
Mag_{Ap}	+0.8	+0.8	+0.7
λ_g (°)	264.8	264.9	264.8
$\lambda_g - \lambda_\odot$ (°)	150.3	151.0	150.9
β_g (°)	–21.3	–20.8	–20.8
a (A.U.)	3.03	3.17	3.19
q (A.U.)	0.898	0.893	0.895
e	0.704	0.718	0.719
i (°)	8.2	8.2	8.3
ω (°)	44.1	44.6	44.3
Ω (°)	294.0	293.8	294.0
Π (°)	338.1	338.4	338.3
T_j	2.79	2.72	2.71
N	43	38	29

Table 2 – Top ten matches of a search for possible parent bodies with $D_D < 0.07$, based upon the mean orbit derived from the radiant classification method.

Name	D_D
2023 VN9	0.033
2016 KB1	0.057
2021 VW1	0.062
2024 TH11	0.062
2020 SP4	0.064
2017 UW5	0.065
2025 UW107	0.066
2016 LX48	0.067
2019 TJ5	0.069
2024 NN1	0.071

5 Past activity

There is extensive clustering of radiants between RA 260° and 280° and Dec –22° and –32° from mid to late July. It appears the first detection of the present "shower" was by R.A. MacIntosh (1935). Given the errors from plotting meteors MacIntosh's shower #190 was the first positive detection. MacIntosh records an activity from 10 to 17 July with radiants at RA 273°, Dec –36° and RA 277.4°, Dec –37°.

The next recording of the shower is by Buhagiar who in his first list records a shower active from 10 July to 22 July with a maximum ZHR of 3 on 16 July and a dispersed radiant at RA 268°, Dec –38° in 1972–1978. Buhagiar later changed the radiant position in his second list (to RA 271°, Dec –34°, although he kept the activity period the same as in his first list.

Both Clark 1972–1980 and WAMS /NAPOMS 1979–2000 did not detect the shower. There were 2 to 3 radiants plotted in the general radiant area but the radiant density was such that a shower could not be positively identified from the sporadic radiants. John Morgan at Renwick New Zealand during the 1970's did not detect the shower either. His skies were greatly affected by the winter weather. Darryl Skelsey at Colo NSW detected a radiant from RA 270°, Dec –39° on the evening of 16 July and at RA 268°, Dec –41° on the evening of 17 July 1971. Skelsey reported the rate on the first night reached 6 slow bright orange-yellow meteors per hour for two hours in the evening of 16 July 1971. Skelsey was out observing again at Colo on 15 July and 16 July 1972 but this time did not see any meteors from this source.

6 Conclusions

This GMN meteoroid orbit data case study documents a new activity source with a radiant in Scorpion and a Jupiter Family comet-type orbit. The best activity occurred around at $\lambda_O = 114.5 \pm 0.5°$. Visual observations from the past suggest a possible periodic activity, being absent in most years. The new shower has been reported to the IAU-MDC and received the preliminary designation M2026-P1.

Acknowledgments

This report is based on the data of the Global Meteor Network (Vida et al., 2020a; 2020b; 2021) which is released under the CC BY 4.0 license[1]. We thank all 927 participants in the Global Meteor Network project for their contribution and perseverance. A list with the names of the volunteers who contribute to GMN has been published in the 2025 annual report (Roggemans et al., 2026b). The following 114 cameras contributed to paired meteors used in this study: AU0006, AU000D, AU001B, AU001F, AU001S, AU001W, AU002A, AU002B, AU0030, BA0003, BA0005, BR000F, BR000J, BR000Q, BR000T, BR000Y, BR0013, BR002B, BR002C, HR000K, HR0024, HR002G, HR002H, HR002J, HR002M, HR002V, HR002X, NZ0004, NZ0007, NZ000H, NZ000P, NZ000R, NZ000S, NZ000X, NZ000Y, NZ000Z, NZ0012, NZ0017, NZ001E, NZ001G, NZ001J, NZ001L, NZ001N, NZ001P, NZ001Q, NZ001R, NZ001S, NZ001V, NZ0021, NZ0023, NZ002C, NZ002D, NZ002H, NZ002K, NZ002N, NZ002R, NZ002T, NZ002U, NZ002W, NZ002X, NZ002Y, NZ0030, NZ0032, NZ0033, NZ0036, NZ0037, NZ003A, NZ003C, NZ003E, NZ003F, NZ003H, NZ003K, NZ003R, NZ003S, NZ003U, NZ003W, NZ0040, NZ0041, NZ0042, NZ0044, NZ0046, NZ0049, NZ004A, NZ004F, NZ004H, NZ004J, NZ004R, NZ004T, NZ004Y, NZ0051, NZ0059, NZ005C, NZ005G, NZ005L, NZ005M, NZ005N, NZ005Q, NZ005R, NZ005S, NZ005T, NZ005U, NZ005Z, NZ0061, NZ0063, NZ0067, NZ0069, NZ006C, NZ006G, NZ006L, NZ006R, NZ006V, NZ007B, NZ007C and NZ007D.

References

Drummond J. D. (1981). "A test of comet and meteor shower associations". *Icarus*, **45**, 545–553.

Jopek T. J. (1993). "Remarks on the meteor orbital similarity D-criterion". *Icarus*, **106**, 603–607.

Jopek T. J., Rudawska R. and Pretka-Ziomek H. (2006). "Calculation of the mean orbit of a meteoroid stream". *Monthly Notices of the Royal Astronomical Society*, **371**, 1367–1372.

MacIntosh R.A. (1935). "An Index to Southern Meteor Showers". *Monthly Notices of the Royal Astronomical Society*, **5**, 709–718.

Moorhead A. V., Clements T. D., Vida D. (2020). "Realistic gravitational focusing of meteoroid streams". *Monthly Notices of the Royal Astronomical Society*, **494**, 2982–2994.

Roggemans P., Vida D., Šegon D., Scott J.M. (2026a). "Meteoroid orbit shower identification". *eMetN Meteor Journal*, **11**, 189–204.

Roggemans P., Campbell-Burns P., Kalina M., McIntyre M., Scott J. M., Šegon D., Vida D. (2026b). "Global Meteor Network report 2025". *eMetN Meteor Journal*, **11**, 89–129.

Southworth R. B. and Hawkins G. S. (1963). "Statistics of meteor streams". *Smithsonian Contributions to Astrophysics*, **7**, 261–285.

Vida D., Gural P., Brown P., Campbell-Brown M., Wiegert P. (2020a). "Estimating trajectories of meteors: an observational Monte Carlo approach - I. Theory". *Monthly Notices of the Royal Astronomical Society*, **491**, 2688–2705.

[1] https://creativecommons.org/licenses/by/4.0/

Vida D., Gural P., Brown P., Campbell-Brown M., Wiegert P. (2020b). “Estimating trajectories of meteors: an observational Monte Carlo approach - II. Results”. *Monthly Notices of the Royal Astronomical Society*, **491**, 3996–4011.

Vida D., Šegon D., Gural P. S., Brown P. G., McIntyre M. J. M., Dijkema T. J., Pavletić L., Kukić P., Mazur M. J., Eschman P., Roggemans P., Merlak A., Zubrović D. (2021). “The Global Meteor Network – Methodology and first results”. *Monthly Notices of the Royal Astronomical Society*, **506**, 5046–5074.

26-Bootids (TSB#571) confirmed

Paul Roggemans[1], Denis Vida[2,3], Damir Šegon[4,5], Milan Kalina[6], James M. Scott[7], Jeff Wood[8]

[1] **Pijnboomstraat 25, 2800 Mechelen, Belgium**
Paul.roggemans@gmail.com

[2] **Department of Physics and Astronomy, University of Western Ontario, Richmond Street, London, N6A 3K7, Ontario, Canada.**
[3] **Institute for Earth and Space Exploration, University of Western Ontario, Perth Drive, London, N6A 5B8, Ontario, Canada**

[4] **Astronomical Society Istra Pula, Park Monte Zaro 2, 52100 Pula, Croatia.**
[5] **Višnjan Observatory, Istarska 5, 52463 Višnjan, Croatia**

[6] **Czech Astronomical Society, Ondřejov, Czech Republic**
kalina@astro.cz

[7] **Department of Geoscience, Aarhus University, Høegh-Guldbergs Gade 2. DK-8000 Aarhus C, Denmark**

[8] **PO Box 162, Willetton, Western Australia 6955, Australia**

A distinct concentration of radiants detected by GMN occurred on 3rd – 4th March 2026 from a source at R.A. 217° and decl. +25° with a geocentric velocity of 49.5 km/s. The activity has been identified as the 26-Bootids (TSB#571), a long-period comet type meteoroid stream. This shower has been recorded by GMN in the previous years and this case study confirms that this annual meteor shower fulfils the criteria in order to be nominated for established status by the IAU-MDC.

1 Introduction

The radiant density map for the 3rd and 4th March 2025 showed a bright spot caused by the 26-Bootids[2] (*Figure 1*). The activity lasted from $\lambda_{\odot} = 340°$ until $\lambda_{\odot} = 345°$. The shower is listed in the GMN meteor shower reference list and has been recently nominated to be established in the IAU-MDC Working List of Meteor Showers. The shower was discovered by Andreić et al. (2014) and later confirmed by Shiba (2023) and (Jenniskens, 2023). The activity has been well observed by the Global Meteor Network and justified a dedicated case study. The best coverage by GMN for this shower occurred in 2025 and 2026.

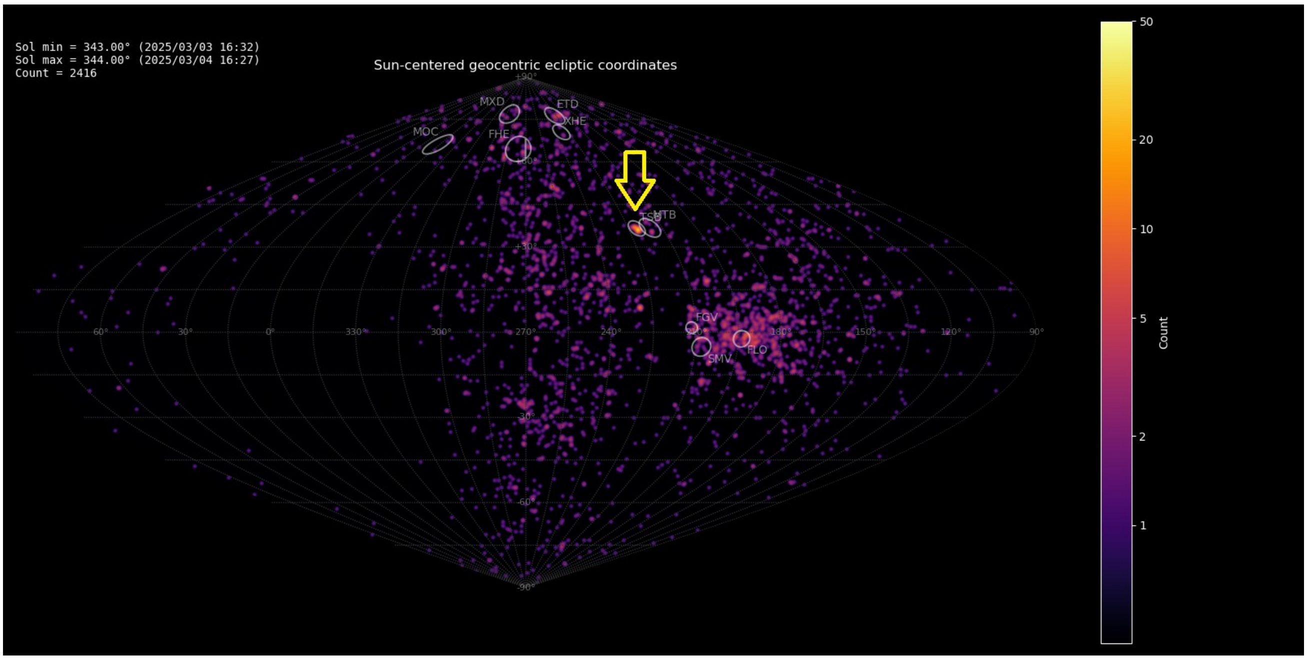

Figure 1 – Radiant density map with 2416 radiants obtained by the Global Meteor Network during the 3rd – 4th March, 2025. The position of the 26-Bootids in Sun-centered geocentric ecliptic coordinates is marked with a yellow arrow.

[2] https://www.ta3.sk/IAUC22DB/MDC2022/Roje/pojedynczy_obiekt.php?lporz=01606&kodstrumienia=00571

2 Shower classification based on radiants

The GMN shower association criteria assume that meteors within 1° in solar longitude, within 1.8° in radiant in this case, and within 10% in geocentric velocity of a shower reference location are members of that shower. Further details about the shower association are explained in Moorhead et al. (2020). Using the 2025 data, initially 102 possible shower members were selected and after removal of outliers, 72 members remained for final analysis. 169 GMN-cameras in 23 countries (Austria, Australia, Belgium, Bulgaria, Brazil, Canada, Croatia, Czech Republic, Finland, France, Germany, Hungary, Ireland, Italy, Netherlands, New Zealand, Poland, Romania, Russia, Slovenia, Slovakia, United Kingdom and the United States) contributed data for this dataset in 2025. The shower parameters as obtained by the radiant method for 2025 are listed in *Table 1* and compared to the results for 2026.

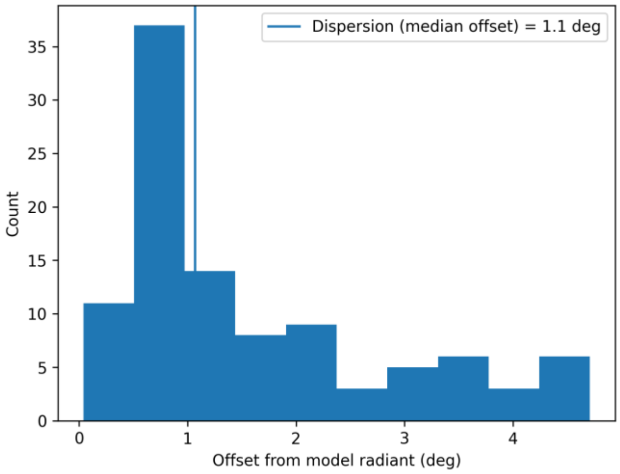

Figure 2 – Dispersion median offset on the radiant position.

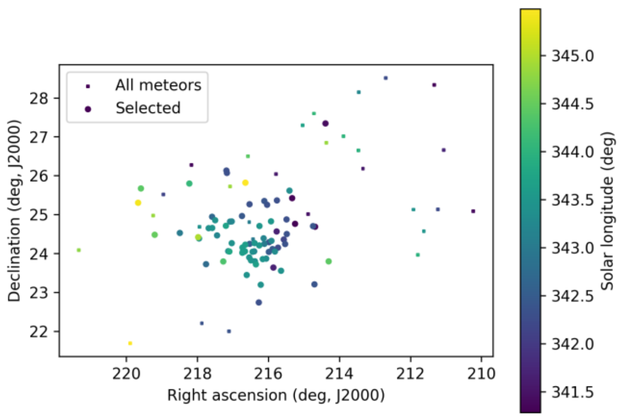

Figure 3 – The radiant distribution in 2025 during the solar-longitude interval 341.2° – 345.5° in equatorial coordinates.

Figure 3 shows a distinct concentration of 26-Bootid radiants. This can also be illustrated when the shower meteors are plotted as grey diamonds and the sporadic background appears randomly distributed in *Figure 5*, compared to the shower meteors plotted as a cluster with the sporadics as grey diamonds in the background (*Figure 6*). In geocentric Sun-centered ecliptic coordinates the compactness of the radiant is even more striking (*Figure 7*). It should be noted that the radiant shower association method results in a short activity interval in solar longitude between 341.2° and 346.5° with best activity around $\lambda_{\odot} = 343.3°$. This activity duration is shorter than given by other researchers (Shiba, 2023; Jenniskens, 2023).

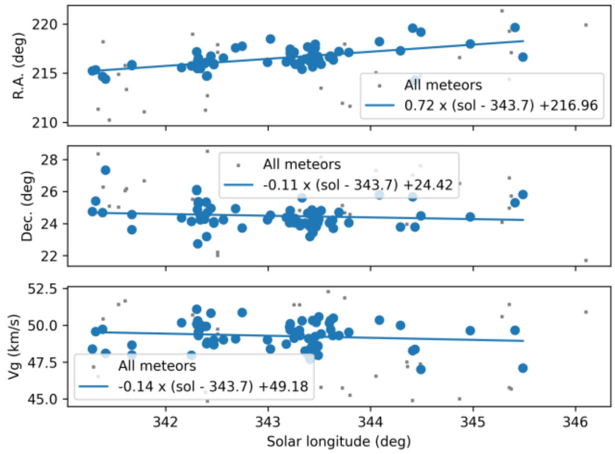

Figure 4 – The radiant drift.

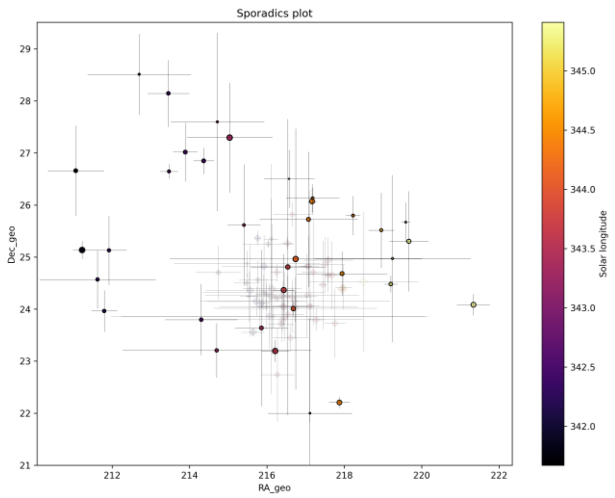

Figure 5 – The sporadic radiant distribution in 2025 during the solar-longitude interval 341.2° – 345.5° in equatorial coordinates with the 26-Booitds as grey diamonds.

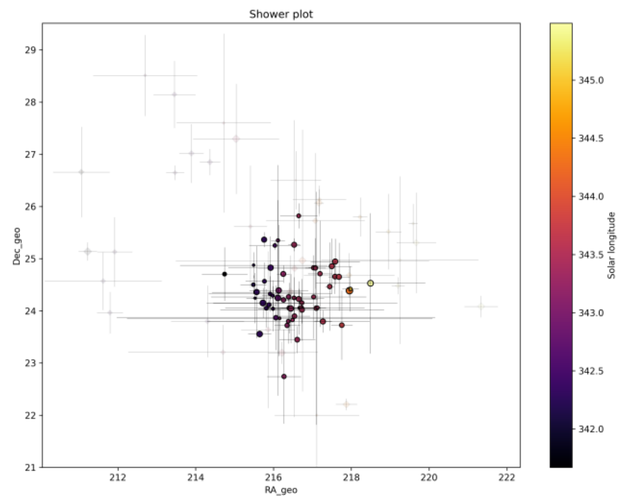

Figure 6 – The 26-Bootids radiant distribution in 2025 during the solar-longitude interval 341.2° – 345.5° in equatorial coordinates with the sporadic background as grey diamonds.

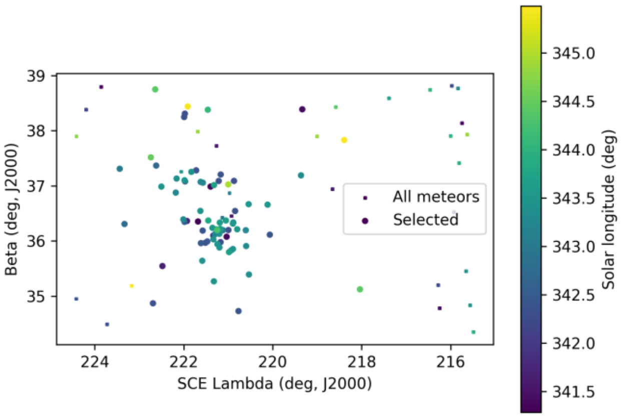

Figure 7 – The radiant distribution during the solar-longitude interval 341.2° – 345.5° in Sun centered geocentric ecliptic coordinates.

3 Shower classification based on orbits

A complete independent meteoroid stream search has been applied to orbit data obtained between solar longitude 337° and 348° during the years 2019–2026. The method has been described in detail in a separate publication (Roggemans et al., 2026a). 74549 orbits were available within this time interval and a final mean orbit has been computed by the method of Jopek et al. (2006) for the thresholds $D_{SH} < 0.125$ and $D_D < 0.05$ and $D_J < 0.125$ (Southworth and Hawkins, 1963; Drummond, 1981; Jopek, 1993), based upon the Rayleigh fit in *Figure 8*. The resulting mean orbit based upon 207 meteors recorded from 2019 until 2026 is listed in *Table 1*.

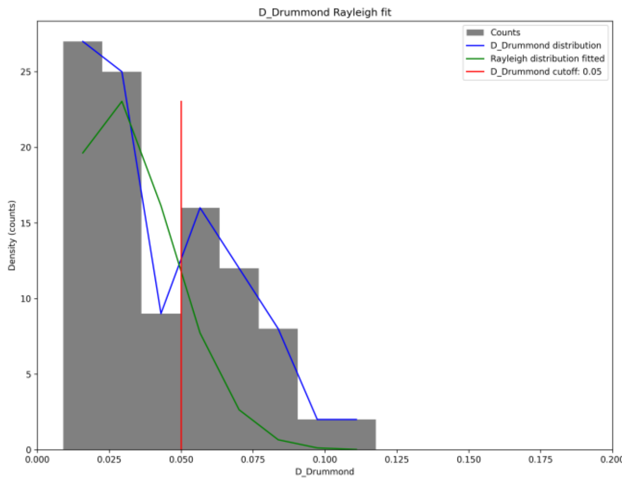

Figure 8 – Rayleigh fit on the Drummond criterion for 26-Bootids. The 2025 data result in a cutoff value of $D_D = 0.05$.

The radiant is very compact in geocentric equatorial coordinates (*Figure 9*). The more dispersed cloud of sporadics at slightly higher declination right of the 26-Bootids are the March 12-Bootids (MTB#859). The compactness of the radiant is very distinct in the geocentric Sun-centered ecliptic coordinates (*Figure 10*). The dark cluster just right from the 26-Bootids are the March 12-Bootids which have their maximum a couple of days later than the 26-Bootids and have a similar orbit apart from a 10° lower inclination. Both showers are very likely related.

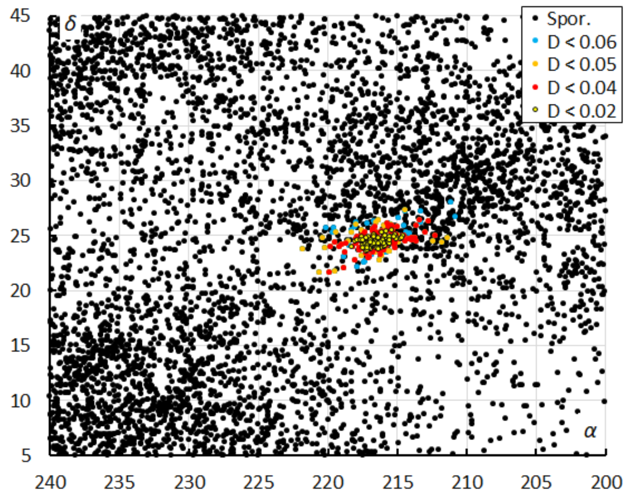

Figure 9 – The radiant distribution during the solar-longitude interval 337° – 348° in equatorial coordinates, color-coded for different threshold values of the combined similarity criteria.

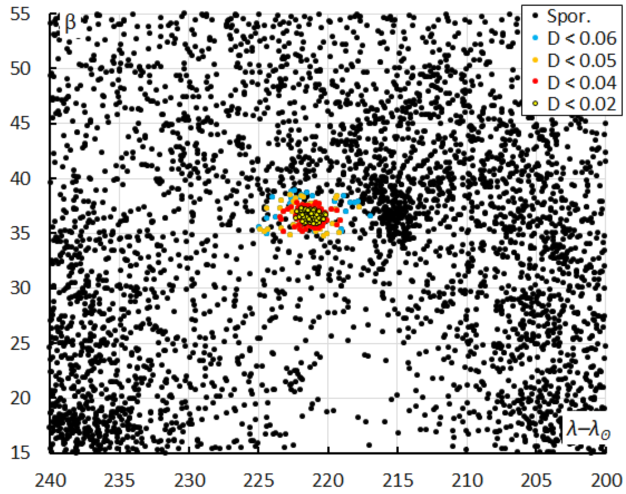

Figure 10 – The radiant distribution during the solar-longitude interval 337° – 348° in Sun-centered geocentric ecliptic coordinates, color-coded for different threshold values of the combined similarity criteria.

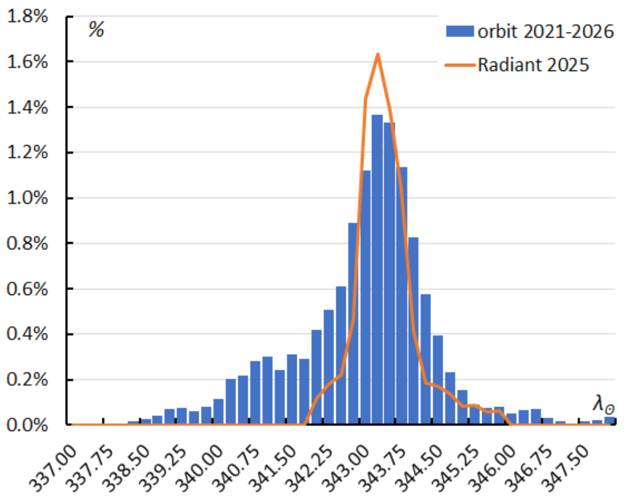

Figure 11 – The percentage of shower meteors relative to the total number of meteors recorded in 2019–2026.

The number of shower meteors as a percentage relative to the total number of meteors recorded in a 24 hours interval results in the profile plotted in *Figure 11*. Best rates occurred at $\lambda_{O} = 343.25 \pm 0.5°$ and the total activity duration spanned a 5 days interval from $\lambda_{O} = 340°$ until $\lambda_{O} = 345°$. This is very well visible in the radiant density maps (*Figure 12*) where almost no 26-Bootids activity is visible after $\lambda_{O} = 344°$ when the March 12-Bootids (MTB in *Figure 12*) becomes stronger. Other possible shower members outside this activity interval are most likely sporadic meteors that fit the similarity criteria by chance. The results obtained by the radiant based classification method for 2025 and 2026 and the orbit method for 2019–2026 are in good agreement.

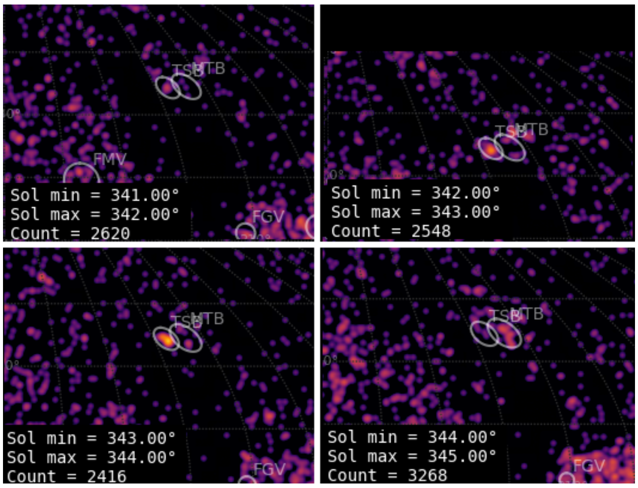

Figure 12 – The radiant density maps show clear activity of the 26-Bootids for a few nights.

4 Orbit and parent body

The diagram of the inclination *i* versus the longitude of perihelion *Π* shows a clear concentration (*Figure 13*). The diffuse cloud at 72° inclination are the March 12-Bootids. The eccentricity *e* versus the longitude of perihelion *Π* also appears concentrated in *e* versus *Π* (*Figure 14*), *e* versus *i* (*Figure 15*), *q* versus *i* (*Figure 16*) and *q* versus *e* (*Figure 17*). Note that the March 12-Bootids only differ about 10° in inclination, best visible in *Figure 16* as the other orbital elements overlap for both showers with the March 12-Bootids being more scattered.

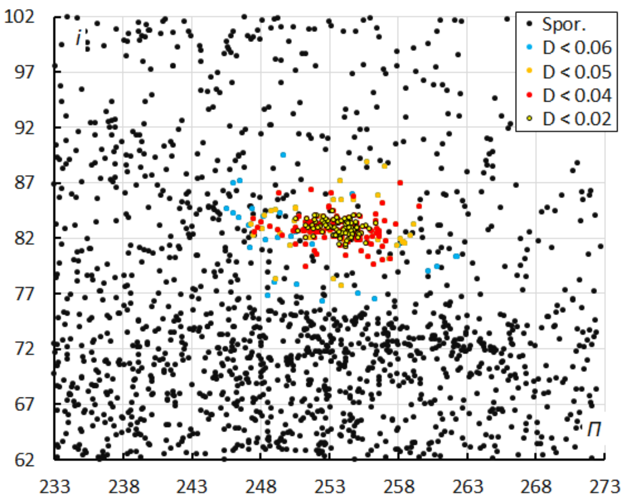

Figure 13 – Inclination *i* versus the longitude of perihelion *Π* color-coded for different classes of D-criteria thresholds, for λ_{O} between 337° – 348°. Spor. = sporadics.

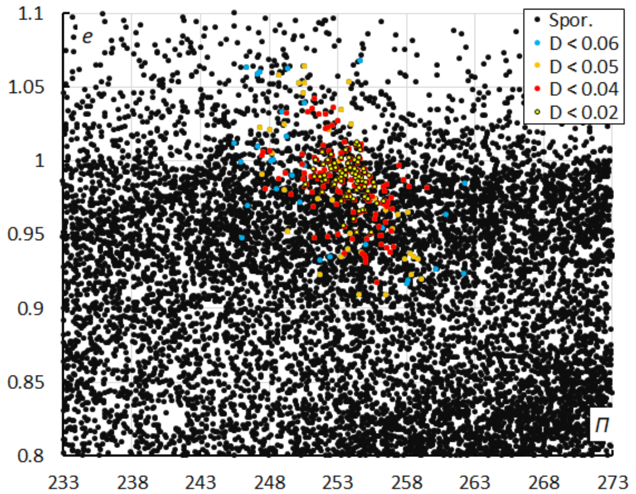

Figure 14 – Eccentricity *e* versus the longitude of perihelion *Π* color-coded for different classes of D-criteria thresholds, for λ_{O} between 337° – 348°. Spor. = sporadics.

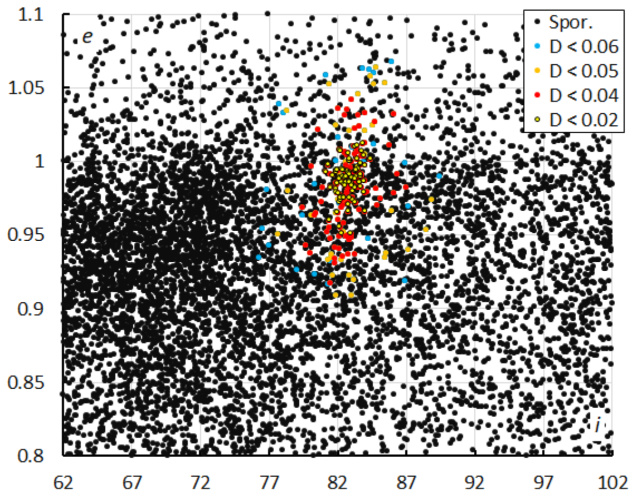

Figure 15 – Eccentricity *e* versus the inclination *i* color-coded for different classes of D-criteria thresholds, for λ_{O} between 337° – 348°. Spor. = sporadics.

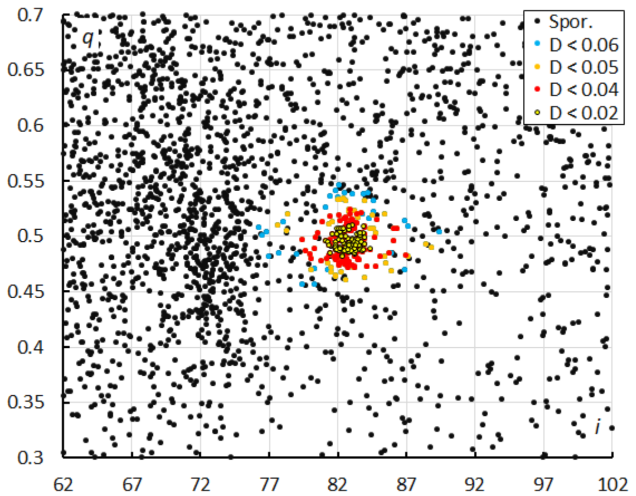

Figure 16 – Perihelion distance *q* versus the inclination *i* color-coded for different classes of D-criteria thresholds, for λ_{O} between 337° – 348°. Spor. = sporadics.

With a Tisserand value relative to Jupiter of 0.30, this shower has a long period comet type orbit. The inclination of ~83° is almost perpendicular to the ecliptic plane (*Figure 18*). With an eccentricity close to the hyperbolic limit, the slightest observational or instrumental uncertainty on the velocity results in a huge difference in aphelion, which reaches far beyond the distance of Neptune to the Sun.

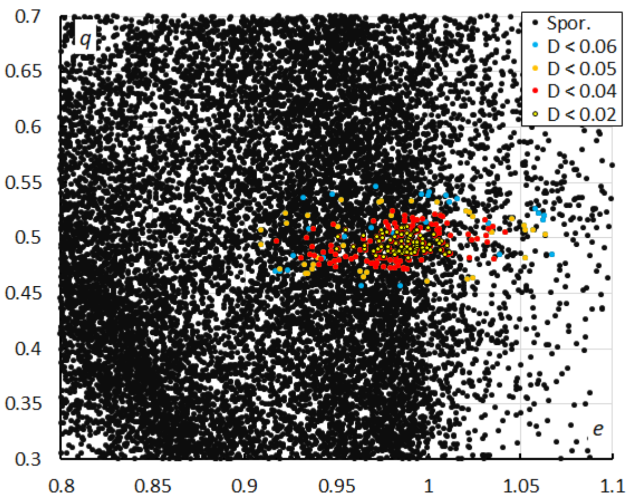

Figure 17 – Perihelion distance *q* versus the eccentricity *e* color-coded for different classes of D-criteria thresholds, for λ_O between 337° – 348°. Spor. = sporadics.

Table 1 – Comparing solutions derived by two different methods, GMN-method based on radiant positions for 2025 and 2026, and the orbit association method for D_D < 0.05 for 2019–2026.

	Radiant method 2025	Radiant method 2026	Orbit method 2019–2026 D_D < 0.05
λ_O (°)	343.3	343.5	343.3
λ_{Ob} (°)	341.2	341.1	338.7
λ_{Oe} (°)	345.5	345.2	348.0
α_g (°)	217.0	216.7	216.4
δ_g (°)	+24.4	+24.5	+24.5
$\Delta\alpha_g$ (°)	0.72	0.67	0.85
$\Delta\delta_g$ (°)	–0.11	–0.31	–0.26
v_g (km/s)	49.2	49.5	49.7
H_b (km)	106.3	105.9	106.7
H_e (km)	92.6	90.6	91.3
H_p (km)	98.2	96.3	97.2
Mag_{Ap}	–0.8	–1.0	–0.8
λ_g (°)	204.5	204.6	204.5
$\lambda_g - \lambda_O$ (°)	221.2	221.1	221.2
β_g (°)	+36.7	+36.7	+36.4
a (A.U.)	16.1	24.7	28.6
q (A.U.)	0.493	0.496	0.494
e	0.969	0.980	0.983
i (°)	82.4	82.4	82.9
ω (°)	271.2	270.5	270.6
Ω (°)	343.1	343.4	343.0
Π (°)	254.3	253.9	253.6
T_j	0.44	0.33	0.29
N	72	44	207

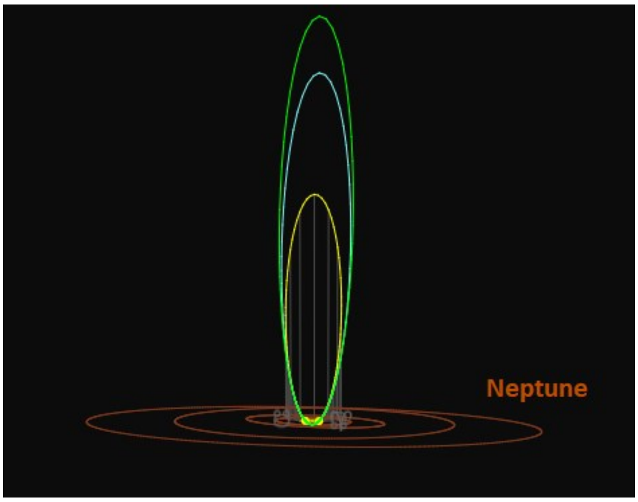

Figure 18 – Comparing the radiant determined 26-Bootids solution for 2025 (yellow), for 2026 (blue) and the orbit determined solution for 2019–2026 (green). (Plotted with the Orbit visualization app provided by Pető Zsolt).

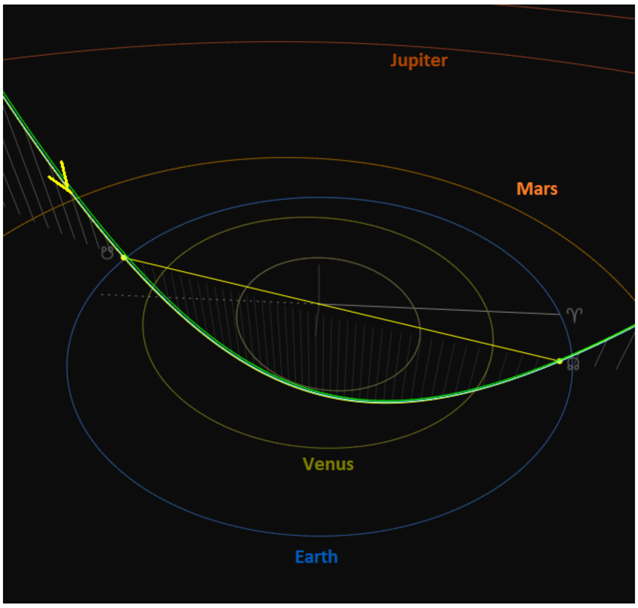

Figure 19 – Close-up in the inner Solar system with the solutions for 2025 (yellow), 2026 (blue) and the orbit determined solution for 2019–2026 (green). (Plotted with the Orbit visualization app provided by Pető Zsolt).

Looking at the orbit solutions within the inner Solar system (*Figure 19*), no difference can be seen in the plotted version of the three solutions. The 26-Bootids encounter the Earth at the descending node. Its ascending node is within the Earth orbit and relatively close to the Earth orbit. In principle this could produce another meteor shower and the orbit shower classification method can detect such orbits. Using the 26-Bootids orbit as a reference we find such orbits between 6 and 8 September from a radiant near R.A. = 116° and Decl. = –15°. There is no such shower known in the IAU-MDC Working List of Meteor Showers.

A search for candidate parent bodies did not yield any convincing similarity in orbit. Jenniskens (2023) suggests C/868 B1 as a vague resemblance but that orbit is uncertain due to poor observations. Our search results in two other slightly better resembling orbits but even here the Drummond criterion with D_D = 0.15 is too poor to associate both orbits. The shower may be related to a long period comet that hasn't yet been discovered.

Table 2 – Top ten matches of a search for possible parent bodies with $D_D < 0.30$, based upon the mean orbit derived from the radiant classification method.

Name	D_D
C/-146 P1	0.15
C/1914 S1 (Campbell)	0.20
C/868 B1	0.20
2020 QH4	0.23
2005 BW1	0.26
2020 CY1	0.26
C/2000 S5	0.27
C/1952 W1 (Mrkos)	0.27
C/2012 F6 (Lemmon)	0.27
(858130) 2012 US136	0.29

5 Conclusions

The existence and annual nature of the 26-Bootids have been confirmed. Meanwhile the shower has been nominated for established status and this study provides some extra solutions to document this shower. The activity duration corresponds best to the initial discovery by the Croatian Meteor Network (Andreić et al., 2014) between solar longitude 341° and 345°. The orbit shower identification method found similar orbits between solar longitudes 338.7° and 348° but the numbers of orbits before 340° and after 345° are statistically insignificant and may concern spurious associations. The activity period given by Shiba (2023) from 330.5° to 358.96° could not be confirmed from the GMN data.

Acknowledgments

This report is based on the data of the Global Meteor Network (Vida et al., 2020a; 2020b; 2021) which is released under the CC BY 4.0 license[3]. We thank all 927 participants in the Global Meteor Network project for their contribution and perseverance. A list with the names of the volunteers who contribute to GMN has been published in the 2025 annual report (Roggemans et al., 2026b). The following 454 cameras contributed to paired meteors used in this study:

AU0002, AU0003, AT0004, AU0006, AU000B, AU000F, AU000G, AU000J, AU000T, AU000X, AU000Z, AU0011, AU001A, AU001L, AU001N, AU001Q, AU001S, AU001V, AU001W, AU001X, AU001Z, AU002B, AU0030, AU0038, AU003G, AU003J, BE0001, BE0002, BE0005, BE0006, BE0007, BE000A, BE000B, BE000C, BE000D, BE000E, BE000G, BE000H, BE000K, BE000P, BE000U, BE000V, BE0010, BE0015, BE0016, BE0019, BG0004, BG000C, BG000K, BR000G, BR001Q, BR001R, CA0005, CA000D, CA000F, CA000S, CA000Z, CA0015, CA0021, CA002R, CA0031, CH0005, CZ0002, CZ0003, CZ0004, CZ0007, CZ0009, CZ000B, CZ000E, CZ000F, CZ000G, CZ000J, CZ000K, CZ000M, CZ000N, CZ000P, CZ000Q, DE0001, DE0004, DE0005, DE0006, DE0007, DE000B, DE000H, DE000Q, DE000R, DE000S, DE000W, DE000Y, DE0013, DK0002, DK0004, DK0007, DK0008, DK0009, DK000A, DK000F, DK000G, DK000J, DK000K, DK000M, DK000N, DK000R, DK000S, DK000T, ES000D, ES000E, ES000L, ES000Q, ES000Z, ES0013, ES0016, FI0002, FI0004, FR0006, FR000A, FR000G, FR000R, FR000U, FR000X, FR000Z, FR0011, FR0013, FR0014, FR0017, GR0006, GR0009, HR0007, HR000K, HR000M, HR000P, HR000S, HR001G, HR001H, HR001Z, HR0024, HR0025, HR0027, HR002F, HR002H, HR002J, HR002K, HR002M, HR002X, HU0001, HU0002, HU0004, HU0005, HU0008, HU000A, IE0005, IE000G, IT0001, IT0004, KR0002, KR0004, KR0009, KR000G, KR000H, KR000K, KR000M, KR000P, KR000R, KR0019, KR001C, KR001J, KR0023, KR0024, KR002F, KR002G, KR002S, KR0036, KR0037, KR003P, KR003Q, KR003W, LU0001, MX0006, MX000A, NL0001, NL0003, NL0009, NL000C, NL000M, NL000P, NL000Q, NL000R, NL000S, NL0010, NZ0001, NZ000D, NZ000G, NZ000M, NZ000V, NZ000W, NZ000X, NZ0015, NZ001Q, NZ001Z, NZ0024, NZ0026, NZ002E, NZ002M, NZ002S, NZ002Z, NZ0046, NZ004E, NZ004Y, NZ005J, NZ0061, NZ0063, NZ007D, PL0005, PL0006, PL0009, PL000B, PT0002, RO0002, RO000B, RO000R, RU0004, RU0007, RU0008, RU0009, RU000M, RU0016, RU0018, SI0002, SI0005, SK0002, SK0004, UK0004, UK0006, UK000D, UK000F, UK000H, UK000R, UK000S, UK000Z, UK001L, UK001M, UK001R, UK001S, UK001Z, UK0021, UK0024, UK0026, UK002F, UK002J, UK002K, UK002L, UK002Y, UK0030, UK0031, UK0034, UK0035, UK003C, UK003D, UK003E, UK003F, UK003N, UK003W, UK003X, UK003Y, UK003Z, UK0041, UK0042, UK0045, UK0049, UK004C, UK004E, UK004F, UK004G, UK004H, UK004M, UK004R, UK0050, UK0057, UK005E, UK005G, UK005J, UK005M, UK005P, UK005S, UK005U, UK0060, UK0062, UK0066, UK0067, UK006D, UK006E, UK006G, UK006H, UK006P, UK006S, UK0070, UK0079, UK007A, UK007B, UK007E, UK007H, UK007P, UK007Q, UK007U, UK007V, UK007Y, UK007Z, UK0083, UK0084, UK008A, UK008C, UK008D, UK008F, UK008J, UK008Q, UK008S, UK008T, UK008U, UK008W, UK008X, UK0092, UK0098, UK0099, UK009A, UK009B, UK009D, UK009G, UK009J, UK009K, UK009L, UK009M, UK009P, UK009S, UK009T, UK009U, UK009W, UK009X, UK00A0, UK00A1, UK00A2, UK00A5, UK00AB, UK00AE, UK00AF, UK00AG, UK00AK, UK00AL, UK00AN, UK00AP, UK00AT, UK00AU, UK00B0, UK00B1, UK00B2, UK00B5, UK00B6, UK00B7, UK00BA, UK00BF, UK00BH, UK00BJ, UK00BK, UK00BL, UK00BW, UK00C1, UK00C2, UK00C9, UK00CC, UK00CE, UK00CJ, UK00CQ, UK00CZ, UK00DH, UK00DL, UK00DN, US0001, US0002, US0003, US0004, US0005, US0006, US0008, US0009, US000A, US000D, US000E,

[3] https://creativecommons.org/licenses/by/4.0/

US000G, US000H, US000J, US000L, US000M, US000N, US000R, US000S, US000U, US001G, US001P, US001Q, US001R, US001U, US001V, US0020, US0021, US0023, US0027, US002A, US0030, US0031, US0039, US003G, US003N, US003S, US004B, US004J, US004N, US004P, US004U, US0051, US005A, US005B, US005C, US005D, US005Y, US0062, USL002, USL003, USL004, USL005, USL006, USL007, USL008, USL009, USL00A, USL00D, USL00F, USL00G, USL00J, USL00L, USL00M, USL00Q, USL00V, USL00X, USL00Y, USL011, USL012, USL014, USL015, USL016, USL01A, USL01B, USL01C, USL01D, USL01E and USV002.

References

Andreić Ž., Gural P., Šegon D., Skokić I., Korlević K., Vida D., Novoselnik F., Gostinski D. (2014). "Results of CMN 2013 search for new showers across CMN and SonotaCo databases I-0.5mm". *WGN, Journal of the International Meteor Organization*, **42**, 90–97.

Drummond J. D. (1981). "A test of comet and meteor shower associations". *Icarus*, **45**, 545–553.

Jenniskens P. (2023). Atlas of Earth's meteor showers. Elsevier, Cambridge, United states. ISBN 978-0-443-23577-1. Page 135.

Jopek T. J. (1993). "Remarks on the meteor orbital similarity D-criterion". *Icarus*, **106**, 603–607.

Jopek T. J., Rudawska R. and Pretka-Ziomek H. (2006). "Calculation of the mean orbit of a meteoroid stream". *Monthly Notices of the Royal Astronomical Society*, **371**, 1367–1372.

Moorhead A. V., Clements T. D., Vida D. (2020). "Realistic gravitational focusing of meteoroid streams". *Monthly Notices of the Royal Astronomical Society*, **494**, 2982–2994.

Roggemans P., Vida D., Šegon D., Scott J.M. (2026a). "Meteoroid orbit shower identification". *eMetN Meteor Journal*, **11**, 189–204.

Roggemans P., Campbell-Burns P., Kalina M., McIntyre M., Scott J. M., Šegon D., Vida D. (2026b). "Global Meteor Network report 2025". *eMetN Meteor Journal*, **11**, 89–129.

Shiba Y. (2023). "Halley Type and Long Period Meteor Shower Luminous Altitude Characteristics". *WGN, Journal of the International Meteor Organization*, **51**, 93–108.

Southworth R. B. and Hawkins G. S. (1963). "Statistics of meteor streams". *Smithsonian Contributions to Astrophysics*, **7**, 261–285.

Vida D., Gural P., Brown P., Campbell-Brown M., Wiegert P. (2020a). "Estimating trajectories of meteors: an observational Monte Carlo approach - I. Theory". *Monthly Notices of the Royal Astronomical Society*, **491**, 2688–2705.

Vida D., Gural P., Brown P., Campbell-Brown M., Wiegert P. (2020b). "Estimating trajectories of meteors: an observational Monte Carlo approach - II. Results". *Monthly Notices of the Royal Astronomical Society*, **491**, 3996–4011.

Vida D., Šegon D., Gural P. S., Brown P. G., McIntyre M. J. M., Dijkema T. J., Pavletić L., Kukić P., Mazur M. J., Eschman P., Roggemans P., Merlak A., Zubrović D. (2021). "The Global Meteor Network – Methodology and first results". *Monthly Notices of the Royal Astronomical Society*, **506**, 5046–5074.

Independent confirmation of the psi-Phoenicids shower with PANSY radar data

John Greaves

The ψ-Phoenicids published in 2017 using data from the Southern Argentine Agile Meteor Radar are reassessed using publicly available data from the Program of the Antarctic Syowa MST/IS Radar.

1 Introduction

The ψ-Phoenicids published in Pokorny et al. (2017) is here assessed via the Jopek (1993) variation of the dissimilarity criterion, D_J, against the approximately 1.6 million orbits recently released by the Program of the Antarctic Syowa MST/IS Radar (PANSY) as sourced from RadiantViz[4] (Vierinen et al., 2026). This follows an earlier temporally shifted independent confirmation of this shower using SAAMER data by Greaves (2026).

2 Methodology

The PANSY radar meteor orbits were tested against the ψ-Phoenicids (PPH#769) using a $D_J < 0.080$. The public PANSY dataset currently contains over 1.6 million radar meteor orbits covering a span of 1.5 years (Vierinen et al., 2026) with the vast majority of radiants being below 0 degrees Declination. New mean, median, standard deviation, maximum and minimum values were then calculated for each or Right Ascension, Declination, Solar Longitude, Perihelion Distance, orbital eccentricity, orbital Inclination, Argument of Periastron and Longitude of the Ascending Node.

3 Results

A total of 156 PANSY meteors were matched with the shower giving a mean geocentric velocity of 37.7 kms^{-1} with standard deviations, σ, of 0.8 kms^{-1}. *Table 1* gives the statistics for these radar meteors.

Figure 1 shows the detected ψ-Phoenicids plotted as black circles with the Right Ascension (α) as the horizontal axis and the Declination (δ) as the vertical axis, whilst the black dots represent the PANSY meteors that occurred during roughly the same time interval for the shower as well as the same celestial coordinate range and show the sporadic meteor background.

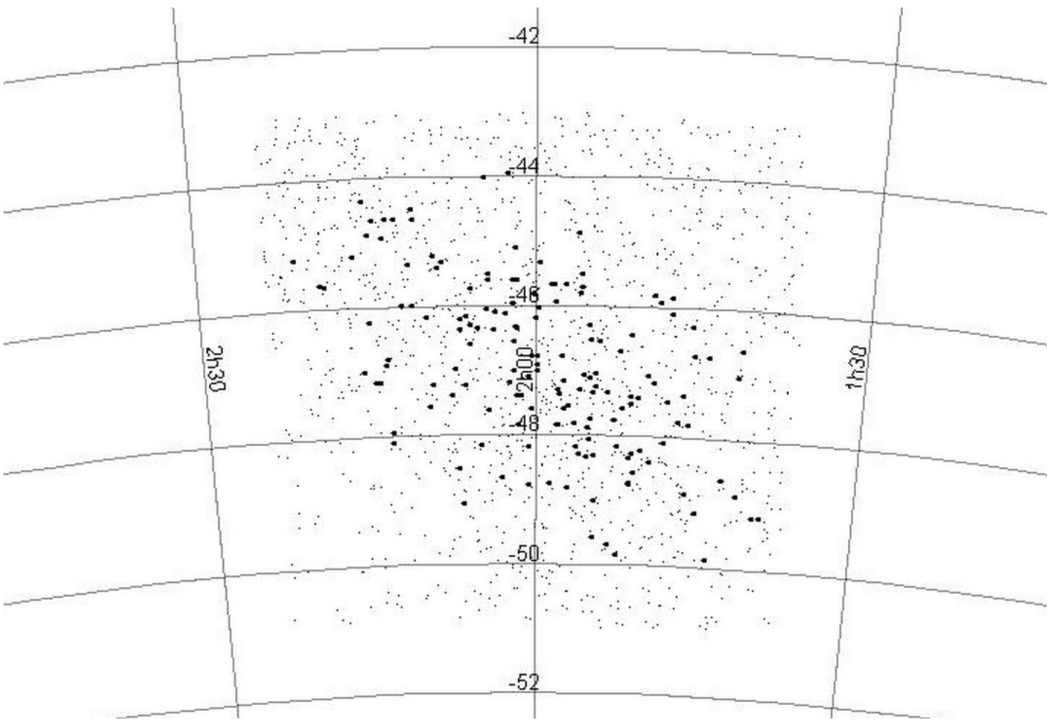

Figure 1 – Sky projection in coordinates of Right Ascension and Declination for a portion of the sky encompassing the area around the ψ-Phoenicids limited to a Solar Longitude range just a little larger than derived shower range. Black circles represent the shower meteors whilst black dots represent the background.

[4] https://juha.no/radiantviz/

Table 1 – Radiant and orbital element details for the ψ Phoenicids.

	R.A. (°)	Decl. (°)	λ_O	q (A.U.)	e	i (°)	ω (°)	Ω (°)
mean	29.8	–47.0	110.613	0.891	0.293	75.02	62.76	290.62
median	29.7	–47.0	110.306	0.894	0.292	75.10	62.14	290.31
stdev	2.3	1.3	1.878	0.024	0.034	1.61	6.35	1.88
min	24.7	–49.9	107.476	0.843	0.226	71.27	49.75	287.48
max	35.3	–43.9	114.888	0.938	0.362	78.39	77.10	294.89

4 Conclusion

The ψ-Phoenicids are reassessed against the newly released PANSY radar meteor orbit dataset using dissimilar orbit criterion.

A total of 156 orbits matching the shower to $D_J < 0.080$ are derived providing further independent confirmation of this shower and its suitability for promotion to an established shower.

Acknowledgments

Juho Vierinen is especially acknowledged for adding a download option to a flat format version of the PANSY level 3 dataset upon request. The entire PANSY team is acknowledged for making their end product data publicly available. Mike Taylor's TOPCAT[5] was used for some data processing and for generating the figure.

References

Greaves J. (2026). "Independent confirmation of meteor shower candidates from the Southern Argentine Agile Meteor Radar". *eMetN Meteor Journal*, **11**, 151–153.

Jopek T. J. (1993). "Remarks on the meteor orbital similarity D-criterion". *Icarus*, **106**, 603–607.

Pokorný P., Janches D., Brown P. G., Hormaechea J. L. (2017). "An orbital meteoroid stream survey using the Southern Argentina Agile MEteor Radar (SAAMER) based on a wavelet approach". *Icarus*, **290**, 162–182.

Vierinen J., Chau J. L., Nishimura K., Hashimoto T., Pfeffer N., Kastinen D., Huyghebaert D. R., Kero J., Tsutsumi M., Sato K. (2026). "The PANSY Meteor Head-echo Orbit Catalogue: Continuous Antarctic Radar Observations of Southern Meteoroid Streams". https://arxiv.org/abs/2608.17589v1

[5] https://www.star.bris.ac.uk/~mbt/topcat

Sporadic meteors Part I
Differences in how sporadic meteors are observed

Masahiro Koseki

The Nippon Meteor Society, 4-3-5 Annaka Annaka-shi, Gunma-ken, 379-0116 Japan
geh04301@nifty.ne.jp

Sporadic meteors are defined as those remaining after meteors belonging to recognized showers have been identified; however, the specific showers detected vary depending on the observation equipment and the classification methods employed. In this study, we utilized sporadic meteors observed by the Global Meteor Network (GMN) (Vida et al., 2019, 2020, 2021). In Part 1 of this paper, we investigated how meteors classified as sporadic by the GMN differ from those identified in other observational datasets, particularly those from the SonotaCo network (Sonota Co, 2009, 2016, 2017). GMN and SonotaCo network differ in their observation equipment and meteor detection methods, and there are also significant discrepancies in the definitions of meteor showers themselves. By comparing the radiant distributions of meteors classified as sporadic by GMN and SonotaCo network respectively, we examined the differences between the two networks regarding the meteors observed and the definitions of meteor showers. While differences attributable to observational equipment and detection methods were observed, the results highlighted that the GMN employs a distinct definition for meteor showers—specifically, setting a longer duration of activity and a smaller radiant spread. However, the distributions of geocentric velocities based on elongation from the Earth-apex were found to be very similar; thus, it was confirmed that GMN observations are suitable for use as video-based sporadic meteor data in the subsequent parts of this study. Part 2 will address the physical characteristics of sporadic meteors, while Part 3 will examine the relationship between sporadic meteors and meteor showers.

1 Introduction

This paper examines sporadic meteors using video observations, for which data is publicly available and abundant. However, sporadic meteors generally refer to those remaining after excluding meteors belonging to meteor showers. Therefore, the composition of sporadic meteors varies depending on what meteors are observed and how meteor showers are excluded. The types of meteors that can be detected differ greatly depending on the observation method, and how meteor showers are defined also varies considerably among researchers. First, we will examine how the appearance of meteor showers differs depending on the observation method and definition, and consequently, how the content of sporadic meteors differs. Through this work, it is first necessary to clarify the nature of sporadic meteors observed via video.

2 Differences in techniques and definitions

2.1 Differences in meteors observed by different observational techniques

The range of geocentric velocities of meteors that are most frequently detected varies depending on the observation method. While we have mentioned this on several occasions (Koseki, 2015), let us reiterate it here. What all observation methods have in common is that there are two peaks in the meteor velocity range, with the dividing line being around 45–50 km/s. However, there are significant differences in which each peak is dominant and to what extent, with photographic observations (*Figure 1*) and video observations (*Figure 2*) being at opposite extremes. Both of the figures shown here are normalized so that the total number of meteors is 10000.

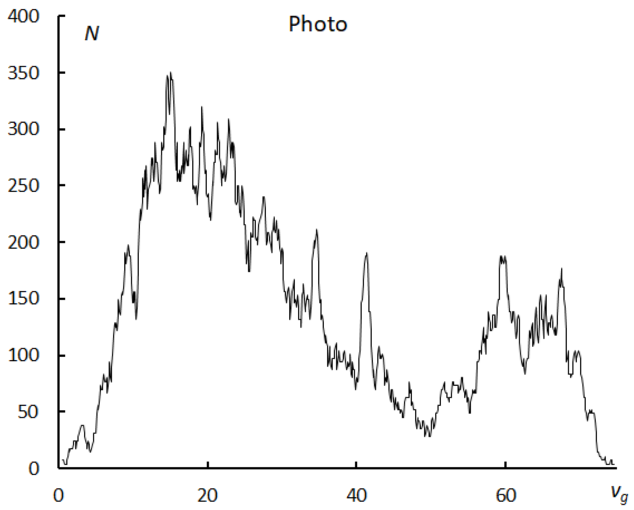

Figure 1 – Geocentric velocity distribution of photographically observed meteors, including data from Super-Schmidt cameras and small cameras used in the former Soviet Union (4451 orbits, *Table 6* of Koseki, 2009). A peak is observed in geocentric velocity at 10–20 km/s. The graph is normalized with a total count of 10000.

These differences arise from a combination of factors, even in optical observations, including the aperture and focal length of the lens used, the sensitivity of the light-receiving unit, the wavelength range in which sensitivity is maximized, and the method used to detect meteor images. In the case of radar observations, there are also complex factors such as the wavelength range used, power output, receiving sensitivity, and the relative positions of the transmission and reception points.

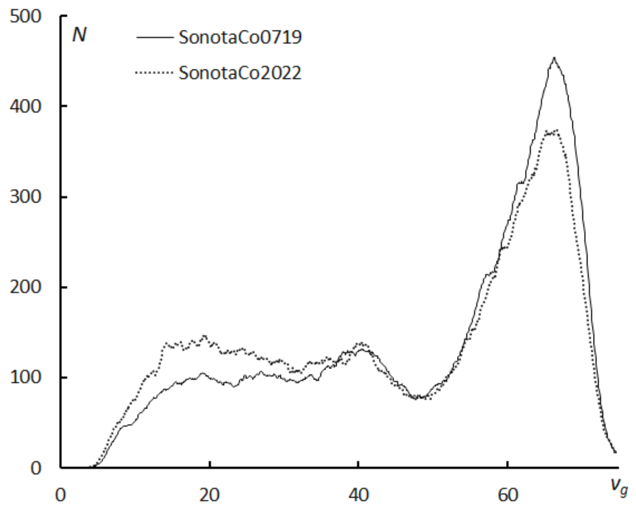

Figure 2 – Geocentric velocity distribution based on video observations by the SonotaCo network. The difference between the two graphs will be explained in the next section, but both have a peak in geocentric velocity at 60–70 km/s, and the peak observed in photographic observations is not clear. The graph is normalized with a total count of 10000.

2.2 Differences in meteor showers detected by different definitions

Meteor showers are detected based on the similarity of orbital elements or on radiant points and geocentric velocities. In either case, a threshold is established to distinguish between shower meteors and sporadic meteors; consequently, a slight difference can result in one meteor being classified as part of a shower while another is deemed sporadic. Since this threshold is not self-evident but is instead determined by a researcher's experience, judgments regarding whether a meteor belongs to a shower or is sporadic may differ among researchers, even when the same data is used.

As discussed later, the spread of the radiant varies according to the angular distance from the "Earth's apex" (the direction of Earth's motion)—hereinafter referred to simply as "elongation" or *εA* (Koseki, 2025). Therefore, even for meteor showers with the same orbital spread, the radiant appears more diffuse when this elongation is large. Consequently, for slow-moving meteors with large elongation angles, a meteor that would be classified as sporadic if identified using the radiant point might instead be broadly classified as belonging to a meteor shower when determined based on orbital elements. Conversely, for meteors with small angular distances and high speeds, errors in velocity determination tend to be significant; in such cases, many meteors belonging to a shower may be misclassified as sporadic. We will now examine in concrete terms how such differences in interpretation regarding meteor showers arise depending on the definition used.

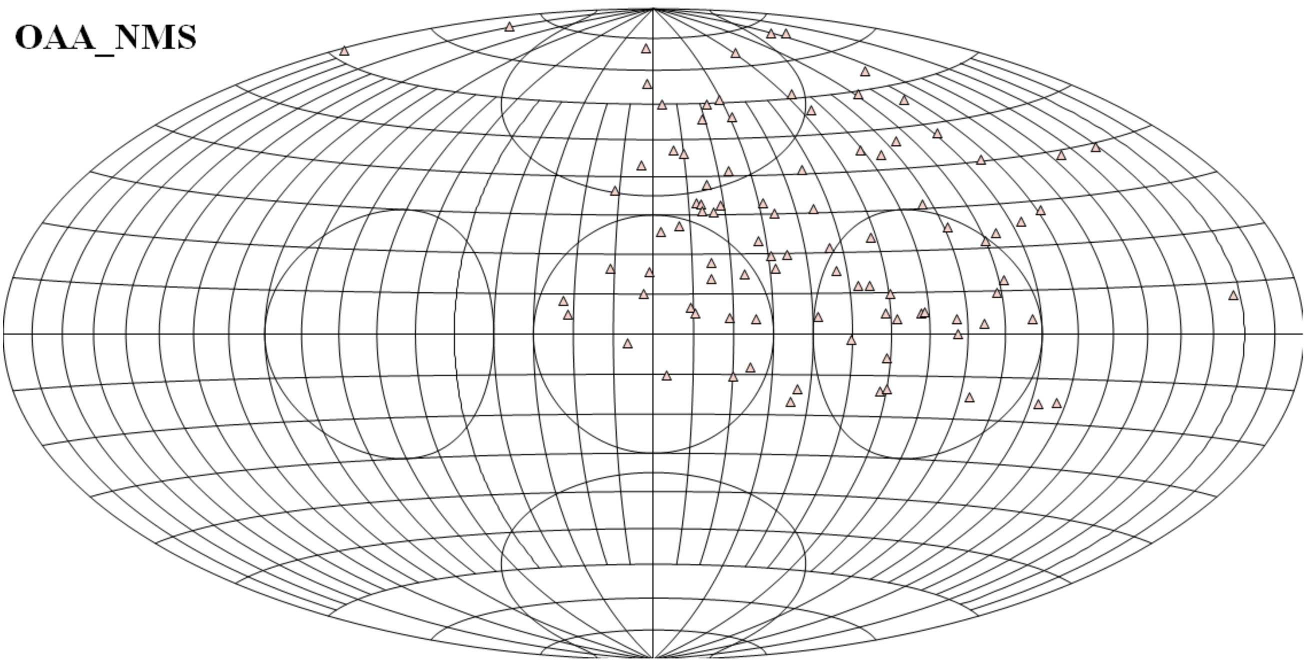

Figure 3 (OAA_NMS): This is a compilation by the author of radiant points obtained through visual observation in Japan between the 1928 and the 1969 (Koseki, 1979).

2.2.1 Differences in radiant point distribution depending on optical observations

First, we compare the radiant point distribution obtained from three different types of optical observations. *Figure 3* shows the radiant points compiled by the author based on visual observations in Japan from the 1920s to the 1960s (Koseki, 1979). In Japan, observation methods heavily influenced by the AMS led by Olivier were adopted, and the objective was often to determine the location of the radiant point of known or under-investigation meteor showers. At the time, many observations were conducted targeting activities such as #0061TAH and #0170JBO, which were attracting attention. As a result, radiant points were detected in regions quite far from the Earth's apex. However, since the number of meteors that can be detected by an individual is limited, it is not particularly strong in terms of detecting minor or new meteor showers.

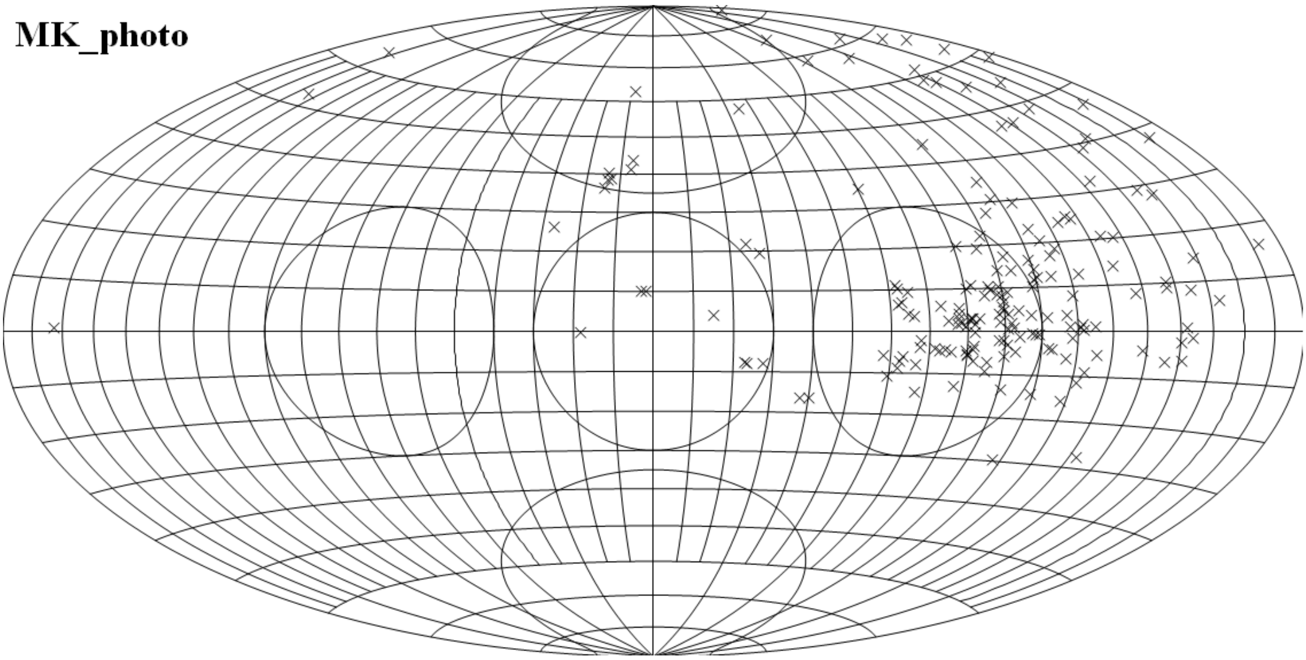

Figure 4 – (MK_photo): This figure shows the results of cluster analysis performed by the author (Koseki, 1982) on photographic observation data using the Southworth-Hawkins D-criterion (Southworth and Hawkins, 1963).

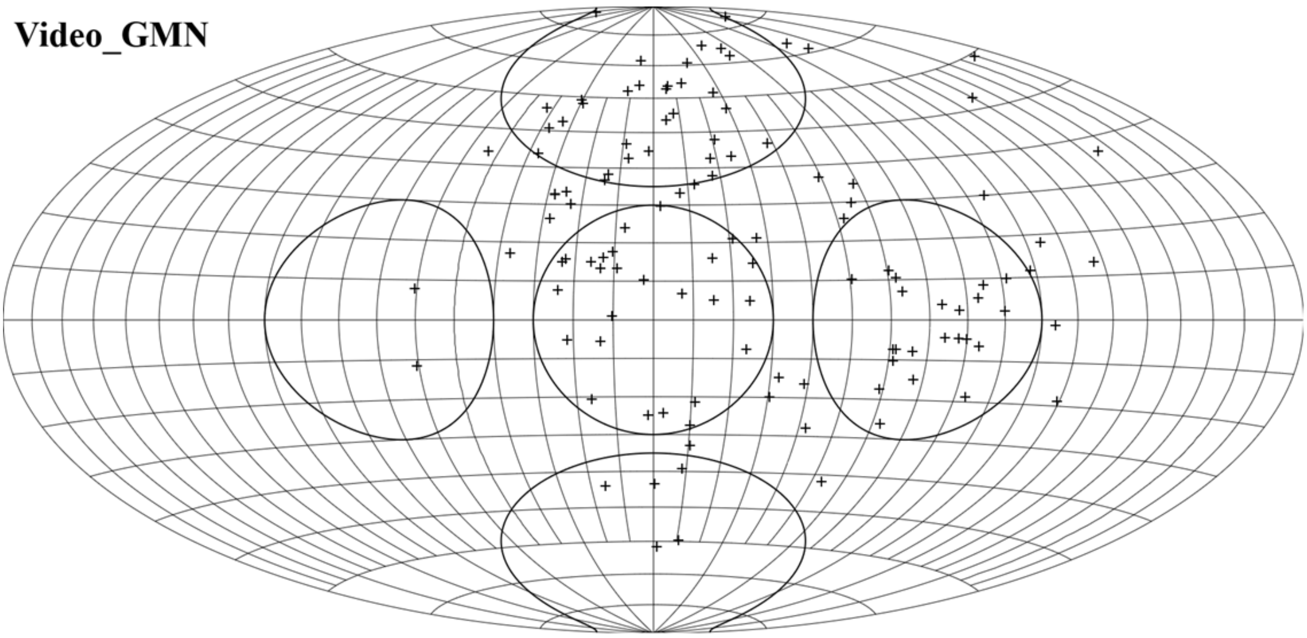

Figure 5 – (Video_GMN): This figure presents the activity confirmed by the author using GMN video observations, verifying the IAU-MDC SD meteor shower list[6]. The analysis is based on the radiant point location and geocentric velocity (Koseki, 2024).

[6] https://www.ta3.sk/IAUC22DB/MDC2022/

Figure 4 shows meteor showers obtained from photographic observations using a Super-Schmidt camera and small cameras from the former Soviet Union, compiled by the author (Koseki, 1982) using the Southworth-Hawkins D-criterion (Southworth and Hawkins, 1963). Due to the use of orbital element similarity and the characteristic of photographic observations to capture many slow-moving meteors, many meteor showers closer to the Earth's dorsal point (antapex) are being detected, not just those from the ANT source.

Figure 5 shows the results (Koseki, 2024a) obtained when verifying the meteor showers listed in the IAUMDC SD using video observations from GMN determination is based on the density distribution of radiant points (Koseki, 2023), and the resulting distribution of radiant points is closer to visual observation than that determined by orbital similarity using photographic observations, as shown in *Figure 4*.

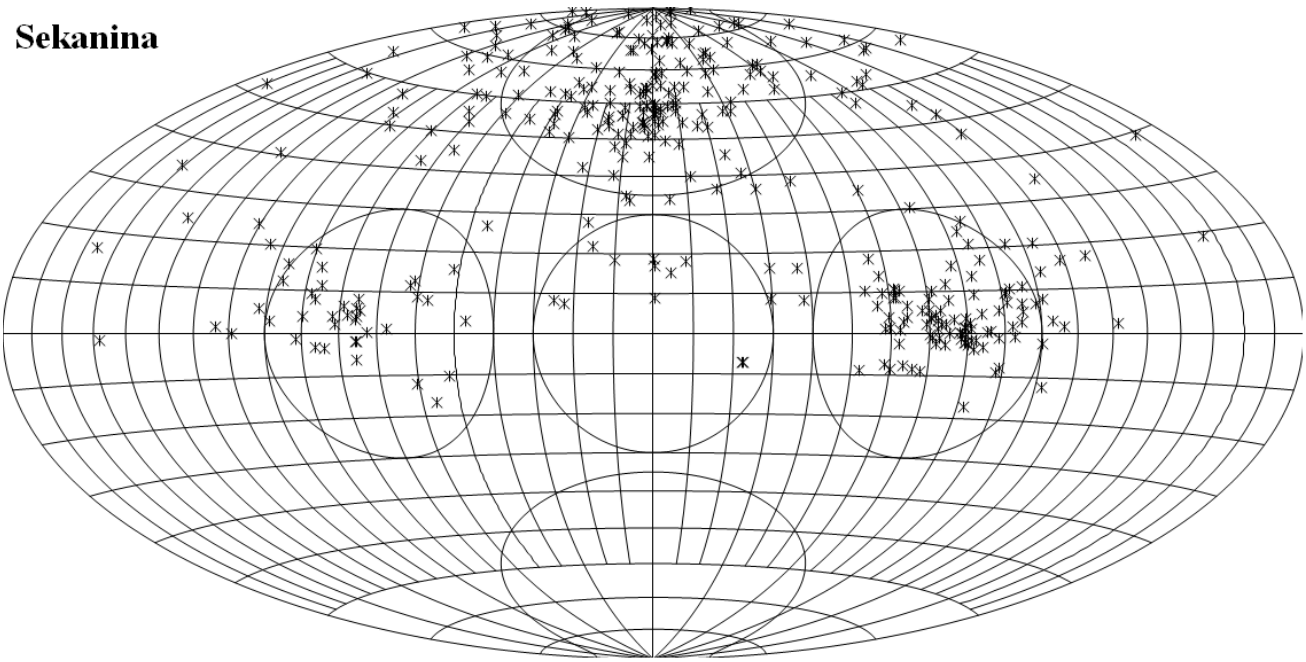

Figure 6 – This shows the radiant points of meteor showers that Sekanina determined to have a higher orbital density than its surroundings (Sekanina, 1970; 1973; 1976), based on two Harvard radio observations conducted in 1961–1965 and 1968–1969, using the Southworth-Hawkins D-criterion (Southworth and Hawkins, 1963).

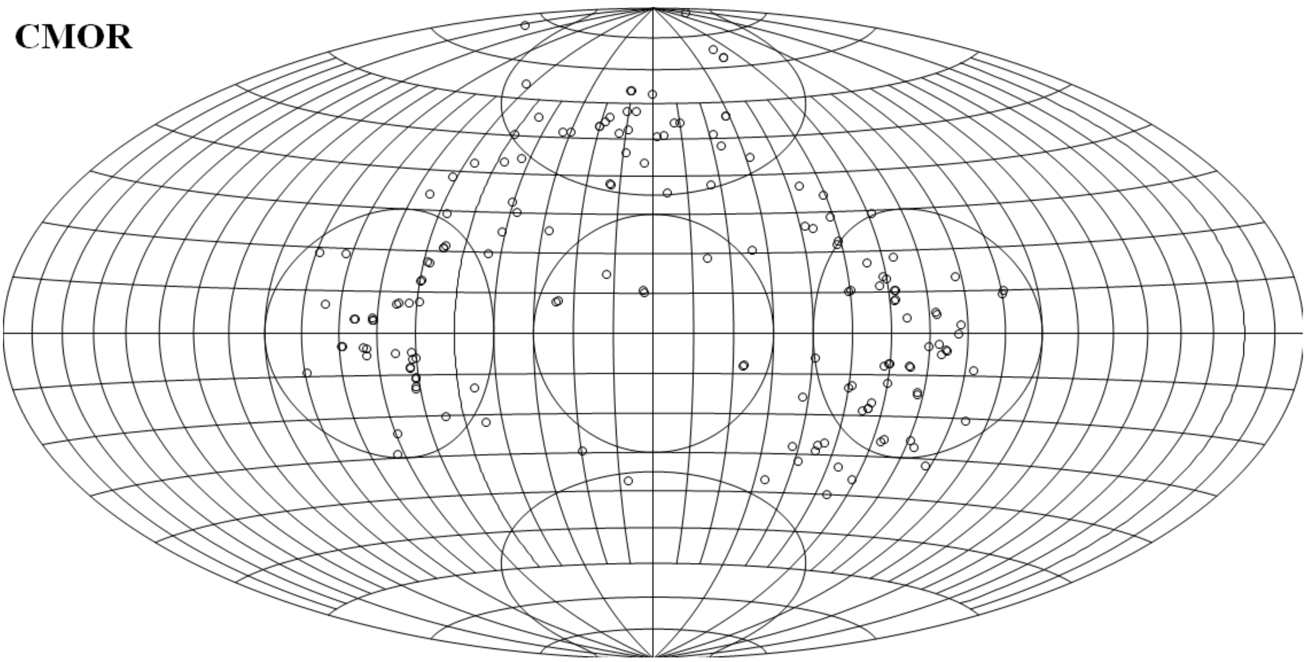

Figure 7 – These meteor showers were detected using the wavelet method based on the distribution density of radiant points and geocentric velocities obtained from CMOR radar observations from 2002 to 2008 (Brown et al., 2008; 2010).

Visual observation captures the faintest meteors, followed closely by video observation, whereas photographic observation primarily captures bright meteors of magnitude 0 or brighter. Additionally, photographic observation mainly records slow-moving meteors, while video and visual observations focus on meteors with medium to high speeds (*Figures 1 and 2*). While these characteristics result in differences in the detected meteor showers, *Figure 4* reveals a significant feature: a large number of meteor showers are detected not only near the Anti-helion (ANT) but also in the region even closer to the Antapex. The effect of differences in heliocentric velocity (differences in orbital elements) on the dispersion of the radiant varies depending on the elongation (εA) from the Earth's apex (Koseki, 2025). A comparison of *Figure 4* with *Figures 3 and 5* reveals that when the same criteria are applied to meteor showers with different angular separations, significant differences in the results arise regardless of whether orbital elements or the spread of the radiant are used as the basis for determination.

2.2.2 Differences in radiant point distribution depending on radar observations

Next, regarding radar observations, we will compare two radiant point distributions that use different methods for determining meteor showers. *Figures 6 and 7* are both maps showing the distribution of radiants based on radar observations. *Figure 6* shows the distribution identified by Sekanina based on the similarity of orbital elements (Sekinina, 1970; 1973; 1976), while *Figure 7* shows the distribution identified by Brown et al. based on radiants and geocentric velocities (Brown et al., 2008, 2010). Radar observations are characterized by the ability to detect a large number of slow-moving meteors, a trait clearly evident when comparing the results with *Figure 5*. Furthermore, a comparison of *Figures 6 and 7* reveals differences arising from the criteria used to identify meteor showers.

Figure 6 shows a concentration of radiant point densities at ANT, Toroidal, and Helion sources, while *Figure 7* shows a ring-shaped distribution connecting these three. Although there are differences in equipment between the two, this difference in distribution is thought to be due to differences in the meteor shower determination methods mainly.

3 Video observations

3.1 Points to consider when using video observations for sporadic meteor research

First, as demonstrated by the comparison between *Figures 1 and 2*, although video observation is a form of optical observation, the velocity distribution of the meteors it captures differs from that of photographic observation. Furthermore, while the brightness of meteors captured via video observation centers around magnitude 0, allowing for the detection of fainter meteors than photographic methods, meteors fainter than magnitude +6 (the primary target range for radio observation) fall outside its scope. While both photographic and radio observations capture many slow-moving meteors, there are significant differences in the distribution of meteor shower radiants; similarly, the method used to identify meteor showers has a major impact on the extraction of sporadic meteors. However, there have been few attempts to detect meteor showers in video observations by applying orbital similarity. Jenniskens (2023), GMN (2019, 2020, 2021), and SonotaCo network (SonotaCo, 2009, 2016, 2017) all use the radiant and geocentric velocity as criteria. SonotaCo et al. (2021) have attempted to detect meteor showers by analyzing the similarity of orbital elements over short time intervals; however, as discussed later, the results do not differ significantly from those obtained using the similarity of radiants and geocentric velocities as criteria. However, in conjunction with this, the settings for meteor showers on SonotaCo network have been modified starting in 2021; consequently, the criteria for classifying "sporadic meteors" have also changed. The data used in this article contains a mixture of classifications based on these differing criteria, and the issues arising from this will be discussed in detail later. With an understanding of these characteristics of video observation, the following section compares observations from the SonotaCo network and GMN to examine the nature of sporadic meteors in video observations.

3.2 SonotaCo network and GMN

SonotaCo network and GMN are two groups that continue to observe meteors via video and also publish their data. This paper uses GMN data, but even though both are video observations, there are differences between SonotaCo network and GMN data. It is important to clarify the differences between the two in order to define what GMN refers to as sporadic meteors.

3.2.1 Differences in observational conditions

Video observations show that both SonotaCo network and GMN primarily feature high-speed meteors. However, GMN has a higher proportion of slower meteors than SonotaCo network. *Figure 8* shows that GMN exhibits two maxima, one at 10–20 km/s and the other at 60–70 km/s, while the former maximum is unclear in the case of the SonotaCo network. As will be discussed later, this is thought to be due to differences in the equipment used by the two systems. *Figure 9* shows the relationship between geocentric velocity and the average magnitudes of captured meteors. It is clear that for slower meteors, the GMN captures fainter meteors than the SonotaCo network. This is also thought to be due to differences in the equipment used by the two groups.

However, measuring the brightness of meteors presents a challenge, and there are systematic differences in magnitude between SonotaCo network and GMN. The difference in the maximum magnitude between SonotaCo network and GMN in *Figure 10* indicates, as mentioned earlier, that GMN is better able to capture fainter meteors at lower speeds than SonotaCo network. Furthermore, the GMN has a narrower distribution. This is clearly evident in the magnitude distribution shown in *Figure 11*. The GMN magnitude distribution fits perfectly within that of the SonotaCo network. Thus, the luminosity scale differs between GMN and SonotaCo network. While this poses a significant problem when determining magnitude ratios, we will only point out here that the luminosity scales for SonotaCo network and GMN are different.

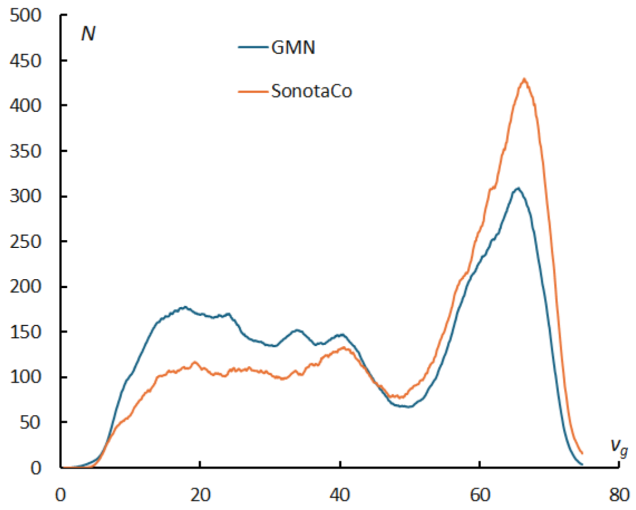

Figure 8 – Distribution of geocentric velocity normalized to 10000 sporadic meteors observed by GMN from 2018 to 2023 and by SonotaCo network from 2007 to 2022. The determination of “sporadic meteors” is based on data from GMN and SonotaCo network.

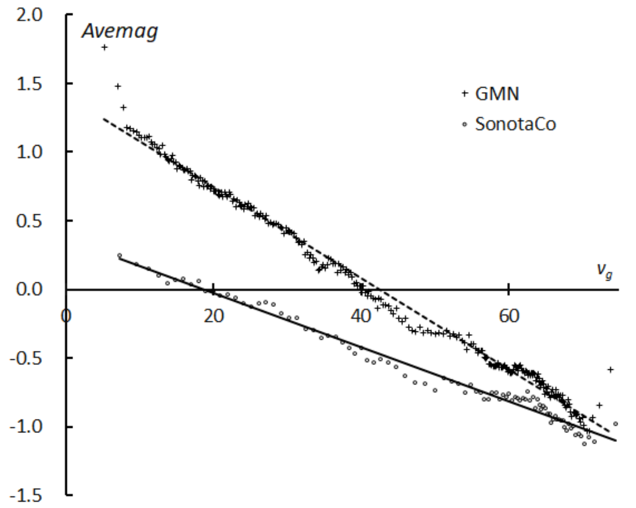

Figure 9 – Relationship between geocentric velocity and average magnitude of sporadic meteors observed by GMN from 2018 to 2023 and by SonotaCo network from 2007 to 2022. The classification of “sporadic meteors” is based on data from GMN and SonotaCo network.

Now, let’s look back at *Figure 2* and compare the meteor detection rate against geocentric velocity for both SonotaCo network’s data from 2007–2019 and 2020–2022. Observations from SonotaCo network between 2020 and 2022 also show that, similar to the GMN case, the proportion of high-speed meteors decreased while the proportion of low-speed meteors increased. This trend aligns with the increased use of lenses with longer focal lengths within the SonotaCo network during this period.

Figure 12 shows the annual variation in meteors classified as sporadic meteors by SonotaCo network and GMN. Japan has two rainy seasons, the rainy season in June (Tsuyu) and in September (Akisame). During these periods, the number of meteors reported by GMN is higher than that reported by

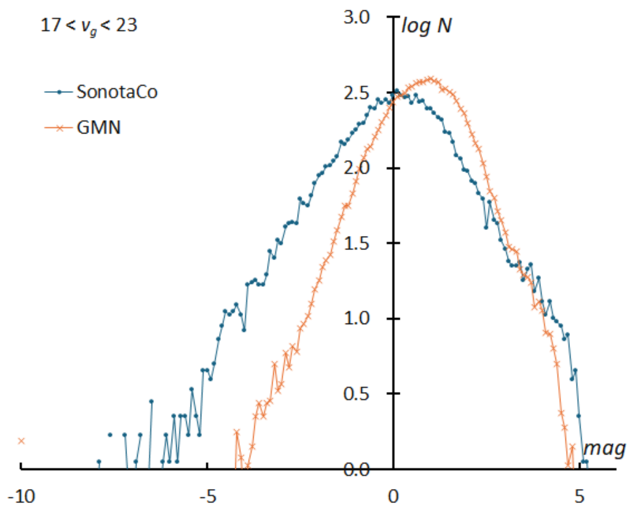

Figure 10 – This figure compares the magnitude distribution of sporadic meteors with a geocentric velocity of $17 < v_g < 23$ (km/s), i.e., an average of 20 (km/s), using SonotaCo network and GMN, normalized to a total of 10000 meteors. (Koseki, 2025).

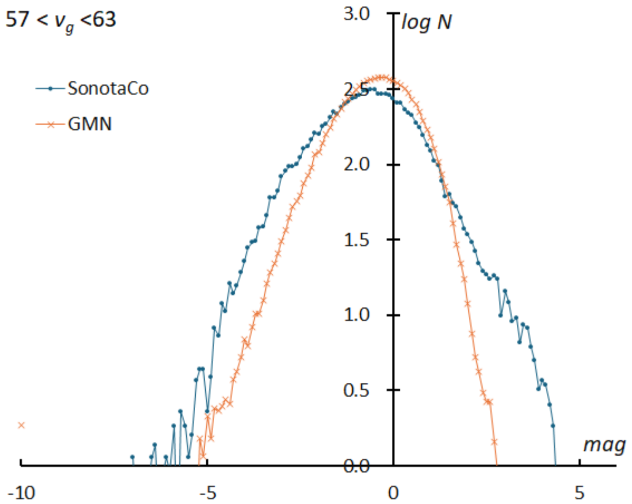

Figure 11 – This figure compares the magnitude distribution of sporadic meteors with a geocentric velocity of $57 < v_g < 63$ (km/s), i.e., an average of 60 (km/s), using SonotaCo network and GMN, normalized to a total of 10000 meteors. (Koseki, 2025).

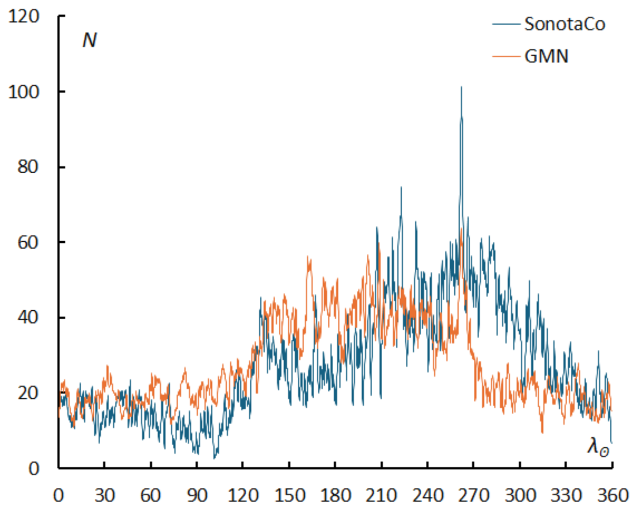

Figure 12 – This figure shows the number of sporadic meteors per degree of solar longitude, normalized to a total of 10000 observed meteors. A moving average of 0.1 degrees solar longitude is used.

SonotaCo network, while in winter, SonotaCo network surpasses GMN. This is due to differences in weather patterns between Japan and Europe, suggesting that meteorological conditions affect the observation of both meteor showers and sporadic meteors. Furthermore, the number of meteors observed during major meteor showers such as the Perseid and the Geminid meteor showers have also increased. This suggests that the number of observations is not constant throughout the year, and that the data is biased.

3.2.2 Differences in criterion on meteor shower definition

There are considerable differences between GMN and SonotaCo network regarding the criteria for determining meteor showers. Firstly, there are differences in the scope of what is recognized as a meteor shower. A typical example is the Taurid meteor shower, which GMN subdivides into multiple components, whereas the SonotaCo network considers them together into just two showers, the Northern and Southern Taurids. The second difference lies in which of the multiple reports published in the IAU-MDC SD is adopted regarding the location of the radiation point. The third difference lies in how far the radiant point's spread extends and where the boundary between it and sporadic meteors is set. This is not included in the IAU-MDC SD, so there are significant differences between the two. The fourth difference lies in the amount of the radiant shift and the coordinate system used to represent it. GMN uses the ecliptic coordinate system, while SonotaCo network uses the equatorial coordinate system. The fifth factor is the activity period of meteor showers, and there are considerable differences between GMN and SonotaCo network regarding this as well. For more information on these differences, please refer to the article I wrote for eMetN Meteor Journal (Koseki, 2024c).

3.2.3 Differences in radiant point distributions between GMN and SonotaCo network

As described above, there are considerable differences between GMN and SonotaCo network, even though both involve video observation. We will now specifically compare how these differences affect the radiation point distribution. Distribution maps of meteors identified as sporadic meteors by GMN and SonotaCo network are shown in *Figures 13 to 20* at 45-degree intervals based on solar longitude, centered on (λ–$\lambda_{\odot}$, β) = (270,0). ANT, Helion, Toroidal (north and south), and Apex sources are indicated by circles with a radius of 30 degrees in the figures. The top row shows the radiant point distribution of sporadic meteors according to GMN, the bottom row shows the distribution of radiant points of sporadic meteors according to SonotaCo Network, and the middle row shows the radiant point distribution of what GMN treats as a "meteor shower".

The differences between what GMN and SonotaCo network classify as "sporadic meteors" can be identified by comparing them with the distribution shown in the middle raw. The notes for *Figure 12 (Figure 12*: $0 < \lambda_{\odot} < 45$) explain the phenomenon where the radiant distribution appears as a ring (with a white center) or, conversely, as a solid black area. For the subsequent figures, the explanatory text is omitted in favor of a detailed examination of the differences between the GMN and the SonotaCo network.

Notes on Figure 13 (0° < $\lambda_{\odot}$ < 45°)

In the GMN distribution at the top, the white area slightly above the center is noticeable, and from the meteor shower distribution in the middle, it can be identified as #0648TAL. This is not included in either the J6 or J14 lists from SonotaCo network, and in the SonotaCo network distribution, it does not show any difference in distribution compared to the surrounding areas (Note: J6 is the list of meteor showers used for classification on SonotaCo Net through 2020, while J14 is the list used from 2021 onwards). This means that the meteor identified as #0648TAL by GMN has incorporated many sporadic meteors, resulting in a lower radiant point density compared to the surrounding sporadic meteors. Also, slightly to the upper right of this is #0006LYR, which in GMN shows a slightly lighter center and a dark, ring-shaped area with a higher radiant point density than the surrounding area. This indicates that, contrary to #0648TAL, GMN underestimated the range of the radiant point for #0006LYR and therefore classified the meteors belonging to #0006LYR as "sporadic meteors".

This phenomenon is not noticeable on the SonotaCo network; in fact, it appears that the radiant point density is lower than in the surrounding area, causing some of the sporadic meteors to be classified as #0006LYR. In the GMN figure, there is a slightly dark area to the lower left of #0648TAL; this corresponds to #0031ETA, which appears in the subsequent period of 45° < $\lambda_{\odot}$ < 90°. Even with this, the same phenomenon as #0006LYR is observed in GMN. Conversely, in the SonotaCo network, areas where radiation points are concentrated can be seen around #0021AVB, #0450AED, and #0827NPE. While #0021AVB and #0450AED appear on the SonotaCo network J14 list, #0827NPE is not listed. Neither #0827NPE nor #0450AED is included in the J6 list. Furthermore, the defined activity period for #0021AVB is shorter in both the J6 and J14 lists compared to the GMN list. As previously mentioned, we used a mixture of SonotaCo network data—specifically, data classified using the J6 list for the years 2007–2020 and the J14 list for 2021–2022, which resulted in the discrepancy with GMN.

Notes on Figure 14 (45° < $\lambda_{\odot}$ < 90°)

There is a region with a high density of radiation points that extends from #0031ETA, as if moving towards #0372PPS, which appears in the next period 90° < $\lambda_{\odot}$ < 135°. The radiant point movement of "PPS" seems to be water flowing from the water bottle to the fishes. In Greek mythology, the water flows from Aquarius to Pisces Austrinus, but in this case, it flows from Aquarius to Pisces. We illustrated this in the eMetNews paper as follows: it can also be compared to water flowing from an aquarium to fishes, Koseki, 2024b. This could be described as the "droppings" of η-Aquariids corresponding to the tail of Orionids. Whether or not to classify such a region as a "meteor shower" is a matter of differing opinions among researchers.

Notes on Figure 15 (90° < λ⊙ < 135°)

In the GMN distribution, ring-shaped black areas are noticeable around #0001CAP, #0005SDA, and #0007PER. In the SonotaCo network, a black ring-shaped area is also seen around #0007PER, but the rings are wider than in the GMN network, indicating that the radiation point spread is set to be larger in the SonotaCo network. The SonotaCo network figure shows a distribution of radiant points around #0175JPE and #0444ZCS. This is because the J6 list previously used by the SonotaCo network for meteor shower determination had a problem with the value of #0175JPE and #0444ZCS was not listed. As previously mentioned, we are using SonotaCo network data that combines classifications based on the J6 list (for 2007–2020) and the J14 list (for 2021–2022). Consequently, for #0175JPE and #0444ZCS, some of these radiants appear in the radiant distribution of sporadic meteors due to the older classification criteria.

Notes on Figure 16 (135° < λ⊙ < 180°)

Following the previous period (*Figure 14*: 90° < $\lambda_{\odot}$ < 135°), both GMN and SonotaCo network show ring-shaped black areas around #0005SDA and #0007PER. Furthermore, the radiant density appears to be high at the location of #0206AUR in both the GMN and SonotaCo network. While #0206AUR is well known for its outburst activity, its activity period seems to have a longer baseline than indicated in each setting (Koseki, 2024c, *Figure 102*). The activity known as the "tail of the Orionids" appears to begin with #0191ERI, but GMN and SonotaCo network differ in how they interpret the activity leading up to the main Orionids. The radiant distribution differs significantly between GMN and SonotaCo networks around #0337NUE and #0552PSO. #0210BAU and #0693ANP are not included in SonotaCo network's J14 list, and these areas are shown as blank in GMN's radiation point distribution. In GMN, the area around #0026NDA is also outlined in white, which differs from the radiation point distribution of the SonotaCo network, and this requires attention for a different reason. The SonotaCo network uses the name #0342BPI, which it proposed for this activity, while the NDA name is used for a different meteor shower activity. Originally, the name NDA was given to the meteor shower activity from the end of July to August, so the name BPI would be more appropriate.

Notes on Figure 17 (180° < λ⊙ < 225°)

Both GMN and SonotaCo network indicate that there is a region with a high density of radiants around the Orionids. Following the previous period (*Figure 15*: 135° < $\lambda_{\odot}$ < 180°), this is because the two groups differ in how they handle the activity known as "the tail of Orionids". GMN subdivides both categories according to Jenniskens' approach, as published in IAU-MDC SD.

The next areas of note are the vicinities of #0002STA and #0017NTA. Following the approach proposed by Jenniskens in the IAU-MDC SD, the GMN subdivides both of these groups. In contrast, the SonotaCo network treats each as a single, unified entity; this difference leads to a significant disparity in the observed distribution of radiant point densities associated with the Taurid complex.

Differences are also observed around #0388CTA between the two networks; GMN shows it as blank, while SonotaCo network retains areas with high radiant density. This is likely because #0388CTA is not listed in the latter J6 list, and the period of activity is set to a shorter duration in the J14 list. This is also thought to be because the latter J6 list has set a shorter activity period for #0023EGE. #0386OBC is shown as blank in GMN, but its density is the same as the surrounding area in the SonotaCo network. This difference arises because neither the J6 nor the J14 list includes #0386OBC. The black areas visible in the SonotaCo network for #0445KUM may be that it is not listed in the J6 list, and the setting for the radiant shift in the J14 list is excessively large. In #0593TOL, black areas remain in both GMN and SonotaCo network. This shower does not appear on the SonotaCo network's J6 list, and the defined period of activity on the J14 list is extremely short. Furthermore, as there are many uncertainties regarding this shower, both GMN and SonotaCo network treat the radiant shift as virtually zero.

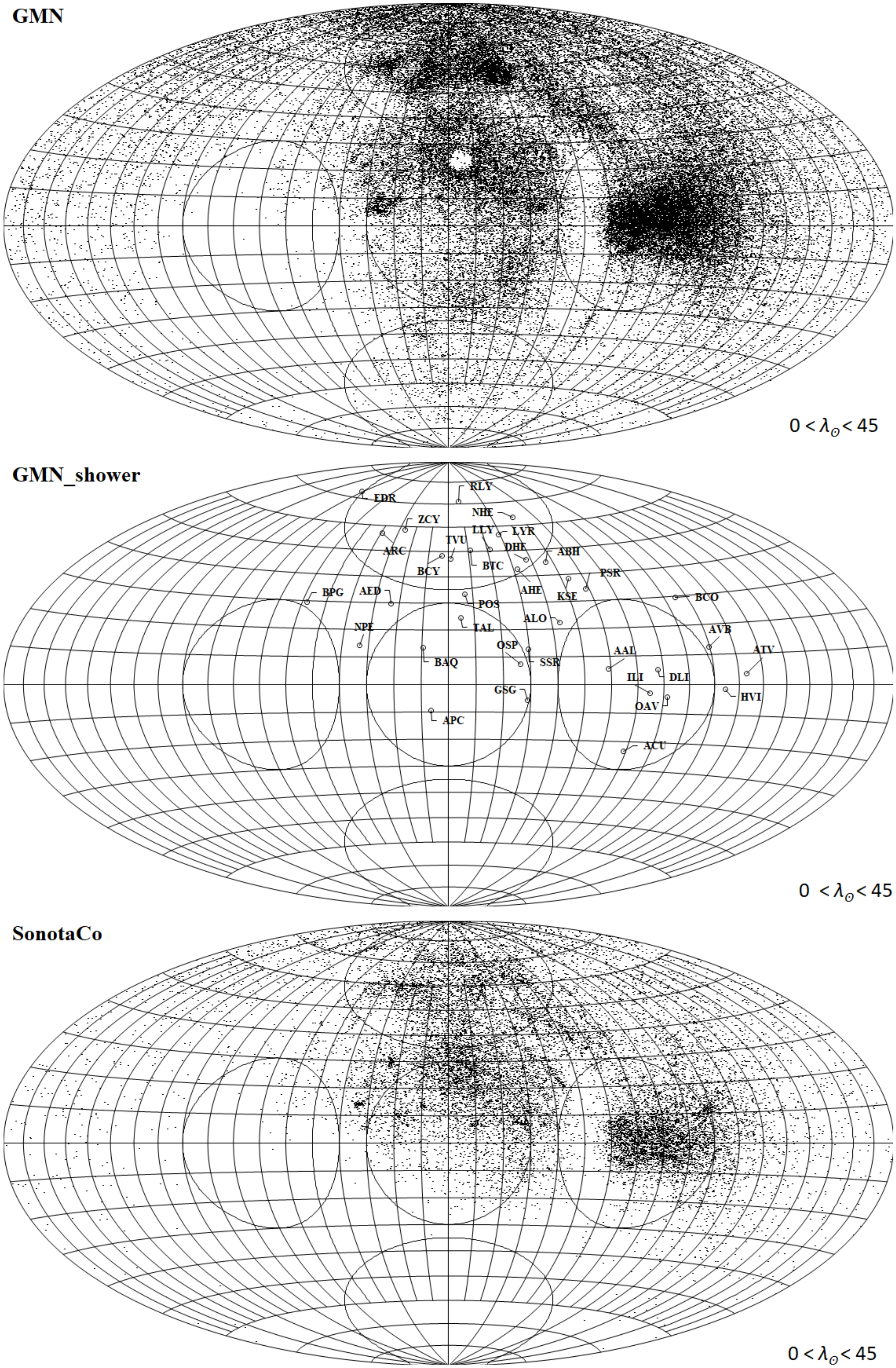

Figure 13 – Radiant point distribution of sporadic meteors identified as such when $0° < \lambda_{\odot} < 45°$. The top row shows sporadic meteors from GMN, the middle row shows those treated as "meteor showers" in GMN, and the bottom row shows sporadic meteors from SonotaCo network.

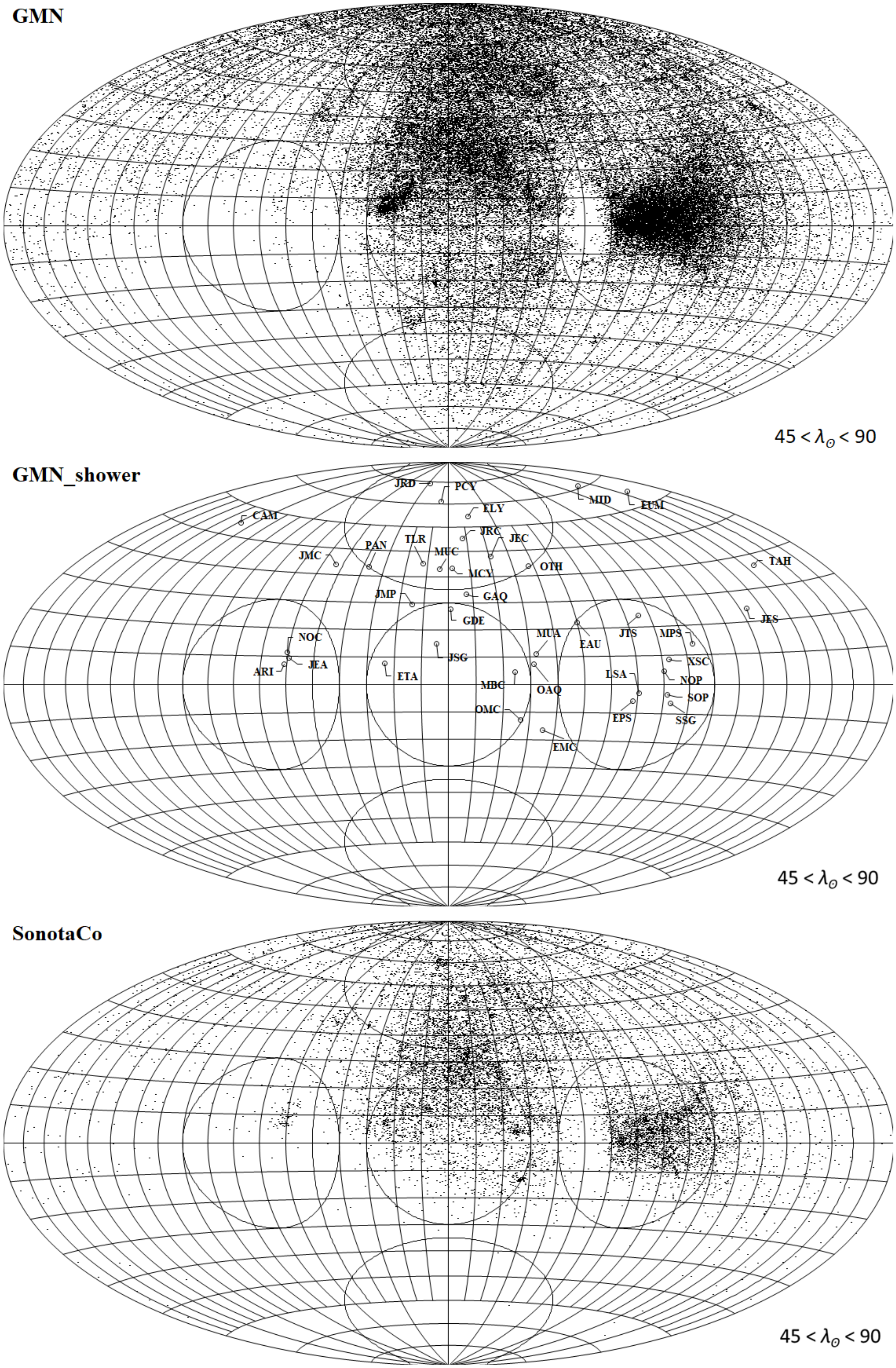

Figure 14 – Radiant point distribution of sporadic meteors identified as such when 45° < λ_{Θ} < 90°. The top row shows sporadic meteors from GMN, the middle row shows those treated as "meteor showers" in GMN, and the bottom row shows sporadic meteors from SonotaCo network.

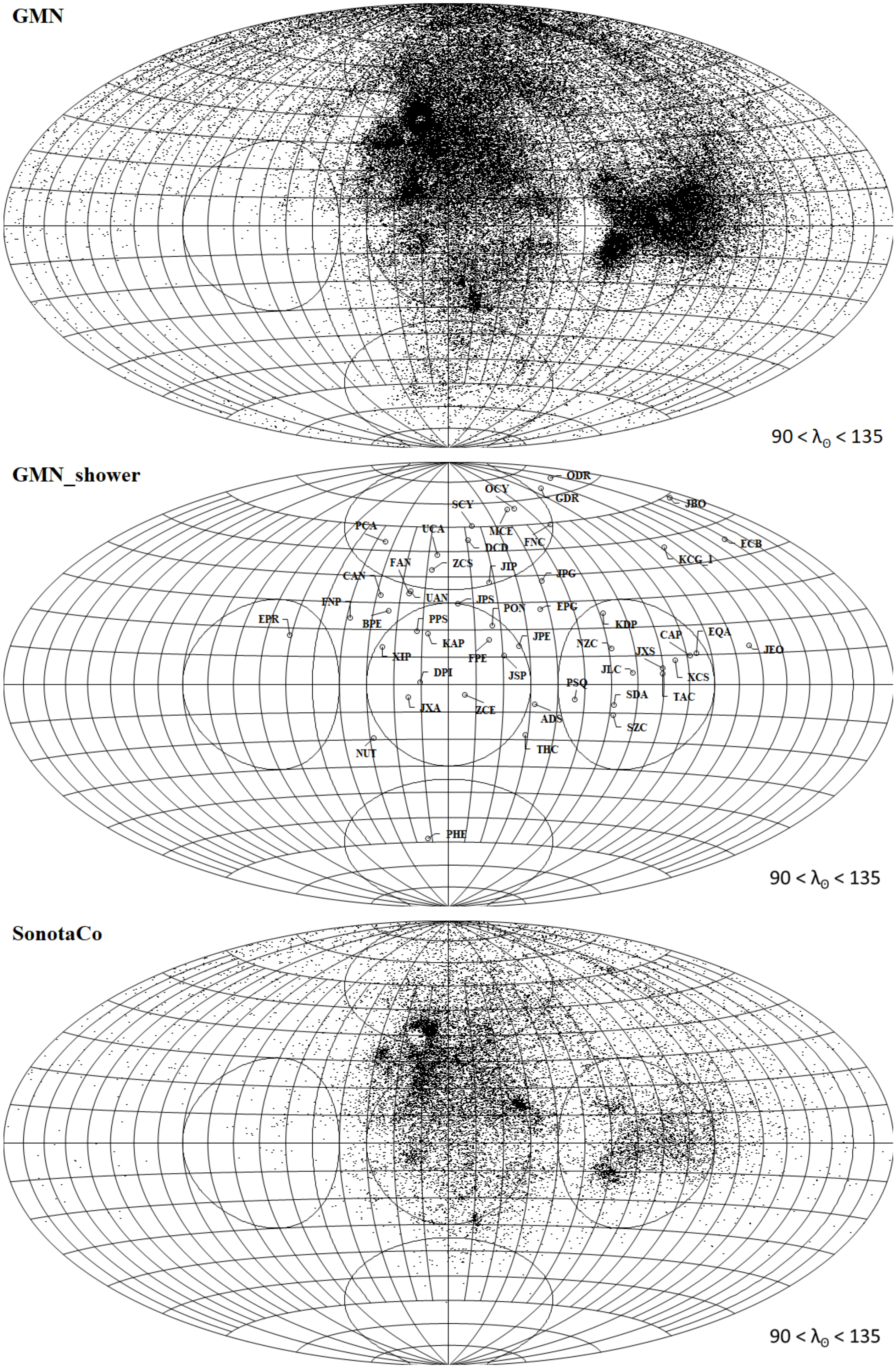

Figure 15 – Radiant point distribution of sporadic meteors identified as such when $90° < \lambda_{\odot} < 135°$. The top row shows sporadic meteors from GMN, the middle row shows those treated as "meteor showers" in GMN, and the bottom row shows sporadic meteors from SonotaCo network.

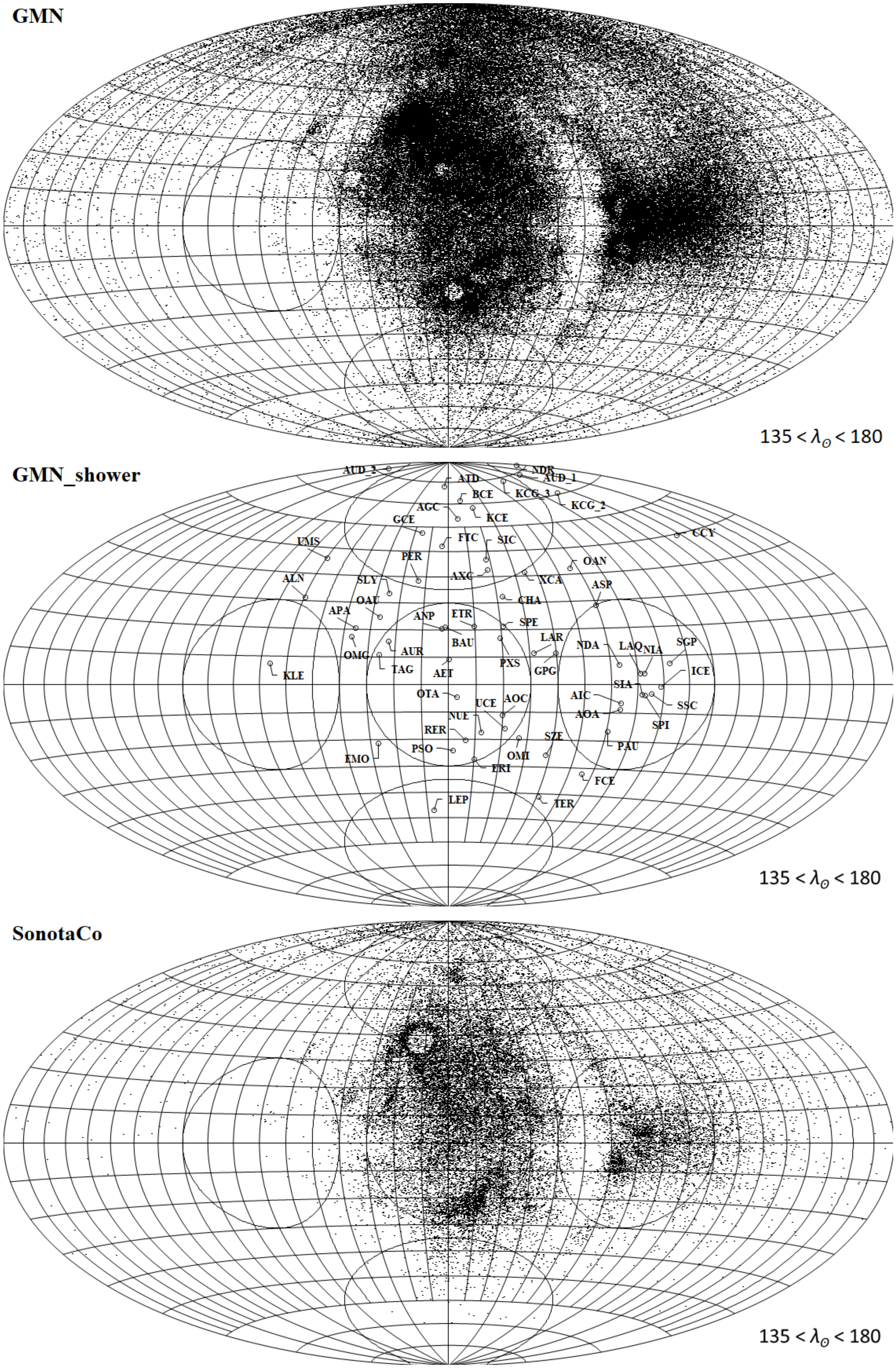

Figure 16 – Radiant point distribution of sporadic meteors identified as such when 135° < λ_O < 180°. The top row shows sporadic meteors from GMN, the middle row shows those treated as “meteor showers” in GMN, and the bottom row shows sporadic meteors from SonotaCo network.

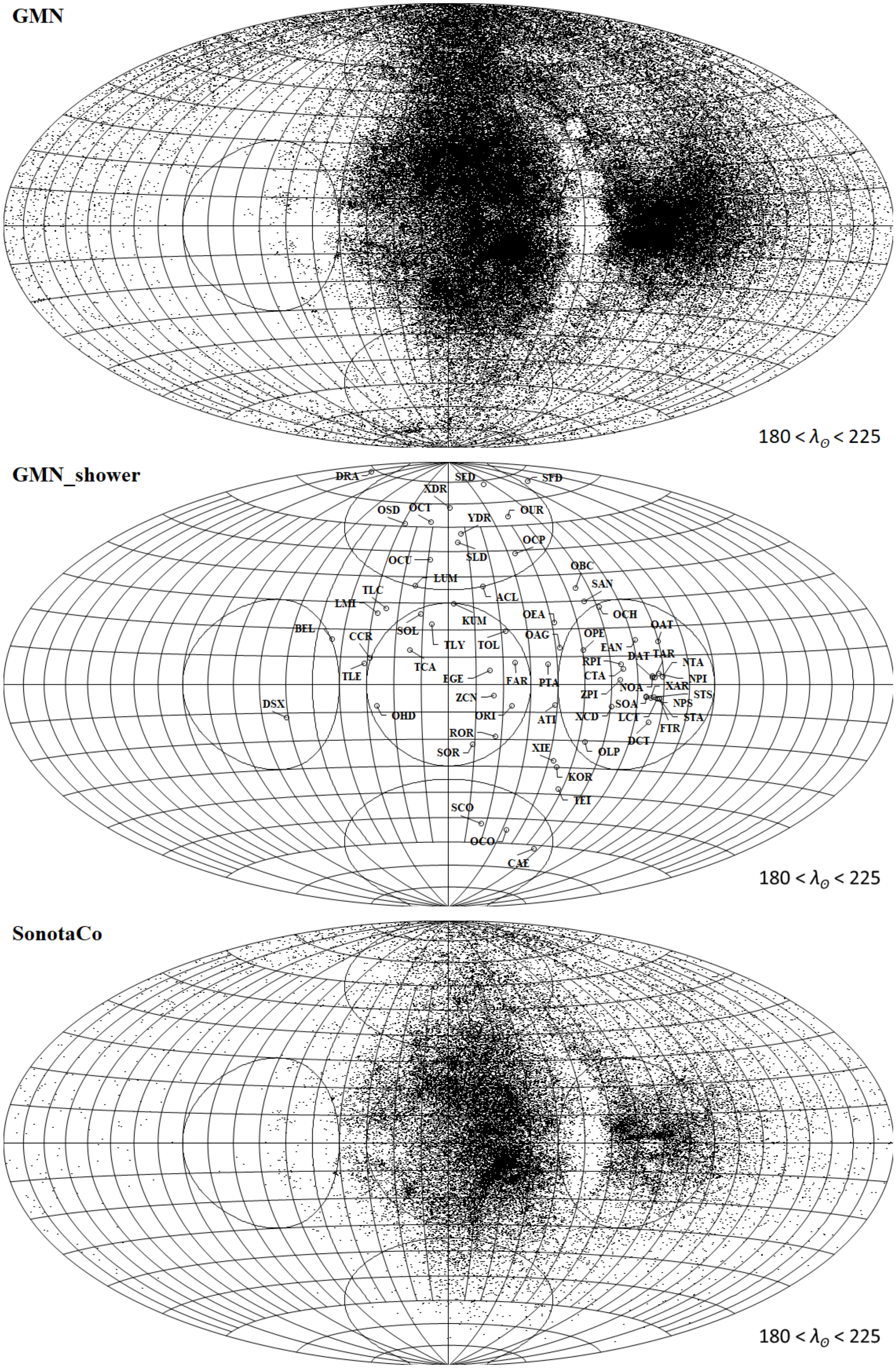

Figure 17 – Radiant point distribution of sporadic meteors identified as such when 180° < $\lambda_\odot$ < 225°. The top row shows sporadic meteors from GMN, the middle row shows those treated as "meteor showers" in GMN, and the bottom row shows sporadic meteors from SonotaCo network.

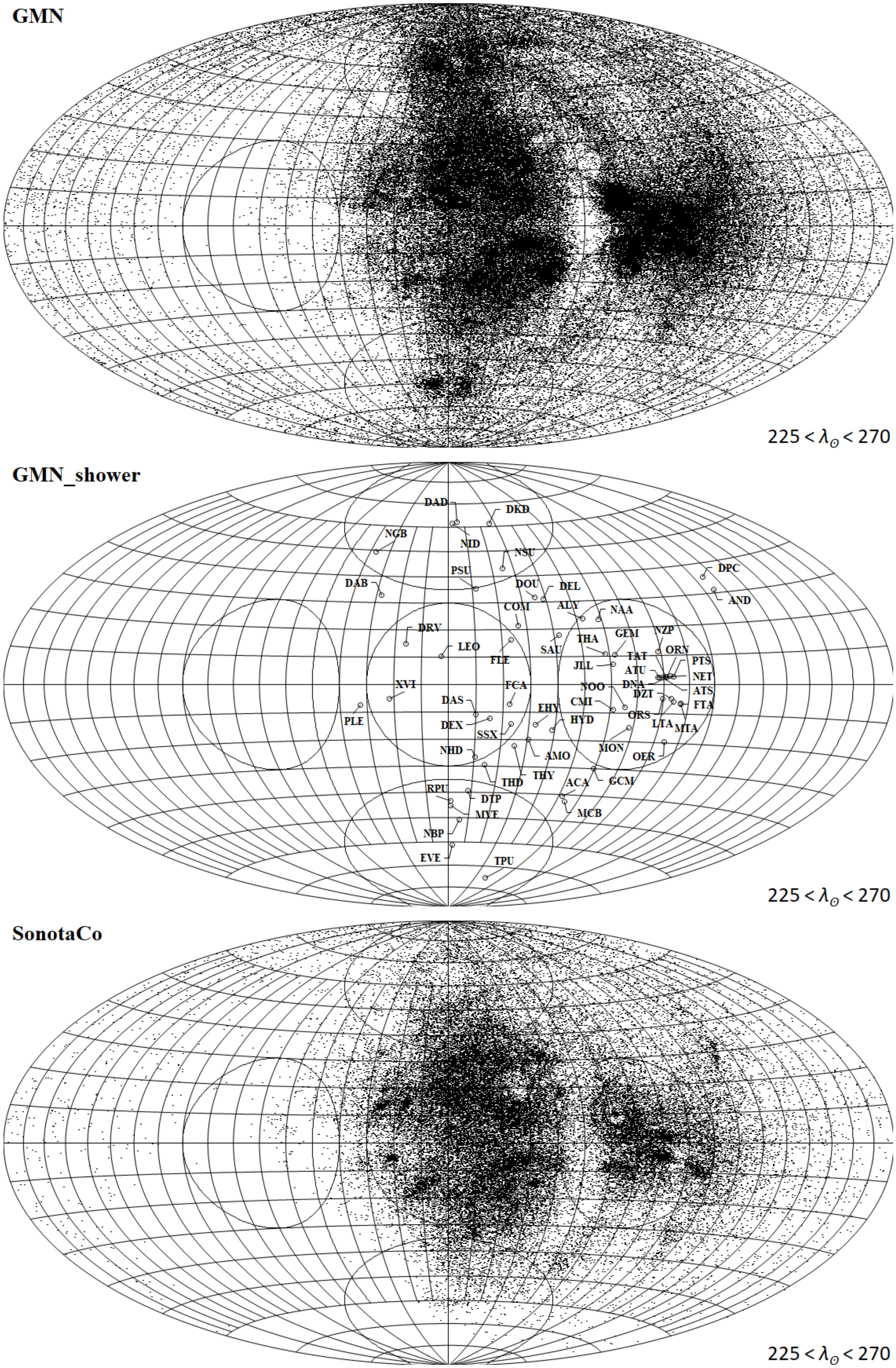

Figure 18 – Radiant point distribution of sporadic meteors identified as such when $225° < \lambda_\odot < 270°$. The top row shows sporadic meteors from GMN, the middle row shows those treated as "meteor showers" in GMN, and the bottom row shows sporadic meteors from SonotaCo network.

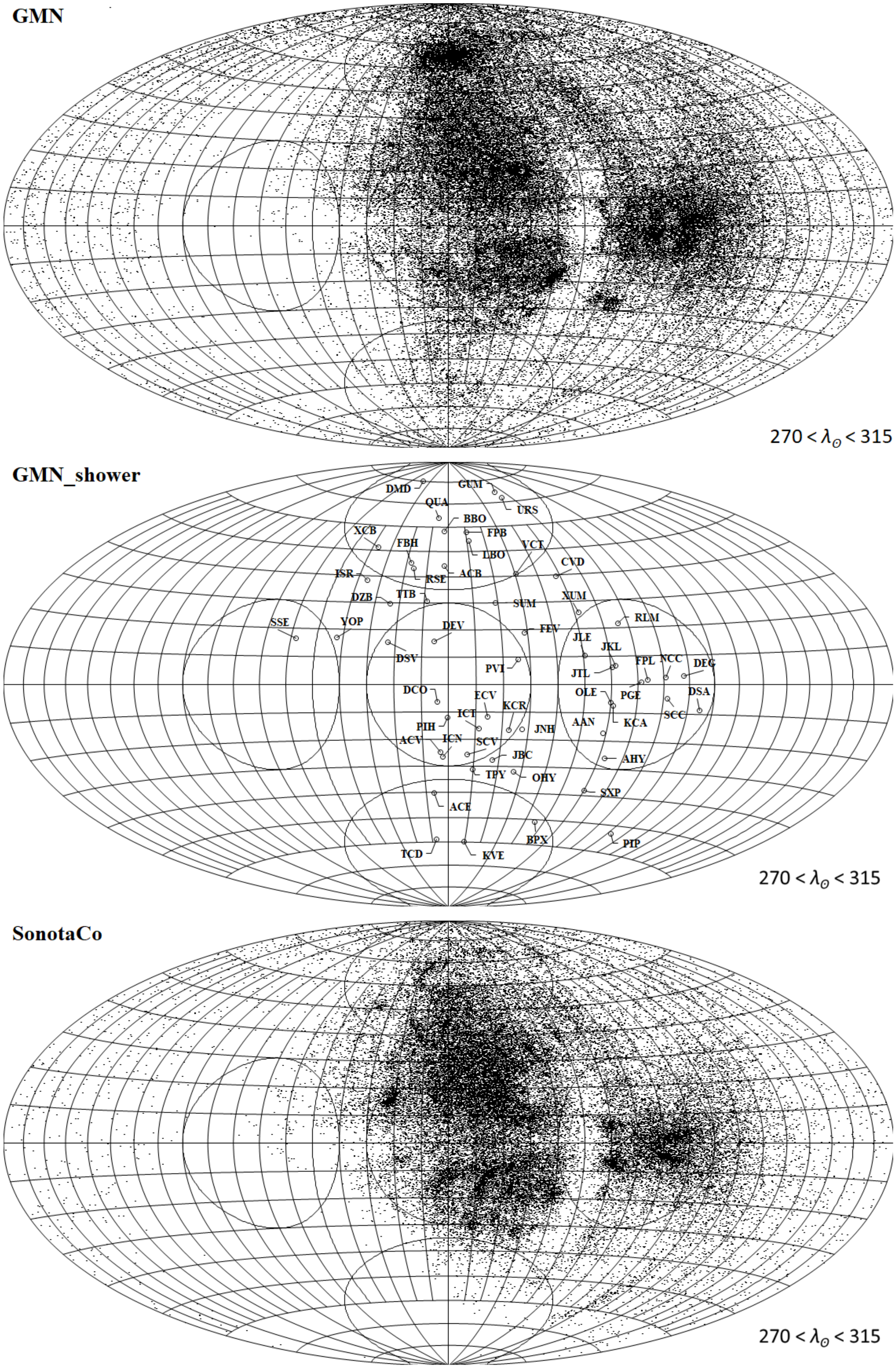

Figure 19 – Radiant point distribution of sporadic meteors identified as such when $270° < \lambda_O < 315°$. The top row shows sporadic meteors from GMN, the middle row shows those treated as “meteor showers” in GMN, and the bottom row shows sporadic meteors from SonotaCo network.

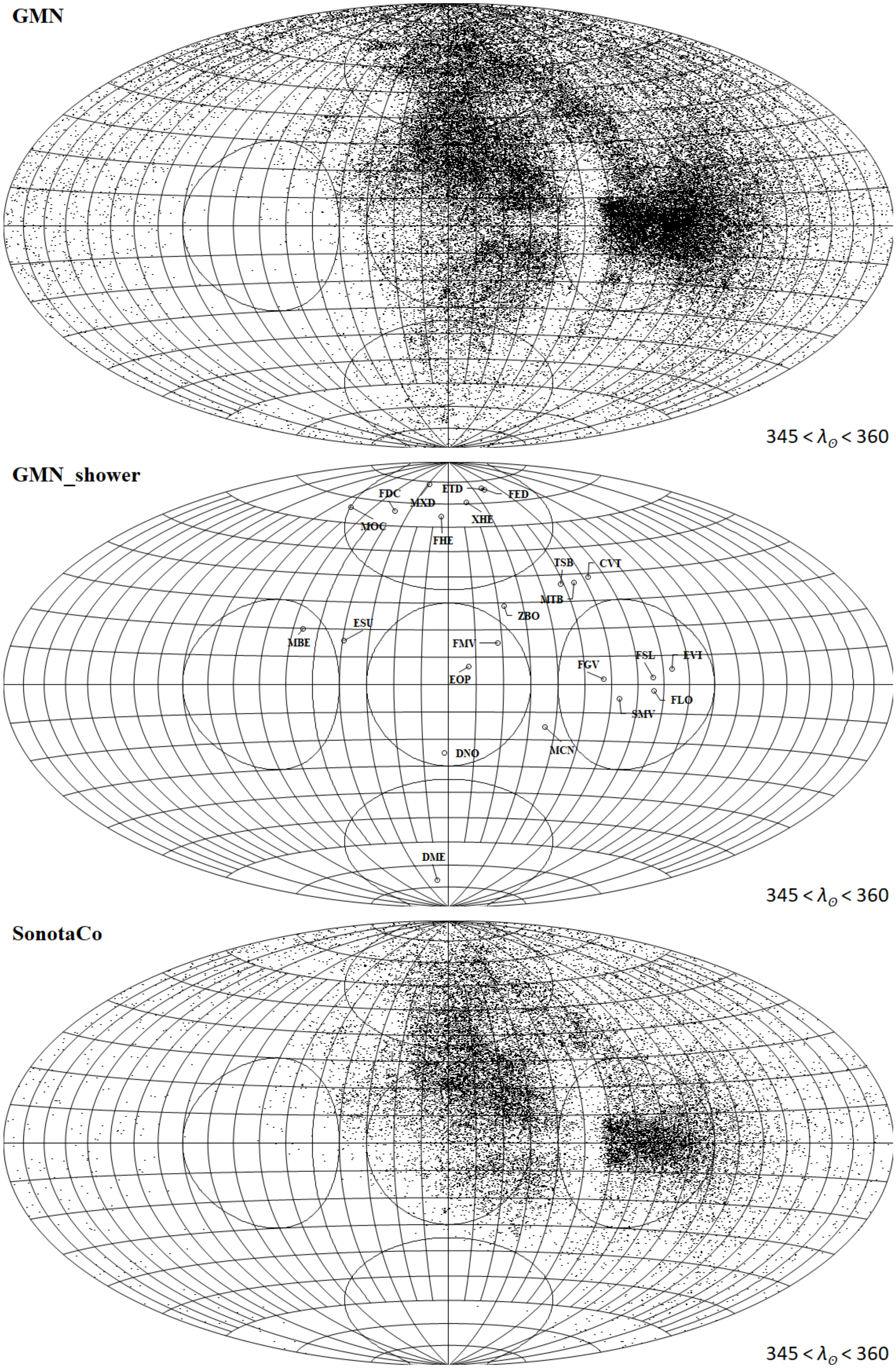

Figure 20 – Radiant point distribution of sporadic meteors identified as such when 345° < λ_{O} < 360°. The top row shows sporadic meteors from GMN, the middle row shows those treated as “meteor showers” in GMN, and the bottom row shows sporadic meteors from SonotaCo network.

Notes on Figure 18 (225° < $\lambda_{\odot}$ < 270°)

During this period, the meteor showers represented by black rings (with white interiors) on the GMN distribution map are the most numerous: 0004GEM, #0013LEO, #0016HYD, #0019MON, #0020COM, #0334DAD/#0392NID, and #0746EVE. On SonotaCo network, #0004GEM and #0020COM have a white interior, while conversely, #0335XVI, #0428DSV, #0445KUM, #0502DRV, and #0529EHY retain their black areas. #0428DSV, 0500JPV, #0513EPV, and #1124HTV represent the same meteor shower activity, and are unified under the name #0428DSV in GMN. However, neither is listed in the SonotaCo network's J6 list, and the J14 list records only #0513EPV and #1124HTV, rather than #0428DSV. Furthermore, the SonotaCo network's J14 list specifies shorter activity periods for #0335XVI and #0502DRV than the GMN data does, and #0502DRV is absent from the J6 list entirely. For #0445KUM, please refer to the description of *Figure 16*. Furthermore, similar to the period 180° < $\lambda_{\odot}$ < 225°, the treatment of #0002STA and #0017NTA differs between GMN and SonotaCo network, resulting in different distributions of radiated points around them in each figure. There are also differences between the two regarding how they handle final activities of #0008ORI.

Notes on Figure 19 (270° < $\lambda_{\odot}$ < 315°)

#0096NCC and #0097SCC are prime examples of how researchers and observers treat ecliptic meteor showers differently. Both are shown as blank in the GMN radiant point distribution map, are not listed in the SonotaCo network's J14 list, and show a dispersed radiant point distribution. Both are listed in the J6 list, but their periods of activity are shorter than that of GMN. Similarly, #0747JKL and #0748JTL are not listed in either the SonotaCo network's J6 or J14 lists, and while SonotaCo network shows a black distribution of radiation points, GMN shows them as blank. #0515OLE, #0643OLS, and #0793KCA are thought to be from the same meteor shower. At this location, the GMN shows a white circle, while the SonotaCo network shows a black distribution of the radiant point. While GMN lists #0515OLE and #0793KCA, neither appears in the SonotaCo network's J6 list, and only #0793KCA is included in the J14 list. The discrepancy in the radiant distribution patterns likely stems from GMN setting an excessively long activity period for #0515OLE, whereas the SonotaCo network sets an overly short activity period for #0793KCA. The activities of #0530ECV and #0601ICT are located next to each other, and their relationship warrants further investigation. SonotaCo network's J14 list does not include #0601ICT, and although #0530ECV is listed, the short duration of its activity likely explains the remaining black area (Neither is listed on the J6 list). Because #0428DSV has been active for a long time, the SonotaCo network still has black areas, following 225° < $\lambda_{\odot}$ < 270°. In GMN, the black area is likely left because the activity period for #0016HYD is set to be short. On the other hand, in GMN, the areas for #0020COM, #0506FEV, and #0331AHY are left white.

Notes on Figure 20 (315° < $\lambda_{\odot}$ < 360°)

#0807FLO is blank on GMN, but it is not included in SonotaCo network's either J6 or J14 list. Meteor activity is low during this period, and there are no other significant differences between the two.

4 Summary and outlook

We have seen that GMN and SonotaCo network differ in their meteor shower settings and in how they classify sporadic meteors. Here, we summarize these differences and identify key points to consider when examining the meteors classified as sporadic by GMN.

While we have observed differences in the radiant distributions between GMN and SonotaCo network, there is also a discrepancy in the baseline number of recognized meteor showers: GMN lists 385 showers, whereas SonotaCo network lists 136. Although this appears to be a significant difference, many of these are minor showers with very low activity levels; furthermore, GMN sometimes splits showers that SonotaCo network groups together as a single entity. Consequently, the impact of this numerical difference is considered to be relatively minor.

Rather, the difference in how the activity periods of meteor showers are defined between GMN and SonotaCo network appears to have a significant impact. There are various criteria for determining when a meteor shower's activity begins and ends. The longest activity period is obtained when the duration is defined based on the range in which meteors appearing to originate from the designated radiant are observed. In this case, the proportion of sporadic meteors mixed in at the start and end points of the activity becomes extremely high. Alternatively, one can identify the period based on when the number of meteors is high relative to the surrounding sporadic background. In practice, however, it appears that both GMN and SonotaCo network determine these activity periods without applying a fixed, standardized criterion; instead, they rely on their own observational data while also referencing other sources, such as the IAU-MDC SD. While the duration naturally varies by meteor shower, SonotaCo network tends to report shorter periods compared to GMN. This appears to have an effect of using short time intervals, as the J14 list employs orbital similarity to identify meteor showers (SonotaCo et al., 2021). However, this tendency is observed only in the case of minor meteor showers with low activity rates, and its impact on the distribution of radiants is not particularly significant.

The primary factor driving the significant difference in radiant distribution between GMN and SonotaCo network lies in the extent to which the spread of the radiant, the basis for determining whether a meteor belongs to a shower or is sporadic, is accepted. However, establishing an objective boundary for this is impossible. Moreover, the spread of the radiant differs for each meteor shower. Consequently, both GMN and SonotaCo network independently define radiant spread settings for each specific meteor shower. Compared to GMN, SonotaCo network generally employs a setting that allows for a wider spread of radiant points. We pointed out that this difference results in the appearance of blank areas, where few radiant points are visible, alongside dark, ring-shaped regions where radiant points are densely concentrated on the radiant point distribution map.

The proportion of "sporadic meteors" within the total number of observed meteors is 62.58% for SonotaCo network and 69.87% for GMN. Given that GMN defines a larger number of meteor showers, this indicates that the broader radiant distributions of meteor showers used by SonotaCo network play a significant role in these figures. In the case of the Perseids and Geminids, we have observed in GMN radiant distribution maps that the radiant points appear as black, ring-like voids. These are good examples how differences in data handling for high-activity meteor showers manifest as numerical discrepancies.

However, there is no absolute criterion for determining whether or not a meteor belongs to a meteor shower. As Part 3 will discuss the boundary region between meteor showers and sporadic meteors we will not elaborate further here, specifically in the context of the Geminids and Taurids, on the distinction between the two.

The upcoming investigation into sporadic meteors is fundamentally statistical in nature and does not aim to examine the physical properties of individual meteors. Let us examine the common characteristics of meteors classified as sporadic by both GMN and SonotaCo network.

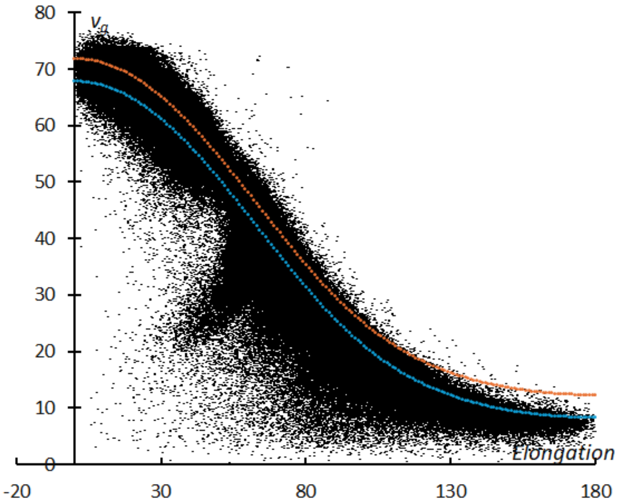

Figure 21 – Geocentric velocity distribution of meteors classified as sporadic by GMN, plotted against the elongation. The upper line shows the relationship between elongation and geocentric velocity for meteors on parabolic orbits colliding with Earth. The lower line represents geocentric velocities 4 km/s lower than those of the upper line.

With very few exceptions, the speed of meteoroids moving within the solar system is capped at the parabolic velocity. Near Earth's orbit, a meteoroid traveling at parabolic velocity moves at approximately 42 km/s; given that Earth's orbital speed is about 30 km/s, the impact speed is approximately 72 km/s for a head-on collision and about 12 km/s if the meteoroid overtakes Earth from behind. The resultant velocity is geometrically determined by the meteoroid's speed and its direction of motion relative to Earth; the velocity distribution of sporadic meteors is determined by the angular distance from the Earth's apex (the direction of Earth's motion) and exhibits nearly the same profile in both GMN (*Figure 21*) and SonotaCo network (*Figure 22*) data. The upper line shows the relationship between elongation and geocentric velocity for meteors on parabolic orbits colliding with Earth. The lower line represents geocentric velocities 4 km/s lower than those of the upper line. The smooth slope appearing on the upper side of the distribution represents the geocentric velocities of meteoroids following approximately parabolic trajectories. We shall liken this distribution to the head, fin, and body of a fish. The two peaks observed in the geocentric velocity distributions each (*Figures 1 and 2*) correspond to the "head" and the "fin plus body" sections seen in the figure of elongation versus geocentric velocity.

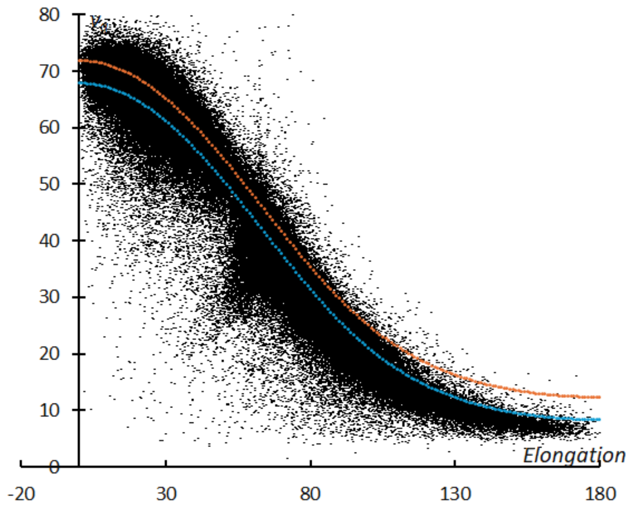

Figure 22 – Geocentric velocity distribution of sporadic meteors classified by the SonotaCo Network, plotted against the elongation. The upper line shows the relationship between elongation and geocentric velocity for meteors on parabolic orbits colliding with Earth. The lower line represents geocentric velocities 4 km/s lower than those of the upper line.

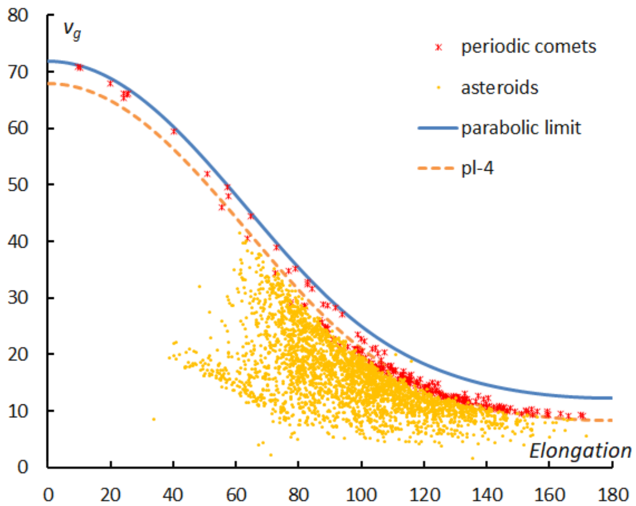

Figure 23: Relationship between elongation and geocentric velocity for the estimated radiants of comets and asteroids approaching Earth. Comets are marked with "×" and asteroids with "−" (Koseki, 2015). As in Figures 20 and 21, the upper and lower lines indicate meteors with parabolic orbits and those with geocentric velocities 4 km/s lower than that, respectively.

Since meteors with hyperbolic orbits are considered virtually non-existent, the portion extending beyond the upper line is attributed to errors in velocity measurement. The distribution at the "head" of the "fish" appears roughly symmetrical about the two lines; therefore, the velocities of meteors in this region are considered to essentially fall between the upper and lower lines.

Figure 22 shows the relationship between elongation and geocentric velocity for the estimated radiants of comets and asteroids approaching Earth. The solid line represents the geocentric velocity for a parabolic orbit, while the dashed line connects values 4 km/s lower than that. It can be seen that comets have geocentric velocities within approximately 4 km/s of the parabolic orbit value, whereas asteroids have velocities lower than that.

A comparison of *Figure 23* with *Figures 21 and 22* reveals that the meteors constituting the "fish's head", specifically, those with an angular distance of within 50 degrees from the apex, are predominantly those with velocities within 4 km/s of a parabolic orbit; in other words, it is inferred that many of them originate from long-period comets. Furthermore, in the region where the apex, which defines the "fish's fins and body", exceeds 50 degrees, it is estimated that objects of cometary origin and asteroidal origin coexist. It is also shown that as the angular distance increases, meaning the geocentric velocity decreases, there is a transition from meteors with velocities within 4 km/s of a parabolic orbit to those with velocities exceeding 4 km/s; the proportion of asteroidal-origin objects is thought to increase relative to those of cometary origin. Furthermore, in the region where the elongation from the apex exceeds 50 degrees, an area likened to the fins and body of a fish, it is estimated that objects of cometary origin and those of asteroidal origin coexist. It is shown that as the elongation increases, meaning the geocentric velocity decreases, the population shifts from meteors with speeds within 4 km/s of a parabolic trajectory to those with speeds exceeding 4 km/s. It is believed that the proportion of asteroid-origin meteors increases relative to those of cometary origin.

There are some differences in the shape of the "fish" between *Figure 20* and *Figure 21*. The head of the fish is larger in the SonotaCo network data than in the GMN data. This is likely because the cameras used in the SonotaCo network generally have shorter focal lengths than those in the GMN, leading to larger measurement errors for fast-moving meteors. Conversely, the body and fins of the fish are thicker in the GMN data than in the SonotaCo Network data; this is because the GMN captures slower and fainter meteors.

While differences arising from the use of distinct equipment for GMN and SonotaCo network are acknowledged, there are no apparent discrepancies regarding the classification of meteor showers versus sporadic meteors. Although the following sections analyze sporadic meteors using GMN data, it can be concluded that the characteristics of sporadic meteors in video observations can be effectively captured, provided that the potential for equipment-related variations is considered.

In Part 2, we examine the physical properties of meteoroids based on GMN sporadic meteor data, analyzing the magnitude distribution and the relationships between beginning height, meteor magnitude, and geocentric velocity. In Part 3, we further utilize GMN sporadic meteor data to focus on the "fin" sections of the distribution, visualized by likening the overall pattern to a fish, and investigate the relationship between meteor showers and sporadic meteors.

References

Brown P., Weryk R. J., Wong D. K., and Jones J. (2008). "A meteoroid stream survey using the Canadian Meteor Orbit Radar. I. Methodology and radiant catalogue". *Icarus*, **195**, 317–339.

Brown P., Wong D. K., Weryk R. J., and Wiegert P. (2010). "A meteoroid stream survey using the Canadian Meteor Orbit Radar. II. Identification of minor showers using a 3D wavelet transform". *Icarus*, **207**, 66–81.

Jenniskens P. (2023). Atlas of Earth's Meteor Showers, Elsevier.

Koseki M. (1979). "Meteor Radiant observed between 1928-69 in Japan". *The Heavens*, **60**, 237, 270 and 295. (in Japanese).

Koseki M. (1982). "Meteor shower research on photographic meteors by cluster analysis". *23rd Japanese Meteor Conference*. (In Japanese).

Koseki M. (2009). "Meteor Shower Records: A Reference Table of Observations from Previous centuries". *WGN, the Journal of the IMO*, **37**, 139–160.

Koseki M. (2015). "What do we see as ANT, Apex and Toroidal sources? - What meteors are, where meteors came from, where meteoroids are going". WGN, the Journal of the IMO, 43:5, 127-146.

Koseki M. (2023). "Grading evaluation of meteor showers' report in the IAU Meteor Data Center Shower Database". *eMetN Meteor Journal*, **8**, 337–367.

Koseki M. (2024a). "Meteor shower data from video observation, Part I, "Research methods and summary of survey results". *eMetN Meteor Journal*, **9**, 166–183.

Koseki M. (2024b). "Meteor shower data from video observation, Part II, Meteor showers that need careful attention". *eMetN Meteor Journal*, **9**, 215–230.

Koseki M. (2024c). "Meteor shower data from video observation, Part III, "Radiant point distribution map and activity profile". *eMetN Meteor Journal*, **9**, 295–349.

Koseki M. (2025). "20 meteor showers observed on video: What can be seen from comparing meteor showers with data from SonotaCoNet and GMN". *eMetN Meteor Journal*, **10**, 170–190.

Sekanina Z. (1970). "Statistical Model of Meteor Streams. II. Major Showers". *Icarus*, **13**, 475–493.

Sekanina Z. (1973). "Statistical Model of Meteor Streams. III. Stream search Among 19903 Radio Meteors". *Icarus*, **18**, 253–284.

Sekanina Z. (1976). "Statistical model of meteor streams. IV - A study of radio streams from the synoptic year". *Icarus*, **27**, 265–321.

SonotaCo (2009). "A meteor shower catalog based on video observations in 2007–2008". *WGN, Journal of the International Meteor Organization*, **37**, 55–62.

SonotaCo (2016). "Observation error propagation on video meteor orbit determination". *WGN, Journal of the International Meteor Organization*, **44**, 42–45.

SonotaCo (2017). "Exhaustive error computation on 3 or more simultaneous meteor observations". *WGN, Journal of the International Meteor Organization*, **45**, 95–97.

SonotaCo, Uehara S., Sekiguchi T., Fujiwara Y., Maeda K., Ueda M. (2021). "J14: A Meteor Shower and Cluster Catalog". *WGN, Journal of the International Meteor Organization*, **49**, 76–97.

Southworth R.B. and Hawkins G.S. (1963). "Statistics of meteor streams". *Smithsonian Contributions to Astrophysics*, **7**, 261–285.

Vida D., Gural P., Brown P., Campbell–Brown M., Wiegert P. (2019). "Estimating trajectories of meteors: an observational Monte Carlo approach – I. Theory". *Monthly Notices of the Royal Astronomical Society*, **491**, 2688–2705.

Vida D., Gural P., Brown P., Campbell–Brown M., Wiegert P. (2020). "Estimating trajectories of meteors: an observational Monte Carlo approach – II. Results". *Monthly Notices of the Royal Astronomical Society*, **491**, 3996–4011.

Vida D., Šegon D., Gural P. S., Brown P. G., McIntyre M. J. M., Dijkema T. J., Pavletić L., Kukić P., Mazur M. J., Eschman P., Roggemans P., Merlak A., Zubrović D. (2021). "The Global Meteor Network – Methodology and first results". *Monthly Notices of the Royal Astronomical Society*, **506**, 5046–5074.

The Ursids filament observed as a small outburst in 2025

Koen Miskotte

Dutch Meteor Society
k.miskotte@upcmail.nl

On the night of December 22, 2025 (UT), the Ursids exhibited a small outburst. Following reports from Pierre Martin and Jürgen Rendtel, it was decided to conduct an analysis to present on April 18 during the annual meeting of the Dutch Meteor Society. This article reiterates the results and provides additional info.

1 Characteristics

The Ursids are a small meteor shower active during the period from December 7 to January 7 (Jenniskens, 2023) The meteors are slow (33 km/s) and are mostly faint (population index $r = 2.8$). The maximum ZHR during a normal Ursid year is usually around 10. The radiant of the Ursids is near RA 217 and Declination +76, which is near the star Kochab (beta Ursa Minor). The Ursids are known to exhibit regular outbursts. Interestingly, these occur both around the time the comet is at perihelion and at aphelion. The meteor shower originates from Comet 8P/Tuttle, which has an orbital period of 13.6 years. The comet was discovered on January 5, 1858, by Horace Parnell Tuttle. The Ursids became known after a major outburst on the evening of December 23, 1945 (Bečvář, 1946), which was observed by observers at the Skalnaté Pleso Observatory. Another major outburst was also observed in 1986 (Jenniskens, 1988). More on this in a future second article.

2 Data collection

For the analysis of the 2025 observations, the "on the fly" ZHR curve of the 2025 Ursids[7] was examined first. See also *Figure 1*.

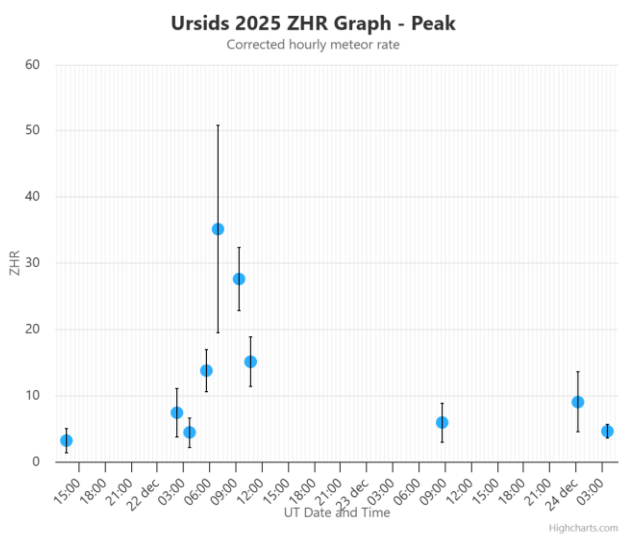

Figure 1 – "On the fly" ZHR curve IMO website Ursids 2025.

On the peak tab, it is clearly visible that a higher-than-normal ZHR was observed. One ZHR point reached ZHR 35. Checking that data point reveals that this ZHR determination was based on only 4 Ursids. Caution is always advised with the "on the fly" curve. It is a handy tool for quickly checking something, but one must always pay attention to the details. Moreover, the amount of data was very meager: only 13 observers provided data for 199 Ursids. The peak ZHR curve (*Figure 1*) is based on only 128 Ursids.

First of all, the data was downloaded. As always, it had to meet the well-known standard requirements:

- Only observers used who observed multiple Ursids.
- Only observers with a reliable C_p value.
- Minimum radiant height 25 degrees.
- Minimum limiting magnitude 5.9.

3 Population index *r*

Due to the small amount of data, it was decided to determine the population index r for only two periods. One during the maximum and one for the period before and after the maximum. From these, a population index r was calculated for the maximum $r[-1{:}5] = 2.50 \pm 0.27$. For the period before and after the maximum, a population index $r[-1{:}5] = 3.00 \pm 0.23$ was calculated (Steyaert, 1981).

4 Zenital Hourly Rate (ZHR)

Based on the population index r calculated above, the ZHR was determined using the formula:

$$ZHR = \frac{n \cdot r^{6.5-lm}}{(\sin h)^{\gamma} \cdot C_p \cdot T_{eff}}$$

The result is *Figure 3*, which gives the ZHR of the Ursids for the period December 15 to 28, 2025. This calculation is based on the data as originally reported on the IMO website:

- Before and after December 22 based on hourly counts (0.75–1.00 hours).

[7] https://www.imo.net/members/imo_live_shower?shower=URS&year=2025

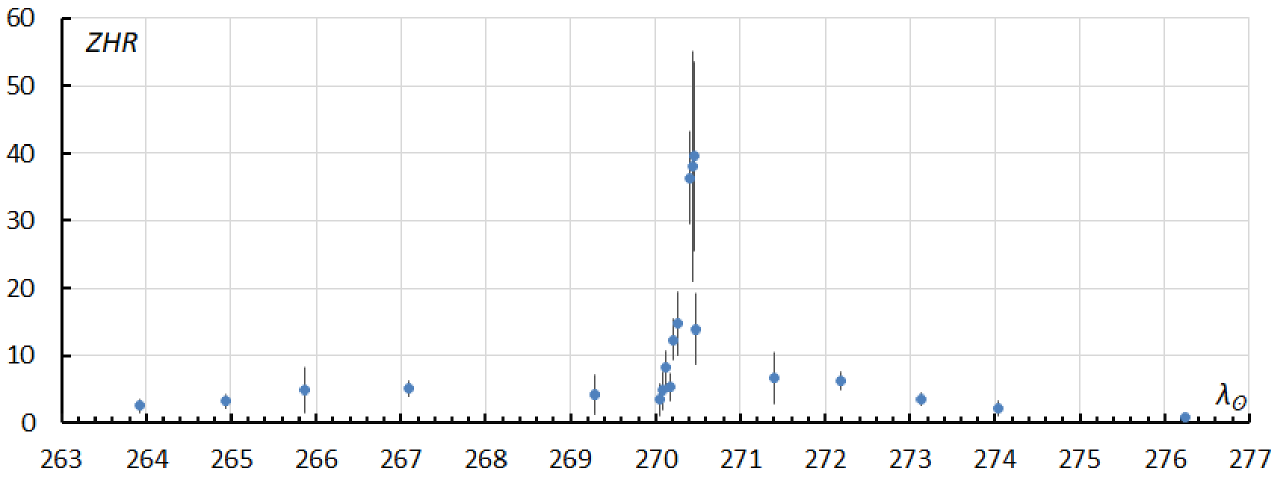

Figure 2 – ZHR of the Ursids in 2025 between December 14–25, 2025. Based on 179 Ursids.

- On December 22, counting periods between 0.3 and 1.0 hours.
- ZHR calculated using weighted averages of individual ZHRs.
- No correction for zenith attraction has been applied yet (Rendtel, 2022).

Figure 3, zooming in on the maximum, looks a bit strange. A slowly rising ZHR, and as soon as the maximum is reached, the ZHR collapses. The graph is based on data from only four observers who provided counting periods between 0.3 and 1.00 hours. These very diverse counting periods may well be the reason why the ZHR curve looks strange.

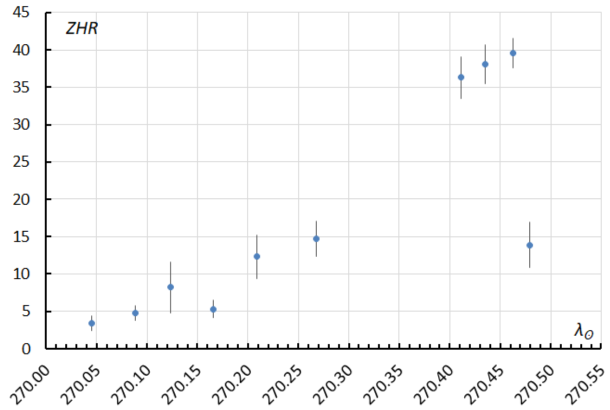

Figure 3 – ZHR curve Ursids 21–22 December 2025. Based on 96 Ursids.

For this reason, the observers who observed the high activity (Terrence Ross and Pierre Martin) were asked to provide data in smaller periods. From the additional data they submitted, counting periods of 0.4 and 0.46 hours could be created. In addition, a correction for zenith attraction was applied for radiant positions below 40 degrees altitude. Subsequently, a ZHR determination was performed every 10 minutes with overlapping counting periods. The results of these calculations are in *Figures 4 and 5* and *Table 1*.

Table 1 – ZHR of the 2025 Ursids, *Tm* is the mean time in UT, *nS* is the number of sessions.

Day	*Tm*	$\lambda_{\odot}$	*nS*	URS	ZHR
16	0.09	263.916	5	6	2.5 ± 1.0
17	0.38	264.946	7	11	3.2 ± 1.0
17	22.00	265.862	1	2	4.8 ± 3.4
19	2.92	267.089	7	19	5.1 ± 1.2
21	6.64	269.284	2	2	4.2 ± 3.0
22	0.58	270.045	1	2	3.4 ± 2.4
22	1.58	270.088	1	3	4.8 ± 2.8
22	2.42	270.123	2	10	8.2 ± 2.6
22	3.42	270.166	2	7	5.3 ± 2.0
22	4.48	270.209	3	16	12.3 ± 3.1
22	5.82	270.268	2	10	14.7 ± 4.6
22	8.88	270.398	2	16	52.1 ± 13.0
22	9.08	270.406	2	13	40.7 ± 11.3
22	9.22	270.412	2	11	30.1 ± 9.1
22	9.31	270.416	2	10	29.8 ± 9.4
22	9.43	270.421	2	11	32.2 ± 9.7
22	9.51	270.424	2	11	32.1 ± 9.7
22	9.62	270.429	2	11	37.1 ± 11.2
22	9.73	270.434	2	10	24.8 ± 7.8
22	9.88	270.440	2	8	17.8 ± 6.3
22	10.02	270.446	2	10	26.0 ± 8.2
22	10.15	270.451	2	10	25.8 ± 8.2
22	10.34	270.459	2	8	22.6 ± 8.0
22	10.59	270.470	2	5	14.7 ± 6.6
22	10.98	270.487	2	2	5.3 ± 3.7
23	8.65	271.407	2	3	6.6 ± 3.8
22	3.15	272.192	7	21	6.1 ± 1.3
25	1.02	273.120	8	15	3.5 ± 0.9
25	22.80	274.045	5	4	2.2 ± 1.1
28	2.47	276.239	9	5	0.8 ± 0.4

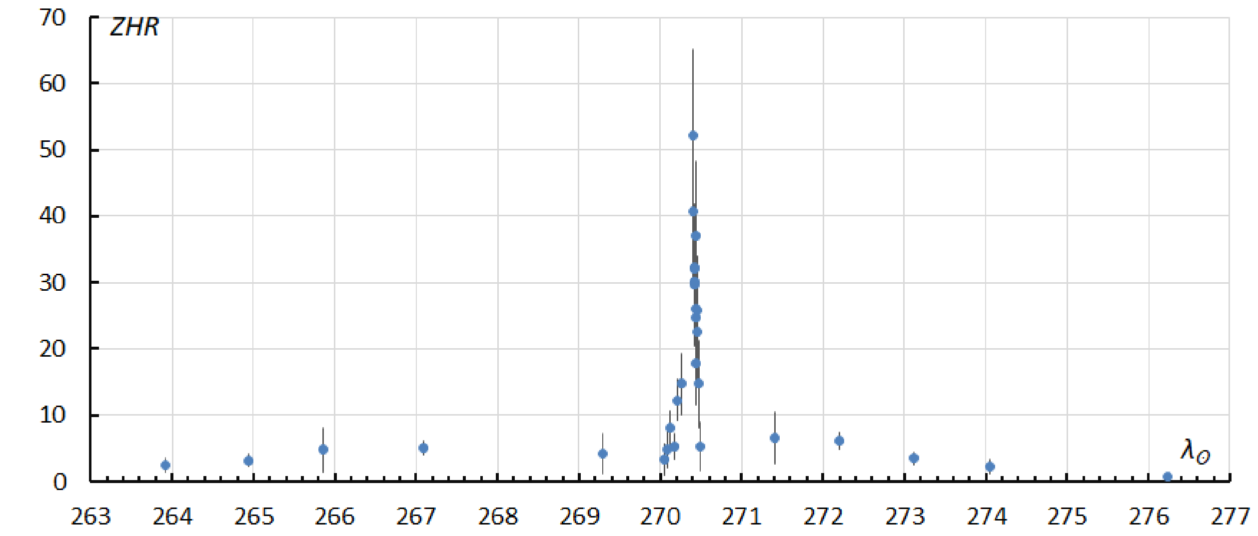

Figure 4 – ZHR for the Ursids for the period 15–28 December 2025.

Few differences are visible over the entire 15–28 December period. However, the maximum in this calculation turns out 20% higher, with a ZHR of 52 compared to 40 in *Figure 1*. To zoom in on the maximum, see *Figure 5*.

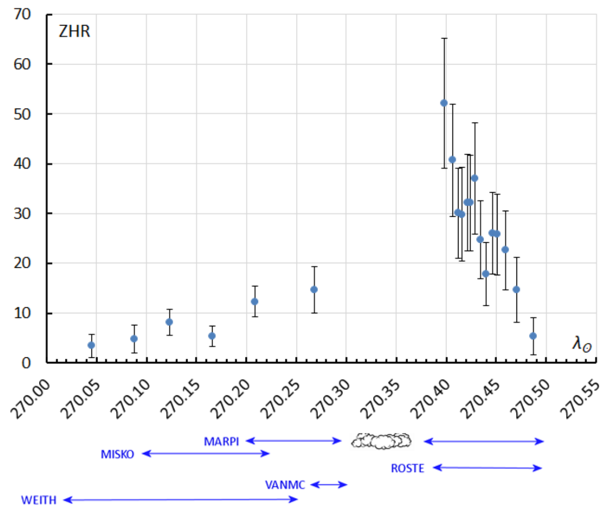

Figure 5 – The Ursid maximum (December 21–22, 2025). The ZHR calculations are based on 1-hour counts for the period prior to $\lambda_\odot$ = 270.30° and subsequently on 0.40 and 0.46-hour counts. Gamma is set to 1 and a population index $r[-1;5]$ = 2.50 is used.

Due to the small amount of data used for this analysis, observations by whom and during which period are indicated below the graph. There we see that Pierre Martin experienced cloud cover for a longer period of time. This is unfortunate, as the built-up and perhaps also the peak were hidden behind this. Nevertheless, the ZHR curve looks much better than the first curve in *Figure 3*. The maximum ZHR is calculated immediately at the (re)start of the observations by Pierre Martin and Terrence Ross. A few sub-peaks also appear to be visible, but these are likely the result of the minimal amount of data on which *Figure 4* is based. The maximum therefore occurred at $\lambda_\odot$ = 270.398° (22 December 2025, 08^h53^m UT) or earlier.

The European part of the graph, which extends to solar longitude 270.30°, is also interesting. Observer Thomas Weiland reports 7 Ursids between solar longitude 270.109° and 270.152° with the following magnitude distribution: –2 (1×), –1 (1×), 0 (2×), +1 (2×) and +4 (1×). The ZHR curve also shows a small peak around that time. This "might" be the annual maximum; the maximum ZHR usually lies between 5 and 10. After solar longitude 270.20, the ZHR starts rising again to the much higher filament peak.

5 Comparison with radio (RMOB) and GMN video observations

Figures 6 and 7 show the results of the radio (RMOB)- and video (GMN) networks.

It is clear that comparing with other observational methods is tricky. In this case, there was a nice agreement between the video and radio observations. Both find a maximum at the same time:

- Maximum visual: $\lambda_\odot$ = 270.398° (22 December 2025, 08^h53^m UT) or earlier. Population index $r[-1;5]$= 2.5.
- Maximum RMOB: $\lambda_\odot$ = 270.382° (22 December 2025, 08^h26^m UT)
- Maximum GMN: $\lambda_\odot$ = 270.38° (22 December 2025, 08^h26^m UT)

Thanks to Hirofumi Sugimoto and Hiroshi Ogawa (Sugimoto, 2017; Ogawa, 2026), the author was able to make a ZHR graph with both visual ZHR and radio ZHRr data. The result is *Figure 8* and shows a reasonably nice comparable progression despite the difference in observational methods.

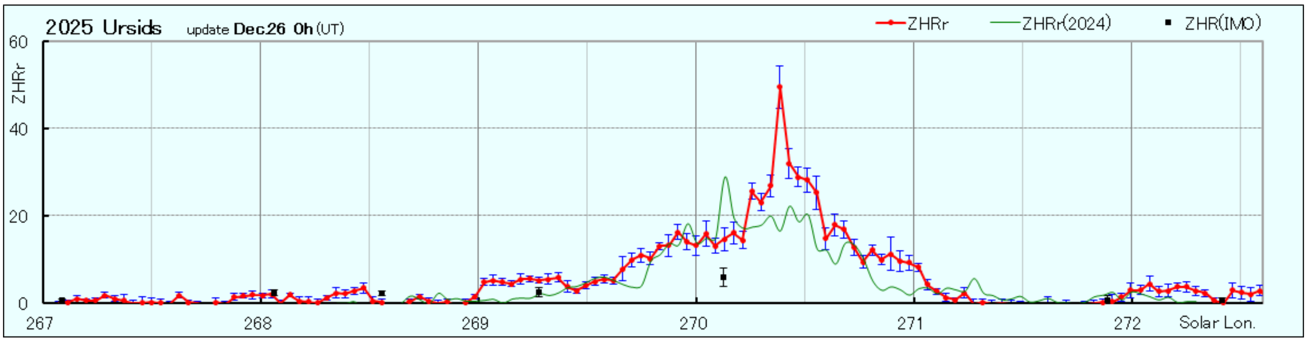

Figure 6 – Radio ZHR r curve of the Ursids 2025 based on radio observation data collected by RMOB[8].

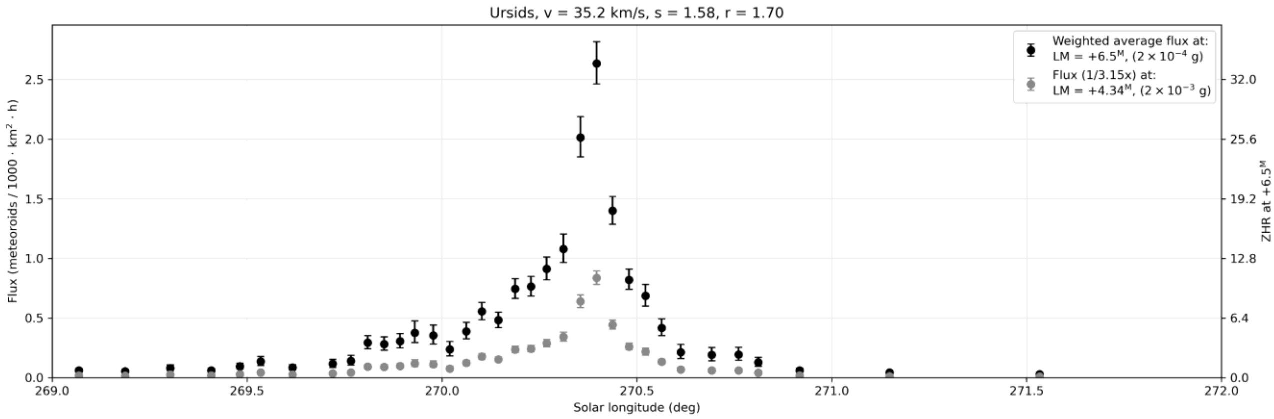

Figure 7 – GMN ZHR curve of the Ursids based on simultaneous Ursids observations.

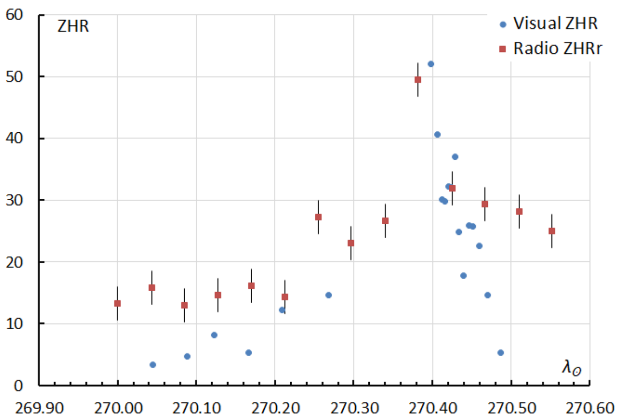

Figure 9 – Radio ZHRr and visual ZHR of the Ursids during 21–22 December 2025.

6 What is the possible cause of this outburst?

Next, attempts were made to determine what caused the increased activity. In the book Meteor Showers and their Parent Comets (Jenniskens, 2006), Peter Jenniskens gives the following for 2025: No dust trails were expected. These structures are very small, with a Width = 0.05° (± 1.2 hours) and a population index *r* = 2.8. However, a filament was expected on 22 December 2025 at 05^h39^m UT with a population index *r* = 2.6 and a ZHR of 25 on top of the annual activity. The expected Width of the filament is 0.35° (~8.4 hours). The same structure was also predicted for 2021, 2022, 2023 and 2024 but was not observed then. In the Meteor Shower Calendar 2025 (Rendtel, 2024), Jeremie Vaubaillon expects the highest activity of the Ursids around 10^h UT; no further information is provided.

The following was observed:

- The duration of the outburst assuming a ZHR exceeding 10: $\lambda_{\odot}$ = 270.20° – 270.48° , W=0.28° (= ±6.7 hours).
- The duration of the outburst assuming a ZHR exceeding 5: $\lambda_{\odot}$ = 270.10° – 270.48° , W=0.38° (=±8.0 hours).
- Maximum ZHR based on visual observations: 50 and possibly slightly higher because the maximum occurred somewhat earlier.
- Calculated population index *r* of the Ursid maximum is *r*[–1;5] = 2.5

7 Conclusion

Visual observations show that the Ursid filament was active on December 22, 2025, with a maximum at 8^h25^m UT (time based on RMOB and GMN observational data). Maximum ZHR 52 (or higher) which is 40% higher than expected in (Jenniskens, 2006). The duration of 6.7 – 8.0 hours and the observed bright meteors resulting in population index *r*[–1;5] = 2.50 indicate that the filament was indeed observed here. Despite the small amount of visual data, a nice result was achieved here, and it aligns well with the

[8] https://www5f.biglobe.ne.jp/~hro/Flash/2025/URS/index-e.htm

radio and video observations. Thumbs up to the visual observers!

Acknowledgments

Many thanks to the observers who braved the December cold to observe the Ursids. These are: *Mark Adams, Jean-Luc Biret, Steve Brown, Pete Kozich, Pierre Martin, Koen Miskotte, Ina Rendtel, Jürgen Rendtel, Terrence Ross, Stefan Schmeissner, Costantine Sigismondi, Michel Vandeputte, Thomas Weiland* and *Roland Winkler*. Also, a thank you to al radio[9] and video observers[10] who contributed to the associated networks and results used in this analysis.

References

Bečvář A. (1946). IAU Circulair 1026.

Jenniskens P. (2006). Meteor showers and Their Parent Comets, Cambridge University Press 2006.

Jenniskens P. (2023). Atlas of Earth's Meteor Showers, Elsevier Inc. 2023, p. 105–107.

Jenniskens P., Hillestad T.E. (1988). "Meteor Section: Ursiden 1986". *Radiant*, **10**, 23. (In Dutch).

Ogawa H. (2026). "Ursids 2025 by worldwide radio meteor observations". *eMetN Meteor Journal*, **11**, 161–163.

Rendtel J. (2024). 2025 Meteor Shower Calendar, IMO.

Rendtel J. (2022). Handbook for meteor observers, IMO.

Sugimoto H. (2017). "The New Method of Estimating ZHR using Radio Meteor observations". *eMetN Meteor Journal*, **2**, 109–110.

Steyeart C. (1981). "Populatie indexbepaling : methode en nauwkeurigheid". Technische Nota nr. 5, VVS Werkgroep Meteoren, september 1981.

Figure 9 – Composite image of 9 Ursids and 3 sporadic meteors captured on December 22–23, 2009. Canon 6D, Sigma 35mm f/1.4 lens. © Pierre Martin.

[9] https://www.rmob.org

[10] https://globalmeteornetwork.org/

June 2026 CARMELo report

Mariasole Maglione[1], **Lorenzo Barbieri**[2], **William Rivato**[3]

[1] **CARMELo network and GAV, Gruppo Astrofili Vicentini, Italy**
mariasole@astrofilivicentini.it

[2] **CARMELo network and AAB: Associazione Astrofili Bolognesi, Italy**
carmelometeor@gmail.com

[3] **CARMELo network and MarSEC, Marana Space Exploration Center, Italy**

The CARMELO network (Cheap Amateur Radio Meteor Echoes LOgger) is a collaboration of SDR radio receivers aimed at detecting meteor echoes. This report presents the data for June 2026.

1 Introduction

In June, during the first half of the month, the CARMELO network detected activity consistent with the daytime shower of the Arietids (ARI#171), which we analyzed using our RZHR algorithm.

2 Methods

The CARMELO network consists of SDR radio receivers. In them, a microprocessor (Raspberry) performs three functions simultaneously:

- By driving a dongle, it tunes the frequency on which the transmitter transmits and tunes like a radio, samples the radio signal and through the FFT (Fast Fourier Transform) measures frequency and received power.
- By analyzing the received data for each packet, it detects meteor echoes and discards false positives and interference.
- It compiles a file containing the event log and sends it to a server.

The data are all generated by the same standard, and are therefore homogeneous and comparable. A single receiver can be assembled with a few devices whose total current cost is about 210 euros.

To participate in the network read the instructions on this page[11].

3 June data

In the plots that follow, all available at this page[12], the abscissae represent time, which is expressed in UT (Universal Time) or in solar longitude (Solar Long), and the ordinates represent the hourly rate, calculated as the total number of events recorded by the network in an hour divided by the number of operating receivers. The time resolution is 15 minutes.

In *Figure 1*, the trend of signals detected by the receivers is given for the month of June.

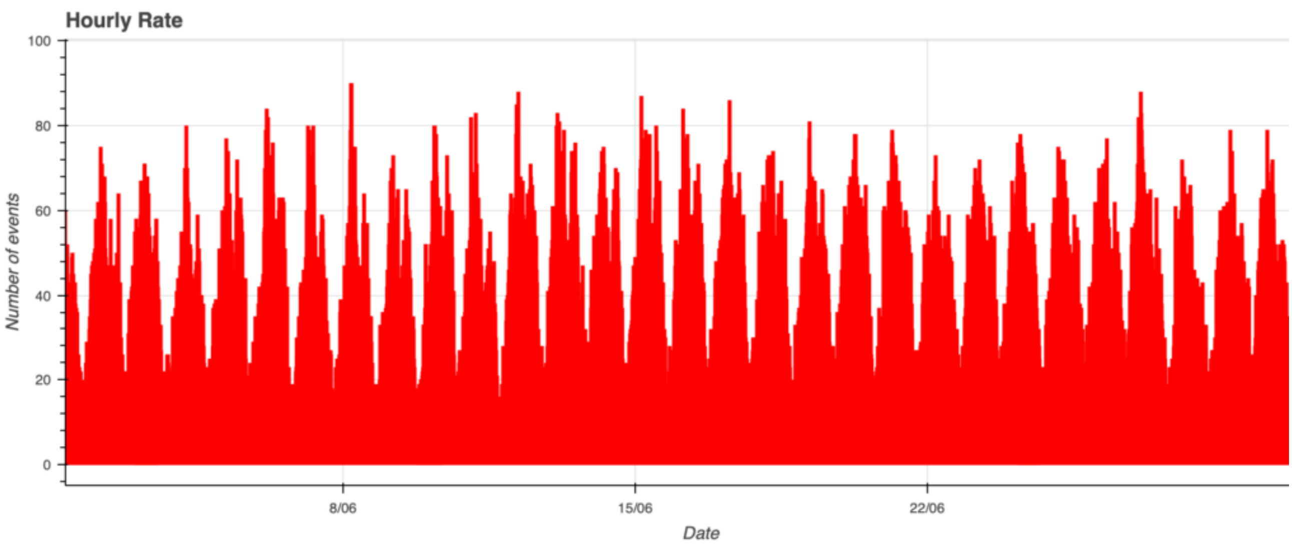

Figure 1 – June 2026 data trend.

[11] http://www.astrofiliabologna.it/about_carmelo

[12] http://www.astrofiliabologna.it/graficocarmelohr

4 Arietids

The Arietids (ARI#171) are a meteor shower active from mid-May to mid-June. It is the most intense daytime meteor shower of the year: its peak occurs when the Sun is already high in the sky, making visual observation extremely difficult, with fewer than one visible meteor per hour. However, Arietid meteors are easily detectable with radio equipment.

The shower's radiant is located in the constellation Aries, about 4 degrees southeast of the star 41 Arietis, and just 30 degrees from the Sun.

The origin of the Arietids has not yet been identified with certainty. The shower's orbit is consistent with both that of asteroid 1566 Icarus and that of comet 96P/Machholz, which are the leading candidates for the parent body (Ohtsuka et al., 2003). It has also been hypothesized that the Tunguska event may have been caused by a fragment of the same parent body as the meteor shower (Serra, 2025), although this theory remains unconfirmed.

The meteor shower was first detected in the summer of 1947 at the Jodrell Bank Observatory through radio observations. Since the peak activity occurs during daylight hours, visual observations are very difficult, and the characteristics of the meteor shower remain partly uncertain even today. Estimates of the active period vary from author to author: some sources indicate it is active from May 22 to July 2, others from May 14 to June 24, while the peak is generally placed around June 7.

The International Astronomical Union adopts a range between solar longitudes 73° and 90°, with a peak at 77°. The entry velocity of the meteors also varies somewhat across different estimates, with values ranging from approximately 35 to 42 km/s.

All of these characteristics make radio observations particularly valuable for studying the meteor shower. The low elevation of the radiant above the horizon, and its overlap with the minor zeta-Perseids (ζ-Perseids) meteor shower, call for some caution in interpreting the data obtained using the RZHR algorithm (Barbieri and Maglione, 2026).

5 The construction of RZHR

By *RZHR* (Radio Zenithal Hourly Rate), we mean the hourly rate of radio meteors in a shower, calculated by processing data from meteor scatter receivers.

This tool allows us to make a significant leap in quality, moving away from the qualitative analysis we have conducted so far (which relied exclusively on graphs) and transitioning to the direct processing of data from our database. To do this, we developed a Python script with the help of the "Cursor" tool, an AI-powered code editor created by Anysphere. This support proved crucial in developing a satisfactory script.

First, it should be clarified that, in calculating the *RZHR*, we make certain approximations, including:

- We do not take into account that the varying geographical distribution of receivers causes them to "see" meteors from slightly different angles.
- We disregard the fact that observations are not isotropic but are influenced by antenna pointing, which favors a specific sector of the sky over the entire sky.
- We define a contribution as "sporadic" even though it may also include meteors from small showers.

The algorithm for this calculation uses data from the database of all meteors recorded by the CARMELo network. First, it asks the user to identify certain days on which no significant meteor shower activity is expected. These days are selected as close as possible to the date being analyzed. This data is then averaged to form a second database called the "sporadic average".

This database is then subtracted from the one for the days under examination, during which a meteor shower is presumed to be present. Any negative values are eliminated, and the profile is smoothed using a smoothing function.

The figure is then divided by the sine of the radiant's altitude above the horizon, calculated for an average Italian location in the same way as the algorithm used to calculate the ZHR (Zenithal Hourly Rate), which, as we recall, is:

$$ZHR = \frac{N \cdot r^{6.5-lm}}{\sin h_R \cdot F \cdot T_{eff}}$$

Where:

- *N*: number of meteors counted.
- L_m: the limiting magnitude of a star that is visible to the observer.
- *r*: shower's density (the ratio indicating how many more meteors are visible for each magnitude; typically ranging from 2.0 to 3.5).
- h_r: angular height of the radiant above the horizon in degrees.
- T_{eff}: actual observation time (in hours).
- *F*: field-of-view correction factor.

The temporal resolution, which is 15 minutes in the original data, is retained at that value; therefore, the term *H* in RZHR should be considered as *H/4*.

To estimate the activity of the Arietids, the sample of sporadic meteors (in *Figure 2*) was collected during the second half of May, when the shower had not yet reached a significant level of activity and no other major meteor showers were active. The analysis was then extended to data collected between June 4 and 21, a period during which the database shows a clear increase in the number of meteors detected.

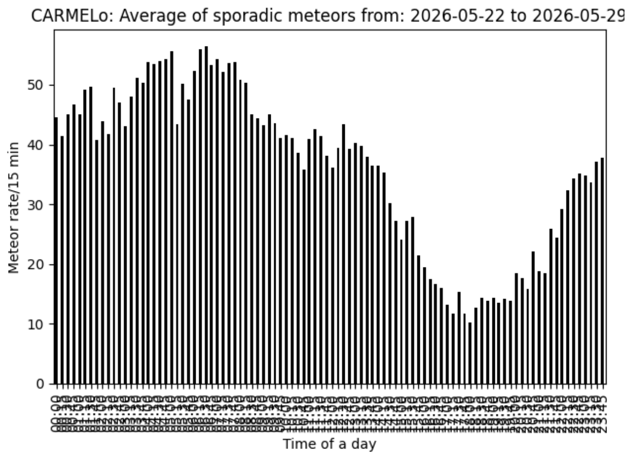

Figure 2 – A sample of sporadic meteors collected in the second half of May 2026.

Figure 3 shows the trend in meteor activity recorded by the network, limited to the hours when the radiant was above the horizon for most of the observing stations, between solar longitudes 73° and 89° (i.e. between June 4 and June 21).

Calculating the *RZHR* using the algorithm we developed (Barbieri and Maglione, 2026) yields the results shown in *Figure 4*.

A first peak is observed at a solar longitude of approximately 77°, which is in good agreement with the predictions reported in the literature. In addition to this, however, a second, more pronounced peak also emerges around a solar longitude of 82°, corresponding to approximately June 13, thus occurring a few days later than the generally predicted peak.

To make the data easier to interpret, we interpolated the maximum values to construct a smoothed curve, which is shown in *Figure 5*.

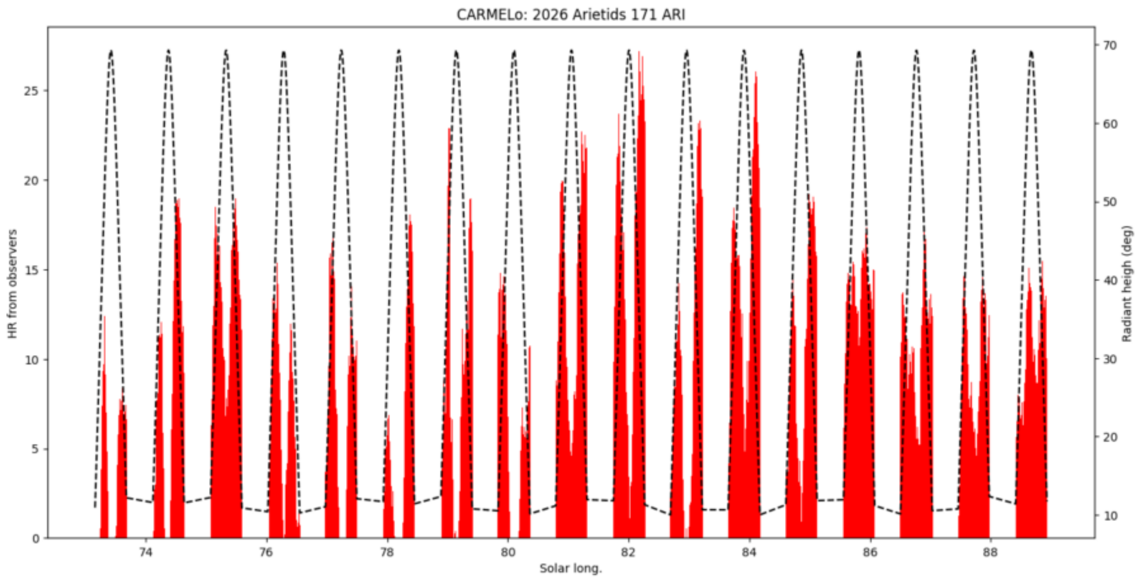

Figure 3 – Meteor activity between June 4 and 21, 2026, limited to the hours when the radiant was at least 10° above the horizon, as a function of solar longitude, and the altitude of the Arietid radiant (dashed line). The contribution of the zeta-Perseids (ζ-Perseids) is neglected.

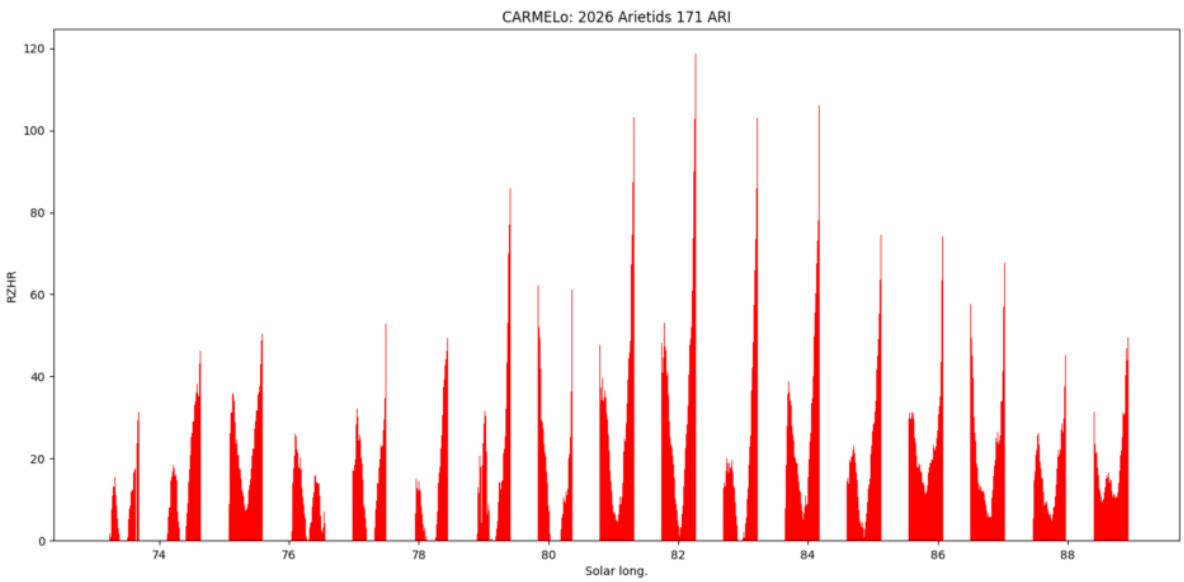

Figure 4 – Residual distribution of events. The contribution of the zeta-Perseids (ζ-Perseids) is negligible.

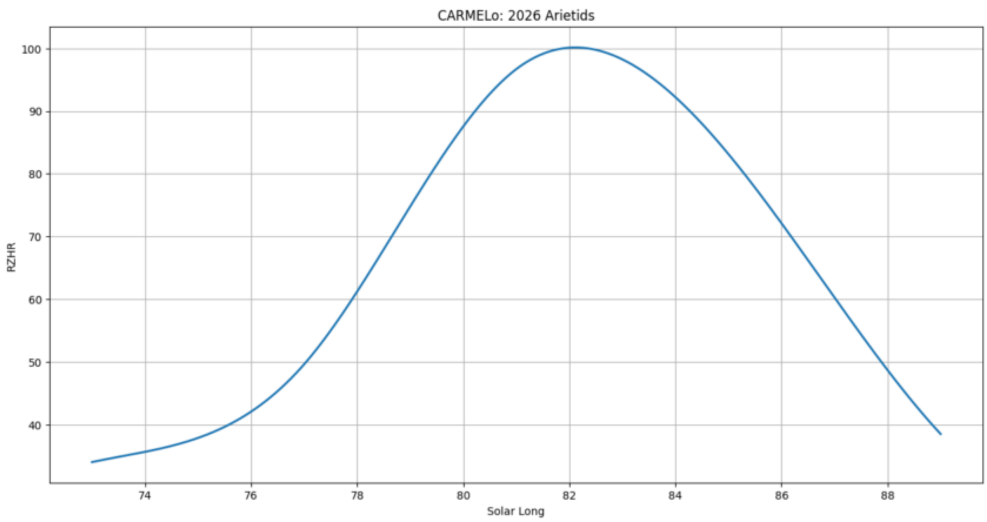

Figure 5 – Distribution of events after interpolation, as a function of solar longitude.

6 Zeta Perseids

The Arietids are not the only daytime meteor shower active in June. As we mentioned at the beginning, the zeta-Perseids (ζ-Perseids) are also expected during the same period; this shower has very similar observing conditions: the radiant is close to the Sun, making visual observations extremely difficult, so much so that, in this case as well, the information available in the literature is rather limited.

Unlike the Arietids, considered the main daytime meteor shower of the year, the zeta-Perseids are generally classified as a shower with low activity. For this reason, no in-depth dedicated analysis has been conducted, particularly in light of two factors. First, data from the Canadian CMOR radar show extremely low activity during the period of interest. Furthermore, when applying the *RZHR* algorithm to the data collected in June, taking into account the radiant of the zeta-Perseids, even after interpolation, no significant deviations emerge compared to the results for the Arietids, confirming the limited impact of this shower on our observations.

7 The CARMELO network

The network currently consists of 17 receivers located in Italy, Spain, the UK, Switzerland and the USA. The European receivers are tuned to the Graves radar station frequency in France, which is 143.050 MHz. Participating in the network are:

- Lorenzo Barbieri, Budrio (BO) ITA;
- Associazione Astrofili Bolognesi, Bologna ITA;
- Associazione Astrofili Bolognesi, Medelana (BO) ITA;
- Paolo Fontana, Castenaso (BO) ITA;
- Associazione Astrofili Pisani, Orciatico (PI) ITA;
- Gruppo Astrofili Persicetani, San Giovanni in Persiceto (BO) ITA;
- Roberto Nesci, Foligno (PG) ITA;
- MarSEC, Marana di Crespadoro (VI) ITA;
- Gruppo Astrofili Vicentini, Arcugnano (VI) ITA;
- Associazione Ravennate Astrofili Rheyta, Ravenna (RA) ITA;
- Mike German a Hayfield, Derbyshire UK;
- Mike Otte, Pearl City, Illinois USA.
- Yuri Malagutti, Comano (TI) CH.
- Leslie Fry, Trawscoed Ceredigion, Wales UK
- Brian Coleman, Redenham Observatory, Andover, England UK
- Radio club La Salle University, Barcellona ESP
- Alberto Latini, Carona (TI) CH

The authors' hope is that the network can expand both quantitatively and geographically, thus allowing the production of better-quality data.

References

Barbieri L., Maglione M. (2026). "May 2026 CARMELo report". *eMetN Meteor Journal*, **11**, 307–310.

Jenniskens P. (2023). Atlas of Earth's meteor showers, Elsevier Science Ltd.

Ohtsuka K., Nakano S., Yoshikawa M. (2003). "On the Association among Periodic Comet 96P/Machholz, Arietids, the Marsden Comet Group, and the Kracht Comet Group". *Publications of the Astronomical Society of Japan*, **55**, 321–324.

Serra Romano, Taddia Lucio, Mazzi Thomas (2025). Sette volte a Tunguska. In riga edizioni. ISBN: 9788893644808

July 2026 CARMELo report

Lorenzo Barbieri[1], **Mariasole Maglione**[2], **William Rivato**[3], **Alberto Latini**[4]

[1] **CARMELo network and AAB: Associazione Astrofili Bolognesi, Italy**
carmelometeor@gmail.com

[2] **CARMELo network, GAV, Gruppo Astrofili Vicentini, Italy**
mariasole@astrofilivicentini.it

[3] **CARMELo network and MarSEC, Marana Space Exploration Center, Italy**

[4] **CARMELo network, Sezione Meteore UAI and IMO, Italy**

The CARMELO network (Cheap Amateur Radio Meteor Echoes LOgger) is a collaboration of SDR radio receivers aimed at detecting meteor echoes. This report presents the data for July 2026.

1 Introduction

In July, the CARMELO network detected moderate meteor activity. Two meteor showers were identified by radio observations in the Northern Hemisphere during the month: the alpha Lacertids (ALA#328) and the psi Cassiopeids (PCA#187). Toward the end of the month, activity increased slightly for the Southern delta Aquariids (5 SDA).

2 Methods

The CARMELO network consists of SDR radio receivers. In them, a microprocessor (Raspberry) performs three functions simultaneously:

- By driving a dongle, it tunes the frequency on which the transmitter transmits and tunes like a radio, samples the radio signal and through the FFT (Fast Fourier Transform) measures frequency and received power.
- By analyzing the received data for each packet, it detects meteor echoes and discards false positives and interference.
- It compiles a file containing the event log and sends it to a server.

The data are all generated by the same standard, and are therefore homogeneous and comparable. A single receiver can be assembled with a few devices whose total current cost is about 210 euros.

To participate in the network read the instructions on this page[13].

3 July data

In the plots that follow, all available at this page[14], the abscissae represent time, which is expressed in UT (Universal Time) or in solar longitude (Solar Long), and the ordinates represent the hourly rate, calculated as the total number of events recorded by the network in an hour divided by the number of operating receivers. The time resolution is 15 minutes.

In *Figure 1*, the trend of signals detected by the receivers is given for the month of July.

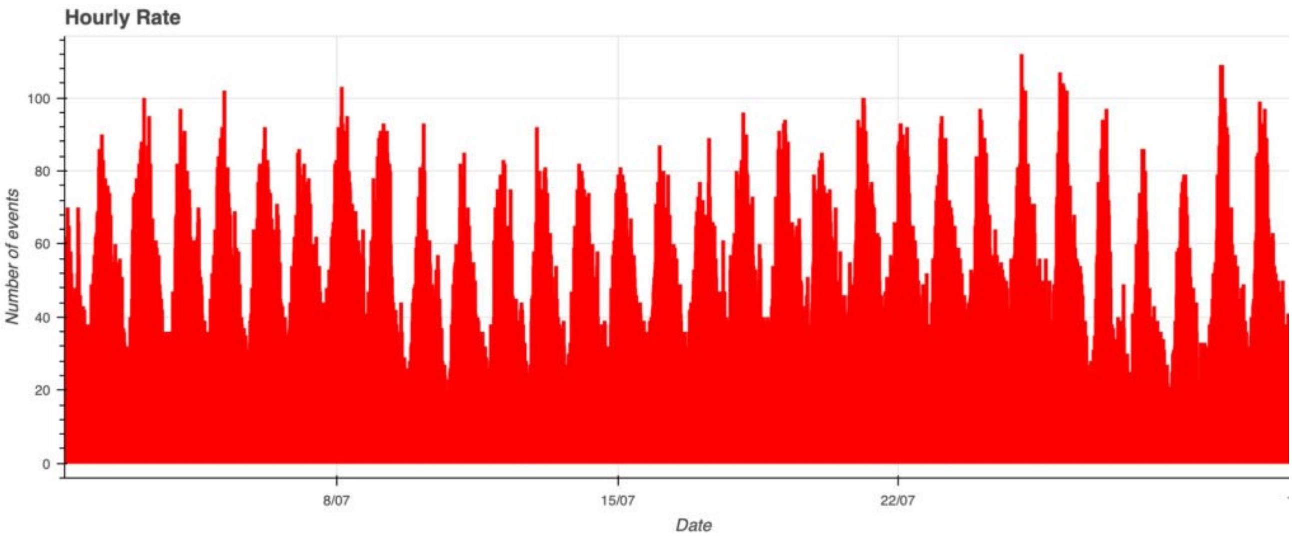

Figure 1 – July 2026 data trend.

[13] http://www.astrofiliabologna.it/about_carmelo

[14] http://www.astrofiliabologna.it/graficocarmelohr

4 Alpha-Lacertids and psi-Cassiopeiids

The alpha-Lacertids (ALA#328) and the psi-Cassiopeiids (PCA#187) are two minor meteor showers associated with the summer sky in the Northern Hemisphere. These showers have been known for some time, but they are much less intense and have been studied far less than the major annual showers: the relatively small number of meteors associated with them makes it difficult to clearly distinguish their activity from the background of sporadic meteors and other showers active during the same period.

The alpha-Lacertids have their radiant in the region of the constellation Lacerta, approximately at RA 343° and Dec +53°, and reach an approximate peak in the first half of July, while the psi-Cassiopeiids have their radiant in the constellation Cassiopeia, at approximately RA 356° and Dec +71°, and reach an approximate peak around the middle of the month.

In July 2026, radio observations conducted in the Northern Hemisphere revealed activity primarily from these two meteor showers. According to data from the CMOR (Canadian Meteor Orbit Radar), the alpha-Lacertids are active roughly from July 9 to 14, while activity from the psi-Cassiopeiids is detectable approximately from July 15 to 25[15].

In data collected by the CARMELo network, however, both meteor showers are difficult to identify. Their weak activity produces relatively small variations compared to the overall meteor background, which can easily be confused with normal fluctuations in the number of sporadic events detected by the network. For this reason, unlike what happens with more intense showers, the graphs (e.g., *Figure 1*) do not show a particularly distinct peak attributable to the ALA or PCA.

5 Southern delta-Aquariids

The Southern delta-Aquariids (SDA#5) are one of the major meteor showers of the summer. They are active for several weeks, roughly from mid-July to the second half of August, with the peak activity concentrated in the last days of July. The radiant is located in the constellation Aquarius, near the star Delta Aquarii, and because of its relatively southern position, the shower is particularly favorable for observers in the southern hemisphere, although it can also be observed from the mid-latitudes of the northern hemisphere.

The meteors of the Southern delta-Aquariids enter Earth's atmosphere at a speed of about 41 km/s, and the shower can reach a ZHR of around 20–25 meteors per hour. Unlike showers characterized by a very brief and well-defined peak, however, the SDA generally exhibit activity that is quite extended over time, with variations that can unfold over the course of several days.

Observations from the Global Meteor Network (GMN) have shown an increase in activity over several years in the region around solar longitudes 126–127°, although the pattern can vary significantly from year to year (Roggemans et al., 2026).

However, analyzing the Southern delta-Aquariids in the data collected by the CARMELo network in July 2026 presents a problem. On July 27, just days before the shower's peak activity, the network's highest-performing receiver malfunctioned due to a lightning strike. The system was restored on July 30, resulting in a gap of about three days in the observations.

This interruption has particularly noticeable consequences for the analysis using the RZHR algorithm (Barbieri and Maglione, 2026), as it affects precisely the most important part of the SDA activity profile.

6 The construction of RZHR

By RZHR (Radio Zenithal Hourly Rate), we mean the hourly rate of radio meteors in a shower, calculated by processing data from meteor scatter receivers.

This tool allows us to make a significant leap in quality, moving away from the qualitative analysis we have conducted so far (which relied exclusively on graphs) and transitioning to the direct processing of data from our database. To do this, we developed a Python script with the help of the "Cursor" tool, an AI-powered code editor created by Anysphere. This support proved crucial in developing a satisfactory script.

First, it should be clarified that, in calculating the RZHR, we make certain approximations, including:

- We do not take into account that the varying geographical distribution of receivers causes them to "see" meteors from slightly different angles.
- We disregard the fact that observations are not isotropic but are influenced by antenna pointing, which favors a specific sector of the sky over the entire sky.
- We define a contribution as "sporadic" even though it may also include meteors from small showers.

The algorithm for this calculation uses data from the database of all meteors recorded by the CARMELo network. First, it asks the user to identify certain days on which no significant meteor shower activity is expected. These days are selected as close as possible to the date being analyzed. This data is then averaged to form a second database called the "sporadic average."

This database is then subtracted from the one for the days under examination, during which a meteor shower is presumed to be present. Any negative values are eliminated, and the profile is smoothed using a smoothing function.

The figure is then divided by the sine of the radiant's altitude above the horizon, calculated for an average Italian

[15] https://aquarid.physics.uwo.ca/research/radar/cmor_intro.html

location in the same way as the algorithm used to calculate the ZHR (Zenithal Hourly Rate), which, as we recall, is:

$$ZHR = \frac{N \cdot r^{6.5-lm}}{\sin h_R \cdot F \cdot T_{eff}}$$

Where:

- N: number of meteors counted.
- L_m: the limiting magnitude of a star that is visible to the observer.
- r: shower's density (the ratio indicating how many more meteors are visible for each magnitude; typically ranging from 2.0 to 3.5).
- h_r: angular height of the radiant above the horizon in degrees.
- T_{eff}: actual observation time (in hours).
- F: field-of-view correction factor.

The temporal resolution, which is 15 minutes in the original data, is retained at that value; therefore, the term *H* in RZHR should be considered as *H/4*.

To estimate the activity of the Southern delta-Aquariids, the sample of sporadic meteors (in *Figure 2*) was collected during the second half of June, when no other major meteor showers were active.

Figure 3 shows the trend in meteor activity recorded by the network, limited to the hours when the radiant was above the horizon for most of the observing stations between July 23 and August 7 (between solar longitudes 120° and 134°).

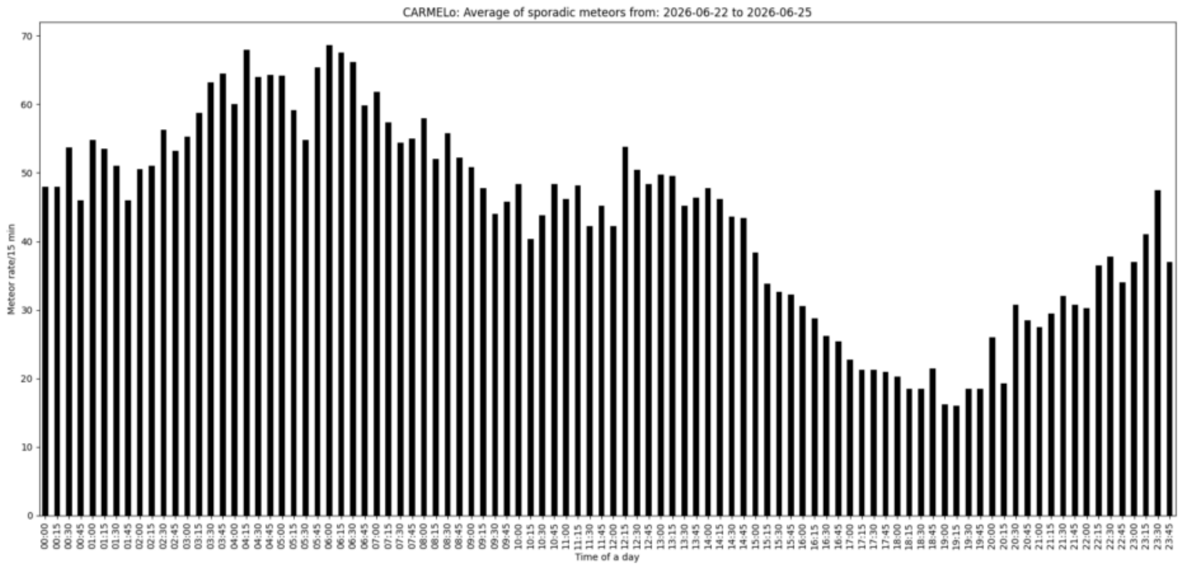

Figure 2 – A sample of sporadic meteors collected in the second half of June 2026 for analysis of the Southern delta-Aquariids.

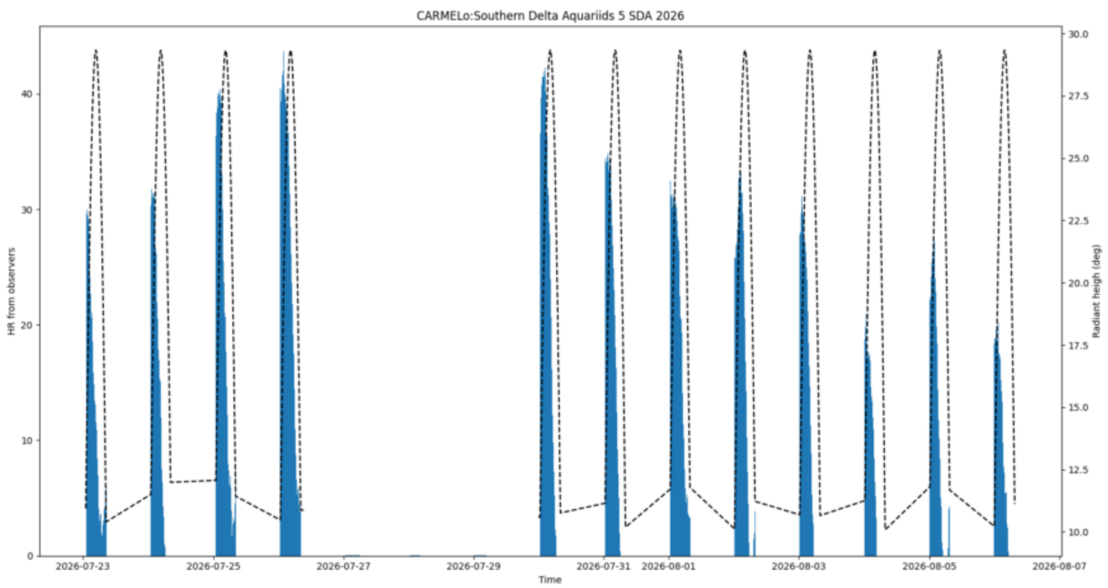

Figure 3 – Meteor activity trend between July 23 and August 7, 2026, limited to the hours when the radiant was at least 10° above the horizon, as a function of solar longitude, and the altitude of the Southern delta-Aquariids' radiant (dashed line). The three-day gap in data is due to the malfunction mentioned above.

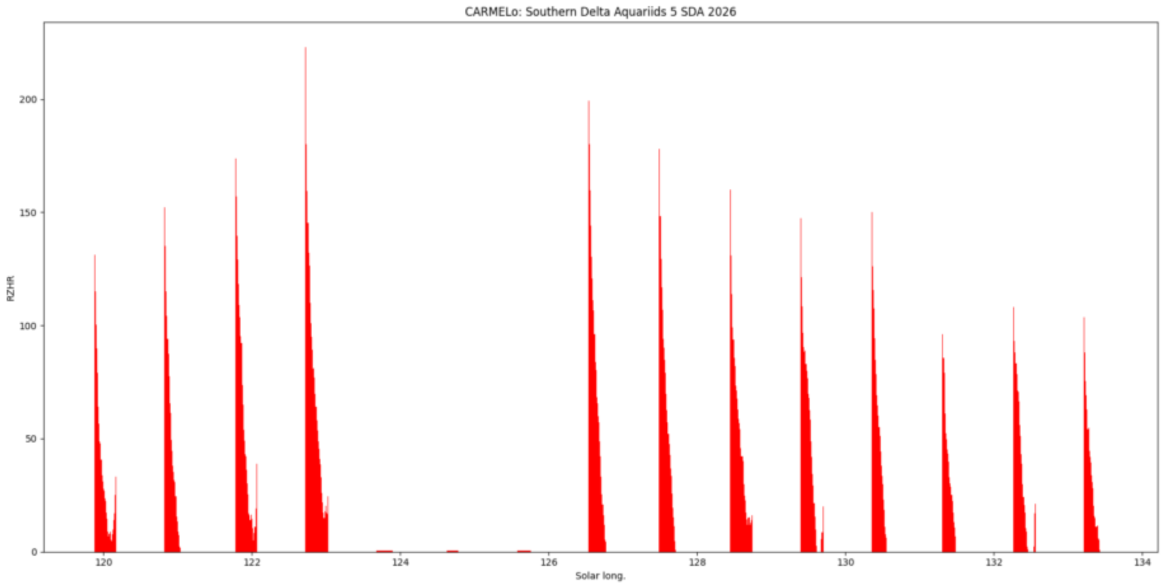

Figure 4 – Residual distribution of events.

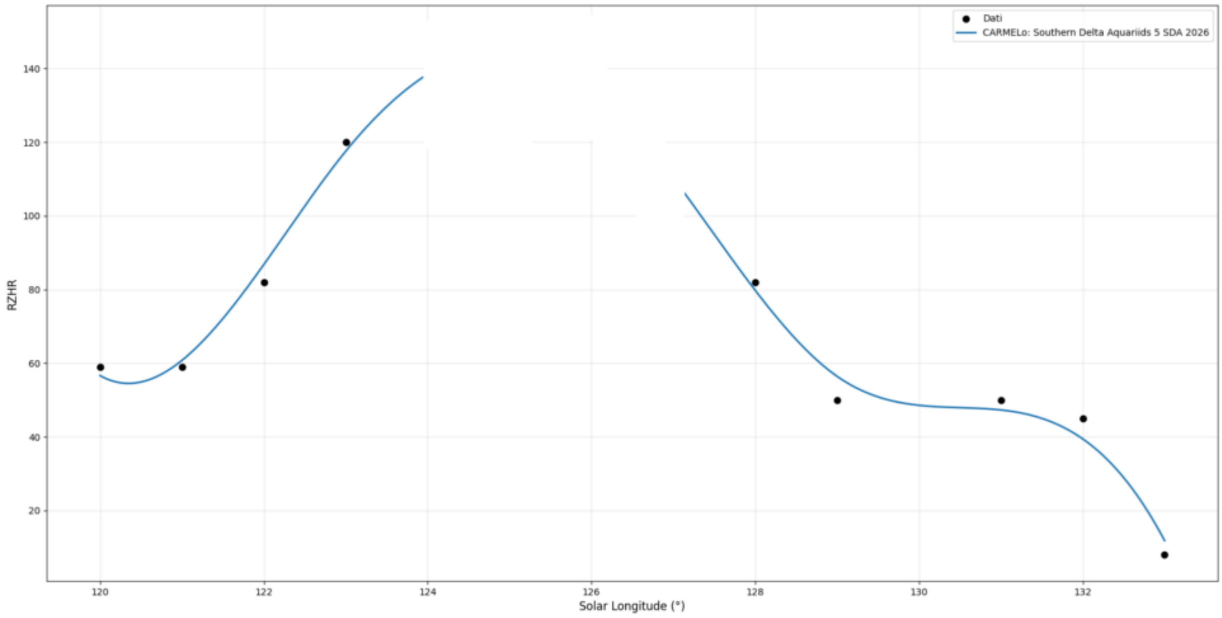

Figure 5 – Distribution of events after interpolation, as a function of solar longitude.

It can be seen that most of the events attributable to the meteor shower are observed in the early morning hours, when the radiant reaches its highest point in the sky.

Calculating the RZHR using the algorithm we developed (Barbieri and Maglione, 2026) yields the results shown in *Figure 4*.

In *Figure 5*, on the other hand, we present a reconstruction of the trend in daily highs, shown as a curve obtained by interpolating the maximum values.

These latest graphs clearly reveal the main limitation of the data collected this year: due to the malfunction mentioned before, observations are missing around solar longitudes 125°–127°, that is, corresponding to a particularly interesting phase of the Southern delta-Aquariids' activity. In fact, video observations from the GMN network place the shower's peak around solar longitudes 126–127°.

The "gap" of about three days in the CARMELo data therefore prevents us from fully reconstructing the peak of the 2026 Southern delta-Aquariids and, above all, from directly comparing its position and intensity with what was observed using other techniques.

7 The CARMELO network

The network currently consists of 18 receivers located in Italy, Spain, the UK, Switzerland and the USA. The European receivers are tuned to the Graves radar station frequency in France, which is 143.050 MHz. Participating in the network are:

- Lorenzo Barbieri, Budrio (BO) ITA;
- Associazione Astrofili Bolognesi, Bologna ITA;
- Associazione Astrofili Bolognesi, Medelana (BO) ITA;
- Paolo Fontana, Castenaso (BO) ITA;
- Associazione Astrofili Pisani, Orciatico (PI) ITA;
- Gruppo Astrofili Persicetani, San Giovanni in Persiceto (BO) ITA;
- Roberto Nesci, Foligno (PG) ITA;
- MarSEC, Marana di Crespadoro (VI) ITA;
- Gruppo Astrofili Vicentini, Arcugnano (VI) ITA;
- Associazione Ravennate Astrofili Rheyta, Ravenna (RA) ITA;
- Mike German a Hayfield, Derbyshire UK;
- Mike Otte, Pearl City, Illinois USA.
- Yuri Malagutti, Comano (TI) CH.
- Leslie Fry, Trawscoed Ceredigion, Wales UK
- Brian Coleman, Redenham Observatory, Andover, England UK
- Radio club La Salle University, Barcellona ESP
- Alberto Latini, Carona (TI) CH
- AstroCampania, Agerola (NA) ITA

The authors' hope is that the network can expand both quantitatively and geographically, thus allowing the production of better-quality data.

References

Barbieri L., Maglione M. (2026). "May 2026 CARMELo report". *eMetN Meteor Journal*, **11**, 307–310.

Roggemans P., Campbell-Burns P., Kalina M., McIntyre M., Scott J. M., Šegon D., Vida D. (2026b). "Global Meteor Network report 2025". *eMetN Meteor Journal*, **11**, 89–129.

Radio meteors June 2026

Felix Verbelen

Vereniging voor Sterrenkunde & Volkssterrenwacht MIRA, Grimbergen, Belgium
felix.verbelen@gmail.com

An overview of the radio observations during June 2026 is given.

1 Introduction

The graphs show both the daily totals (*Figure 1 and 2*) and the hourly numbers (*Figure 3 and 4*) of "all" reflections counted automatically, and of manually counted "overdense" reflections, overdense reflections longer than 10 seconds and longer than 1 minute, as observed here at Kampenhout (BE) on the frequency of our VVS-beacon (49.99 MHz) during the month of June 2026.

The hourly numbers, for echoes shorter than 1 minute, are weighted averages derived from:

$$N(h) = \frac{n(h-1)}{4} + \frac{n(h)}{2} + \frac{n(h+1)}{4}$$

Local interference and unidentified noise remained very limited, but severe lightning activity was recorded on 11 days. On 6 of these days, this also occurred in the immediate vicinity of the beacon, which made the automatic counting of meteors during those periods very difficult (*Figure 5*). The automatic counts of "all" meteors were therefore manually corrected for those periods. There were also numerous strong solar flares, mostly of type III, and occasionally type II.

The main highlights of the month were the daytime showers, primarily the Arietids, but smaller showers such as the zeta Perseids and others also made the month particularly interesting.

Over the course of the entire month, 9 reflections lasting longer than 1 minute were observed here. A selection of these, along with several other interesting reflections, is shown in *Figures 6 to 20*. Many more are available upon request.

In addition to the usual graphs, you will also find the raw counts in cvs-format[16] from which the graphs are derived. The table contains the following columns: day of the month, hour of the day, day + decimals, solar longitude (epoch J2000), counts of "all" reflections, overdense reflections, reflections longer than 10 seconds and reflections longer than 1 minute, the numbers being the observed reflections of the past hour.

[16] https://www.emeteornews.net/wp-content/uploads/2026/07/202606_49990_FV_rawcounts.csv

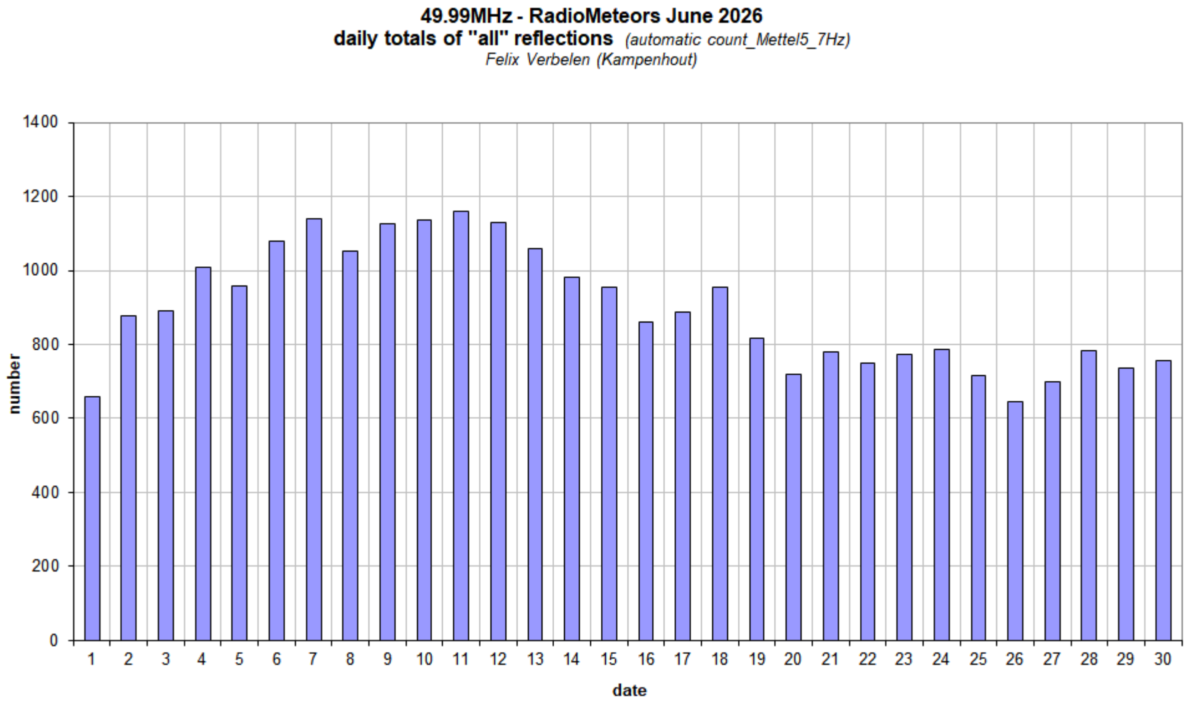

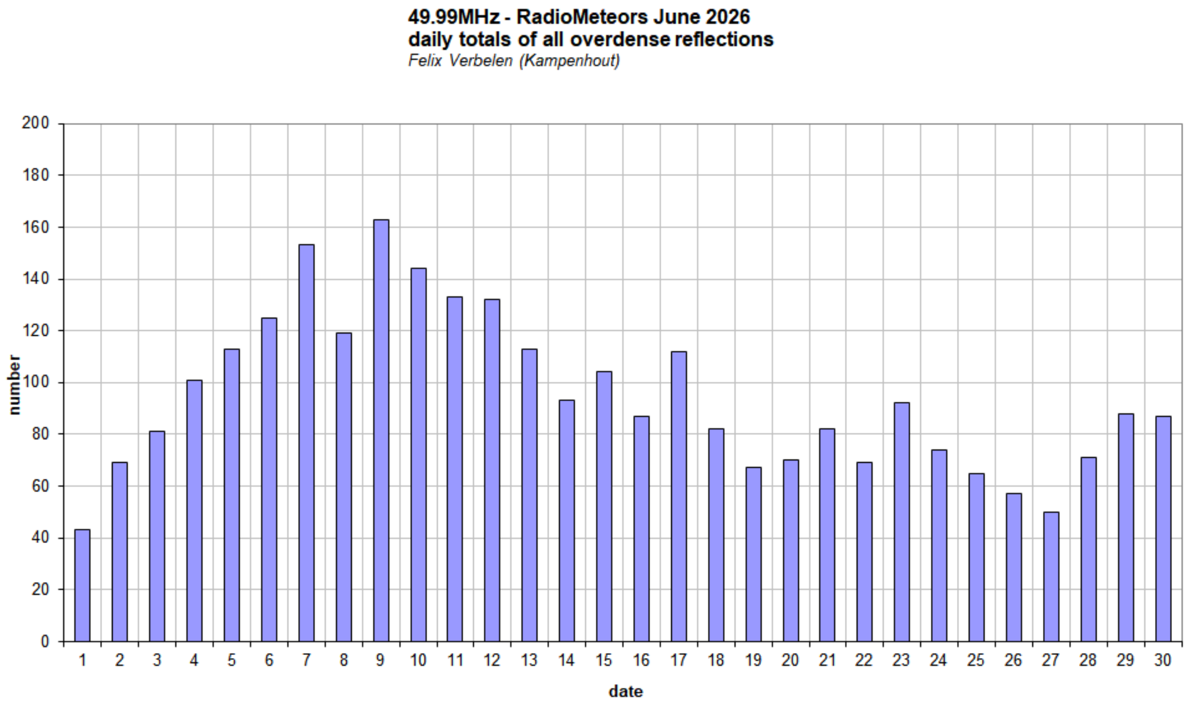

Figure 1 – The daily totals of "all" reflections counted automatically, and of manually counted "overdense" reflections, as observed here at Kampenhout (BE) on the frequency of our VVS-beacon (49.99 MHz) during June 2026.

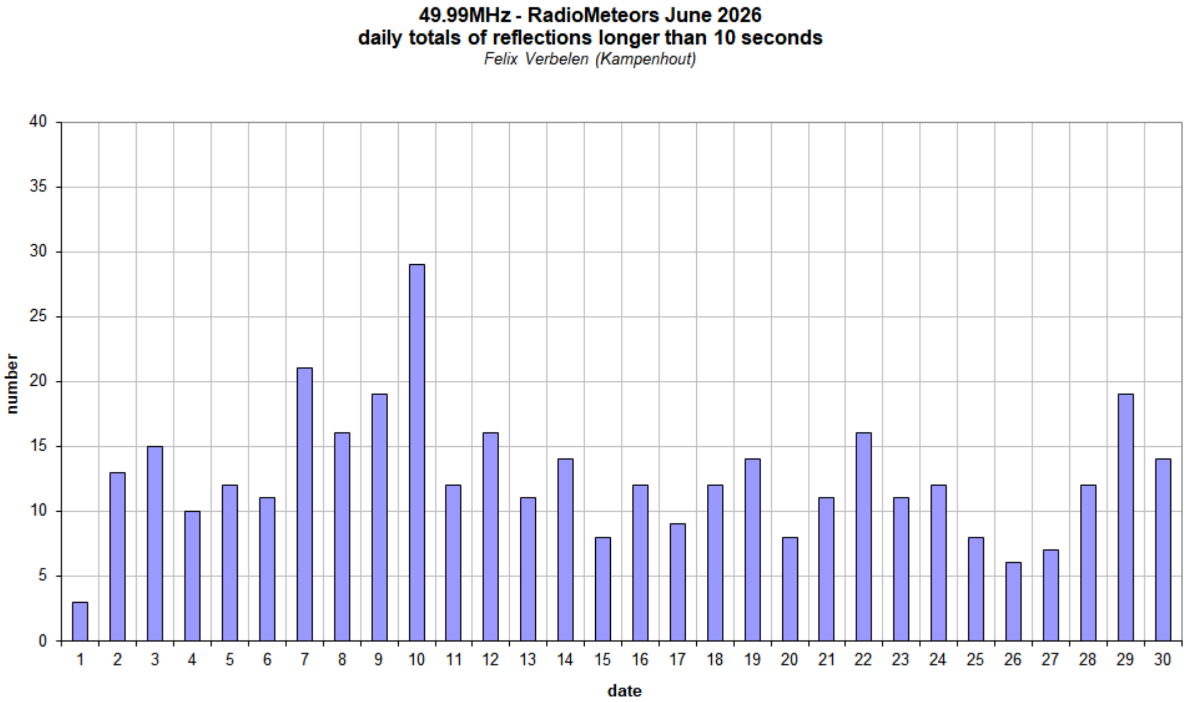

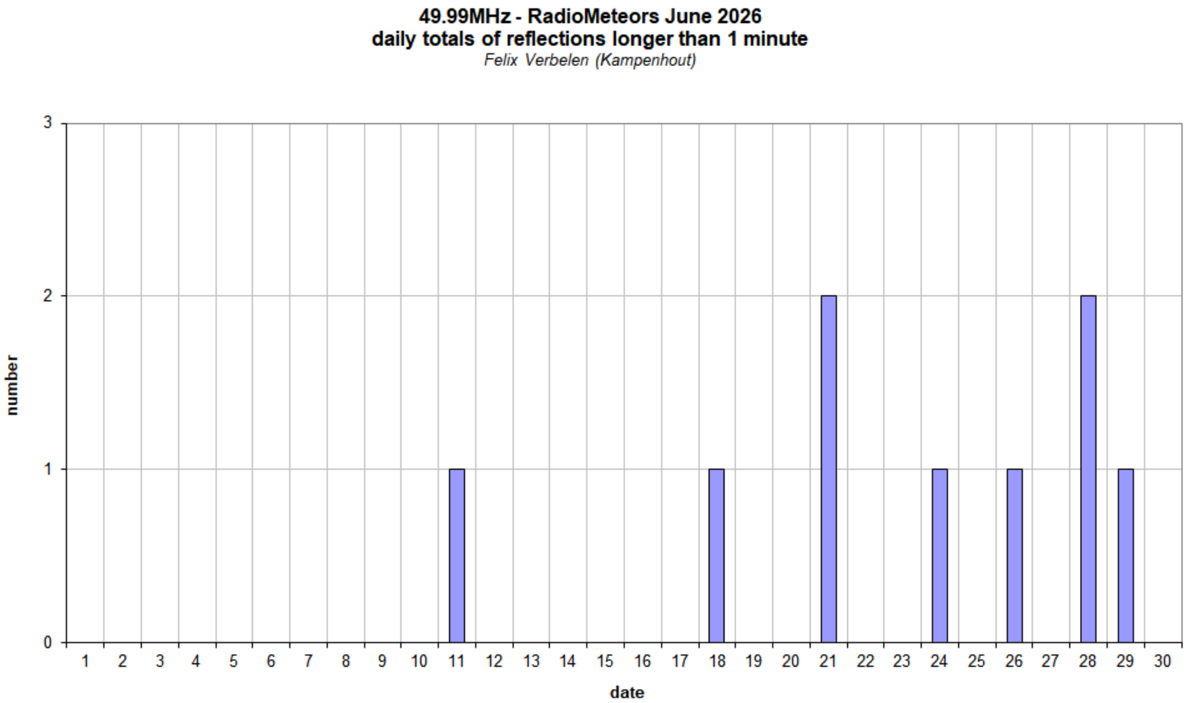

Figure 2 – The daily totals of overdense reflections longer than 10 seconds and longer than 1 minute, as observed here at Kampenhout (BE) on the frequency of our VVS-beacon (49.99 MHz) during June 2026.

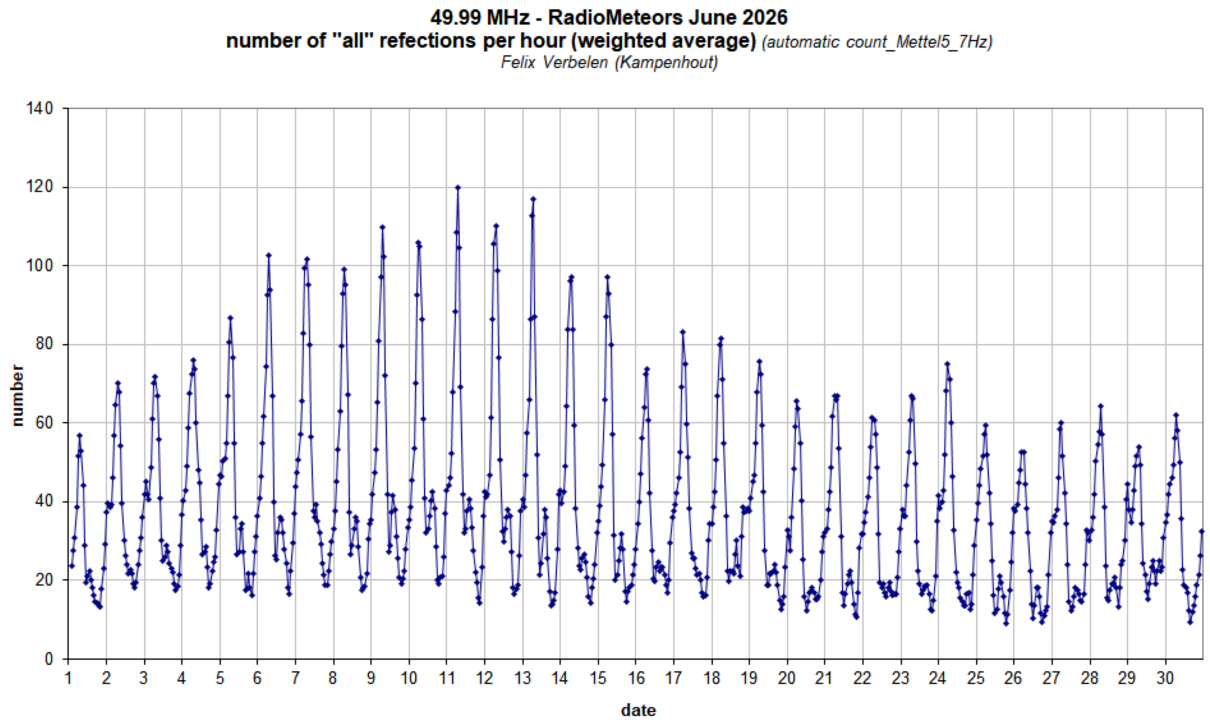

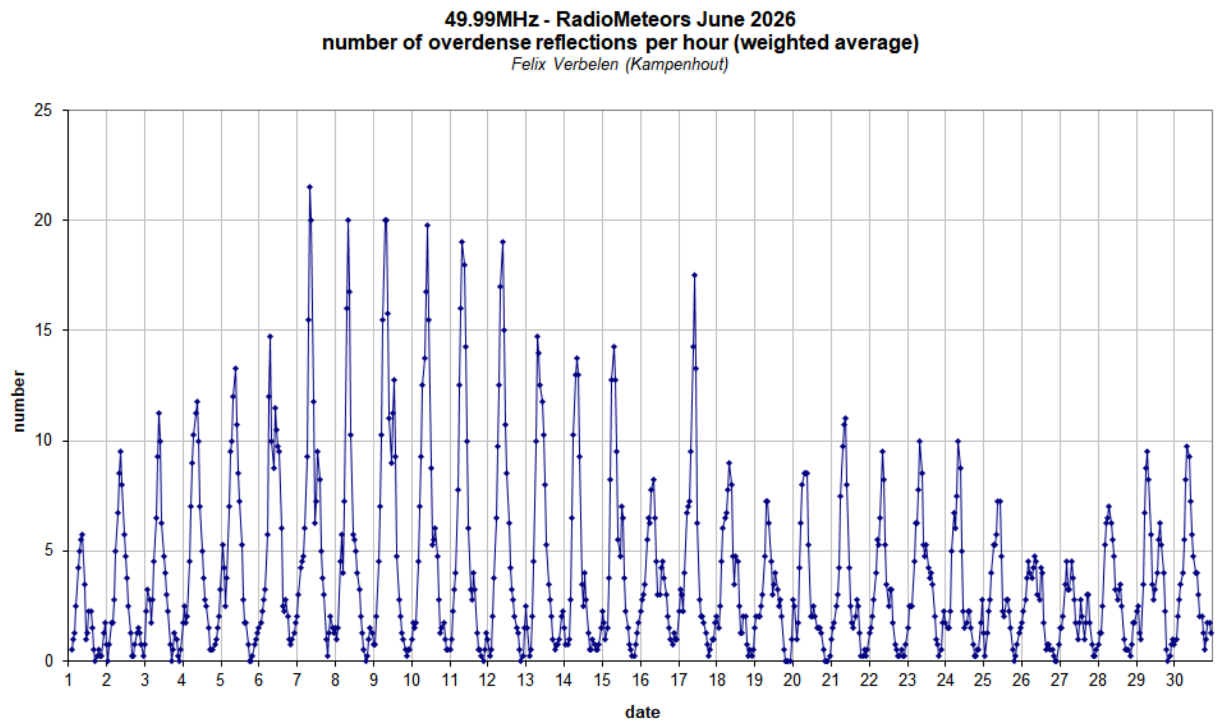

Figure 3 – The hourly numbers of "all" reflections counted automatically, and of manually counted "overdense" reflections, as observed here at Kampenhout (BE) on the frequency of our VVS-beacon (49.99 MHz) during June 2026.

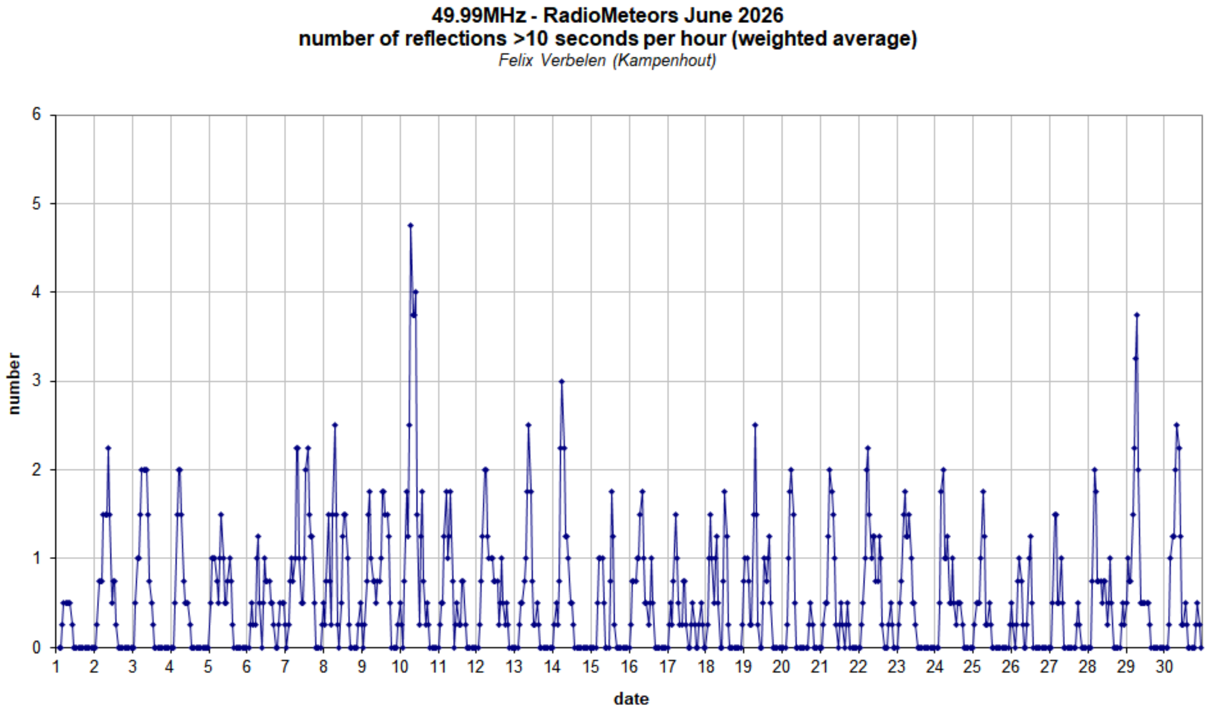

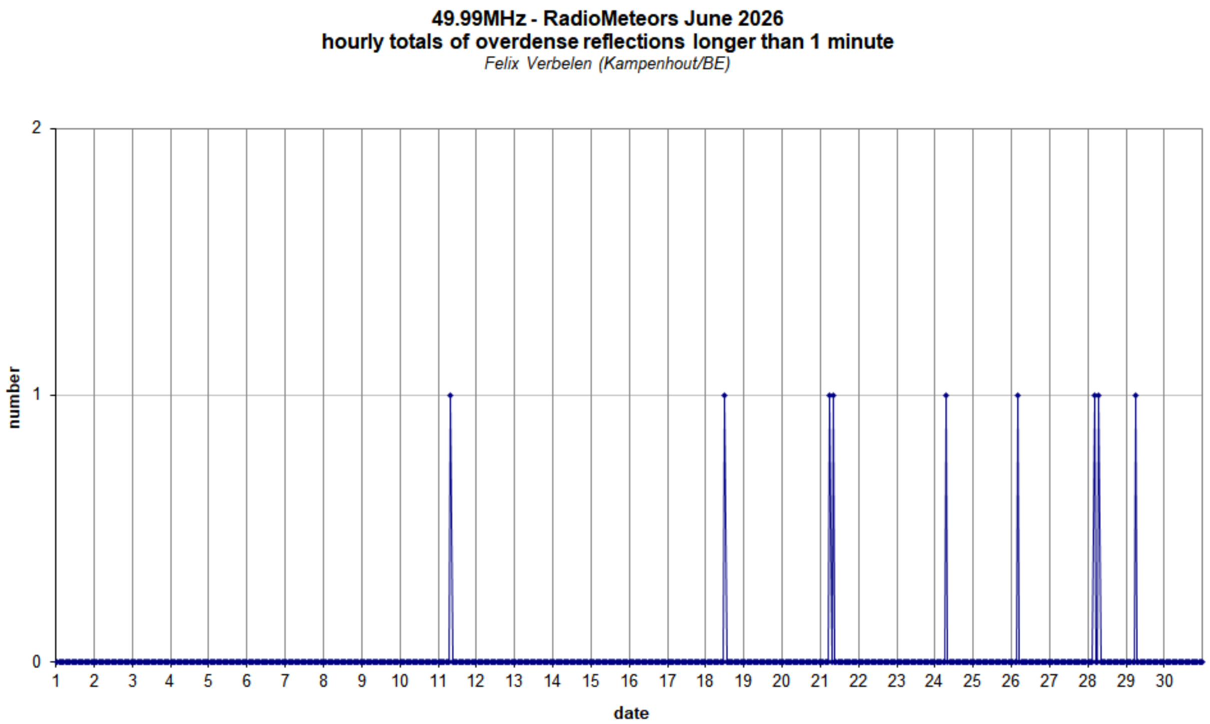

Figure 4 – The hourly numbers of overdense reflections longer than 10 seconds and longer than 1 minute, as observed here at Kampenhout (BE) on the frequency of our VVS-beacon (49.99 MHz) during June 2026.

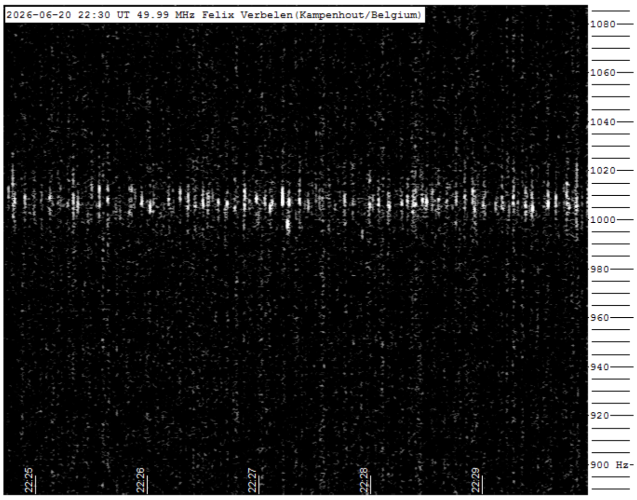

Figure 5 – Severe lightning activity occurred in the immediate vicinity of the beacon, which made the automatic counting of meteors during those periods very difficult.

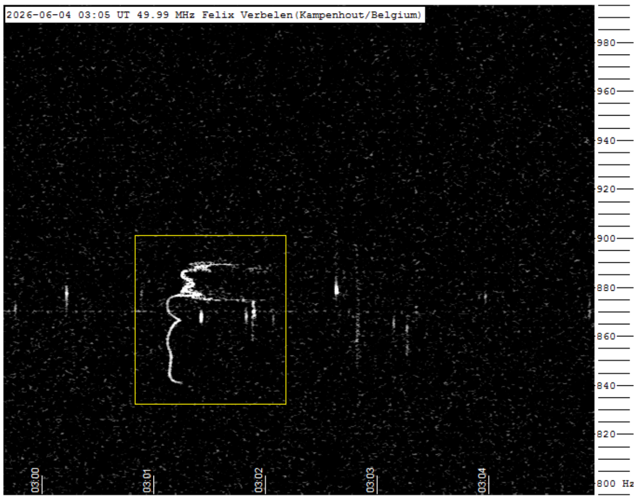

Figure 6 – Meteor echo June 4, 03^{h}05^{m} UT.

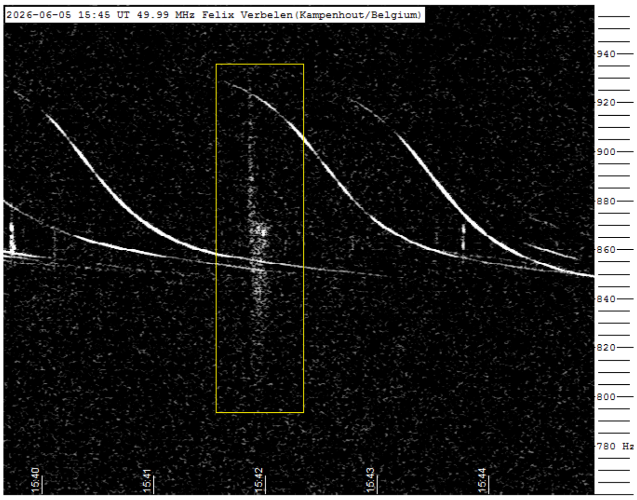

Figure 7 – Meteor echo June 5, 15^{h}45^{m} UT.

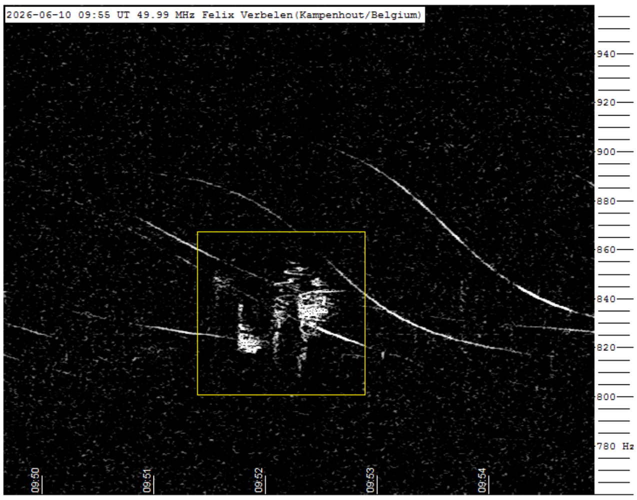

Figure 8 – Meteor echo June 10, 9^{h}55^{m} UT.

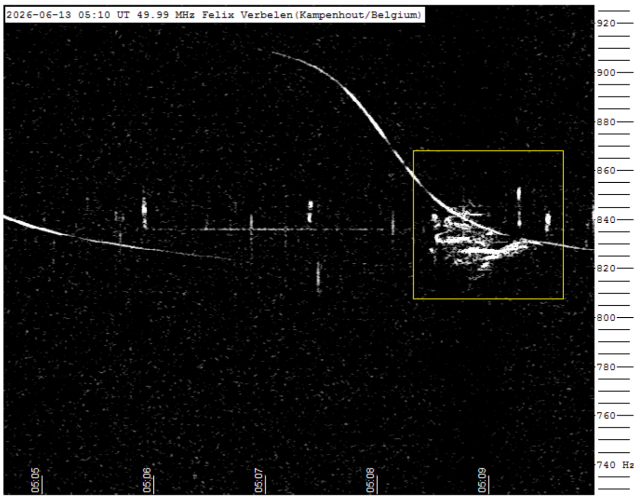

Figure 9 – Meteor echo June 13, 5^{h}10^{m} UT.

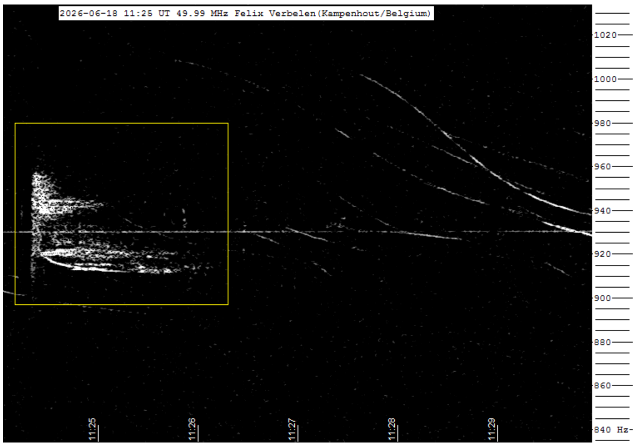

Figure 10 – Meteor echo June 18, 11^{h}25^{m} UT.

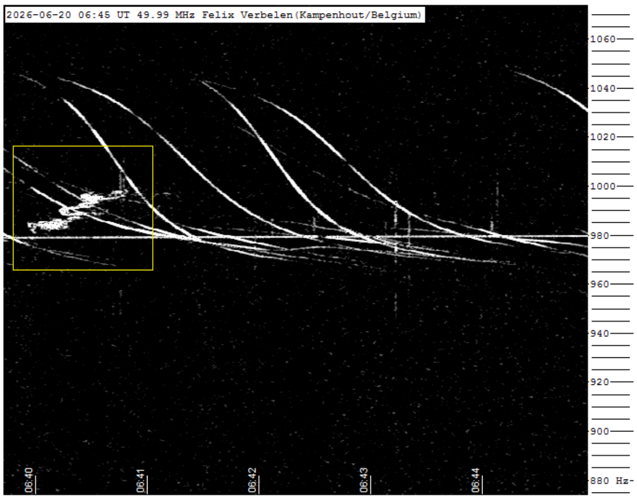

Figure 11 – Meteor echo June 20, 6^{h}45^m UT.

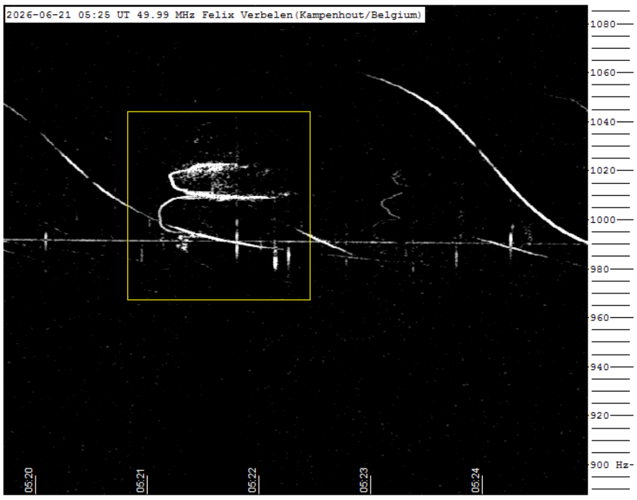

Figure 12 – Meteor echo June 21, 5^{h}25^m UT.

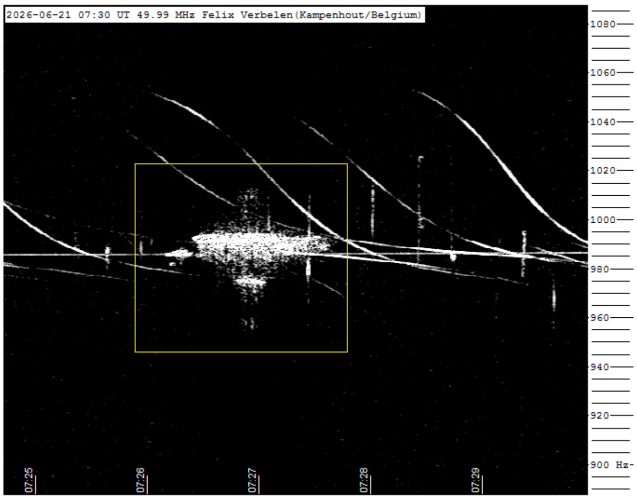

Figure 13 – Meteor echo June 21, 7^{h}30^m UT.

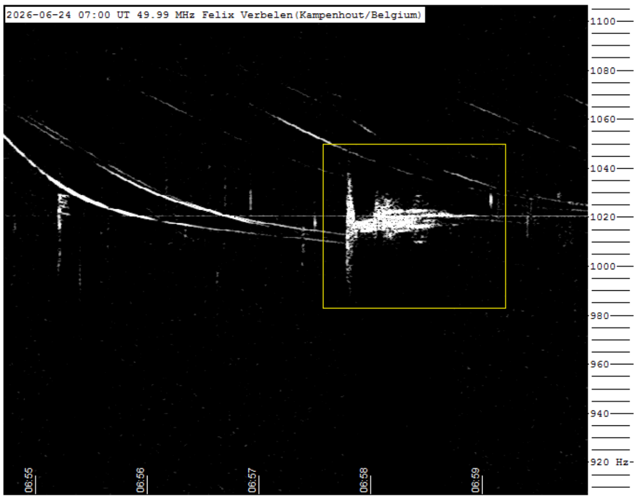

Figure 14 – Meteor echo June 24, 7^{h}00^m UT.

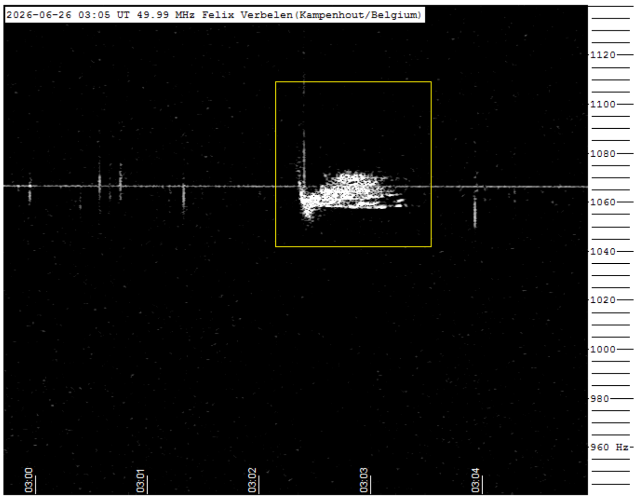

Figure 15 – Meteor echo June 26, 3^{h}05^m UT.

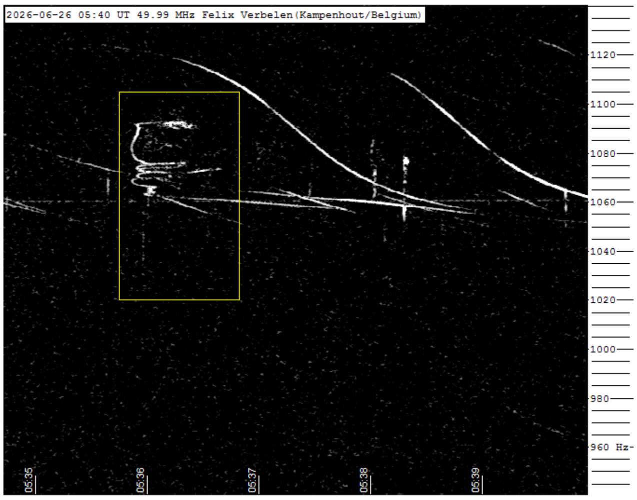

Figure 16 – Meteor echo June 26, 5^{h}40^m UT.

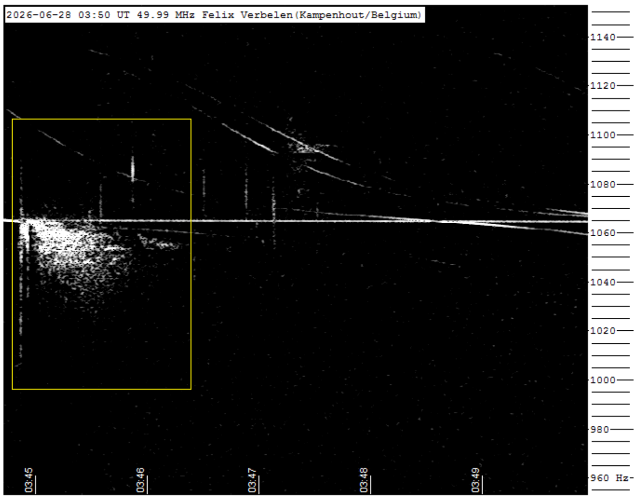

Figure 17 – Meteor echo June 28, 3^{h}50^m UT.

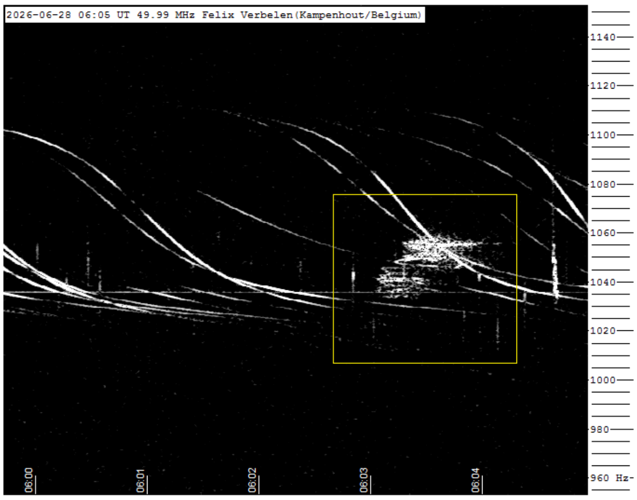

Figure 18 – Meteor echo June 28, 6^{h}05^m UT.

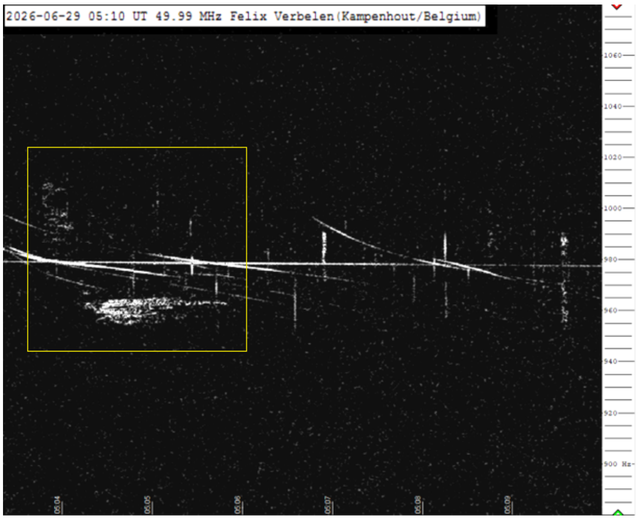

Figure 19 – Meteor echo June 29, 5^{h}10^m UT.

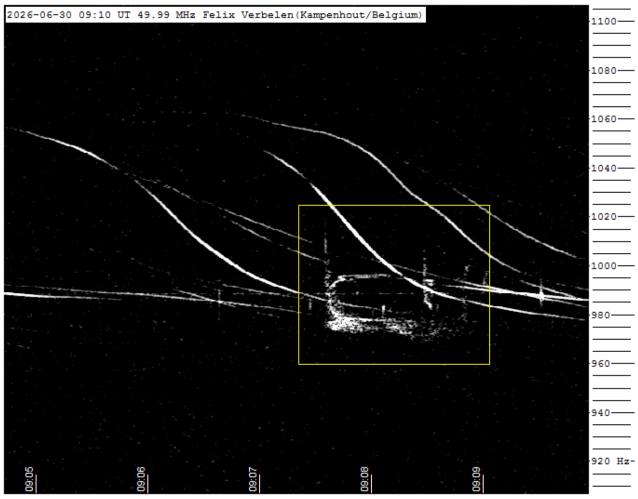

Figure 20 – Meteor echo June 30, 9^{h}10^m UT.

Radio meteors July 2026

Felix Verbelen

Vereniging voor Sterrenkunde & Volkssterrenwacht MIRA, Grimbergen, Belgium
felix.verbelen@gmail.com

An overview of the radio observations during July 2026 is given.

1 Introduction

The graphs show both the daily totals (*Figure 1 and 2*) and the hourly numbers (*Figure 3 and 4*) of "all" reflections counted automatically, and of manually counted "overdense" reflections, overdense reflections longer than 10 seconds and longer than 1 minute, as observed here at Kampenhout (BE) on the frequency of our VVS-beacon (49.99 MHz) during the month of July 2026.

The hourly numbers, for echoes shorter than 1 minute, are weighted averages derived from:

$$N(h) = \frac{n(h-1)}{4} + \frac{n(h)}{2} + \frac{n(h+1)}{4}$$

Local interference and unidentified noise remained moderate to low for most of the month, except on July 11 when no observations were possible for several hours due to local disturbances.

No lightning activity was observed; however, there were strong solar flares on several days.

General meteor activity was fairly normal for the time of year, with clear increases around July 2, 6, 15, and 30–31. Further investigation is still needed to identify the showers – particularly the minor ones.

Over the course of the entire month, 12 reflections lasting longer than 1 minute were observed here. A selection of these, along with several other interesting reflections, is shown in *Figures 5 to 21*. Many more are available upon request.

In addition to the usual graphs, you will also find the raw counts in cvs-format[17] from which the graphs are derived. The table contains the following columns: day of the month, hour of the day, day + decimals, solar longitude (epoch J2000), counts of "all" reflections, overdense reflections, reflections longer than 10 seconds and reflections longer than 1 minute, the numbers being the observed reflections of the past hour.

[17] https://www.emeteornews.net/wp-content/uploads/2026/08/202607_49990_FV_rawcounts.csv

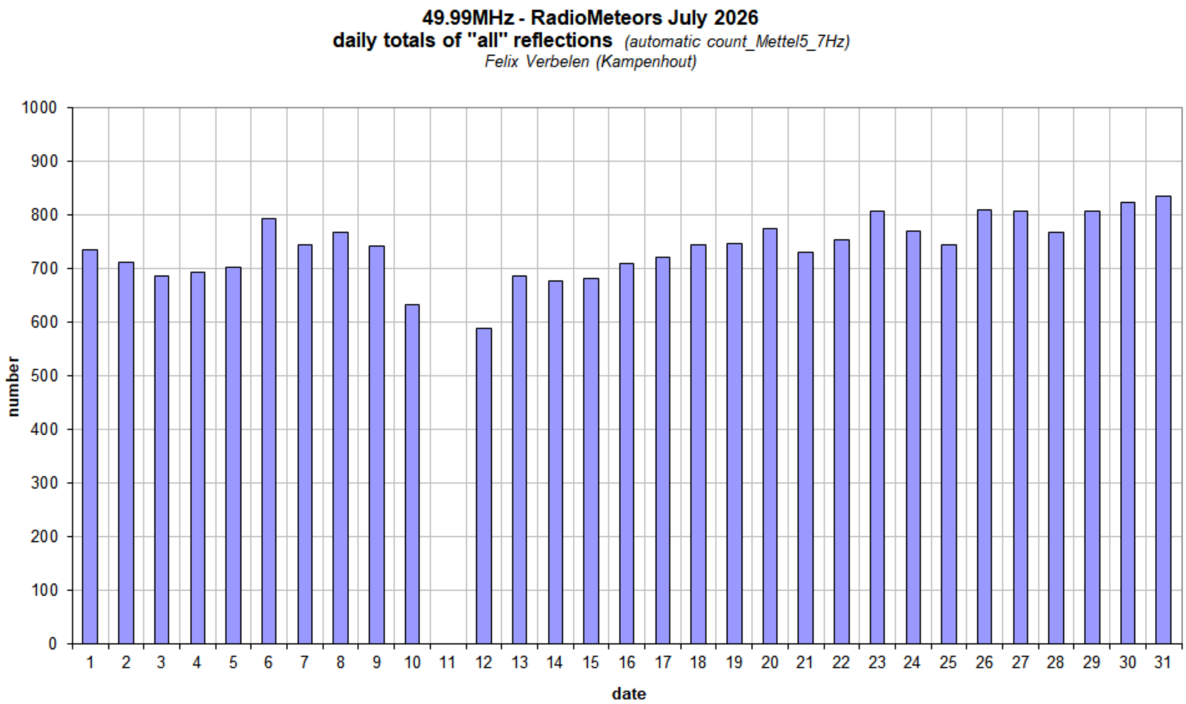

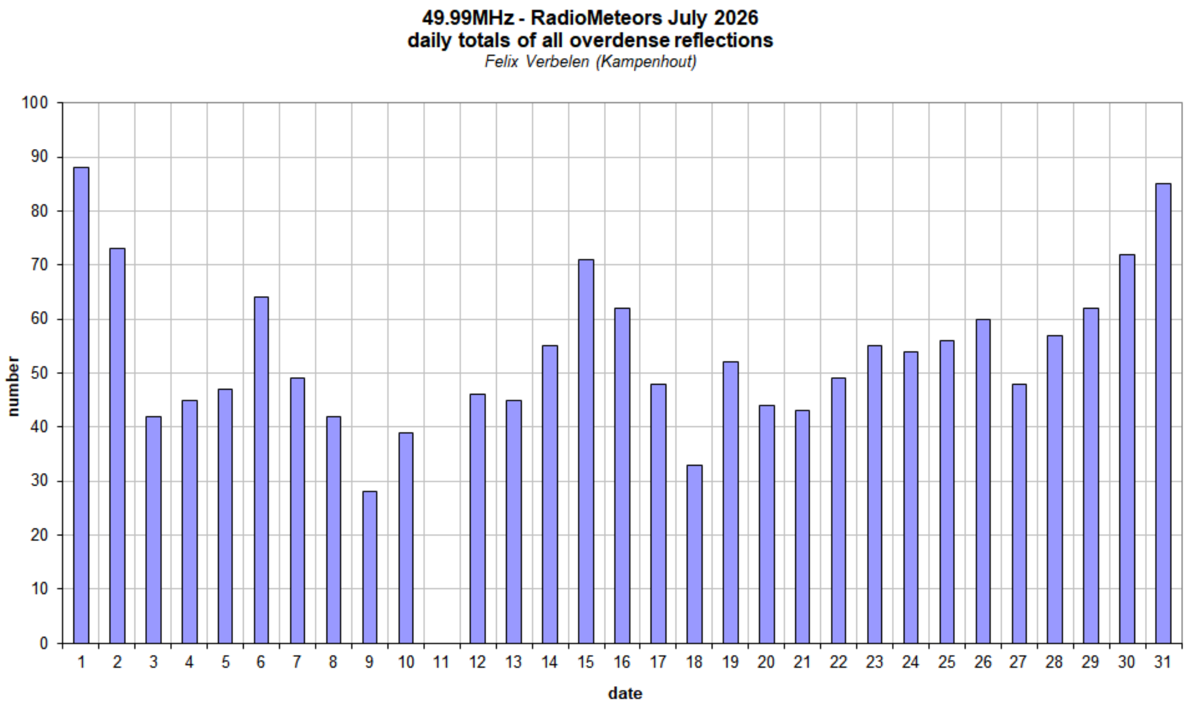

Figure 1 – The daily totals of "all" reflections counted automatically, and of manually counted "overdense" reflections, as observed here at Kampenhout (BE) on the frequency of our VVS-beacon (49.99 MHz) during July 2026.

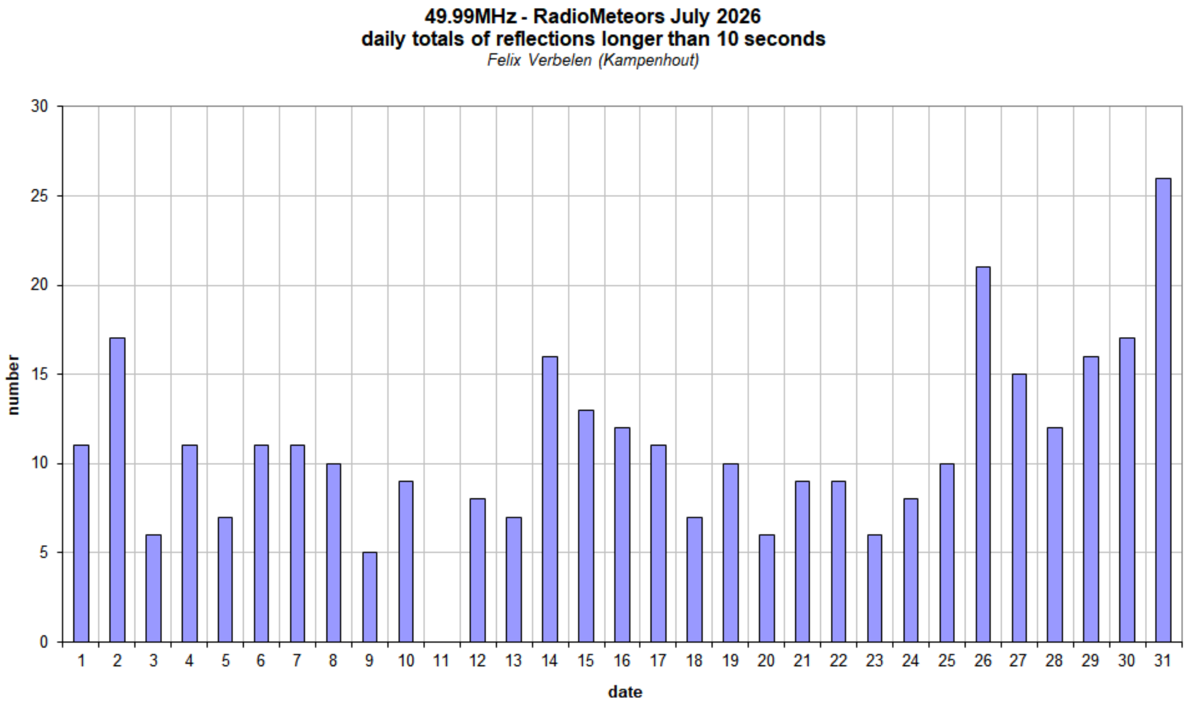

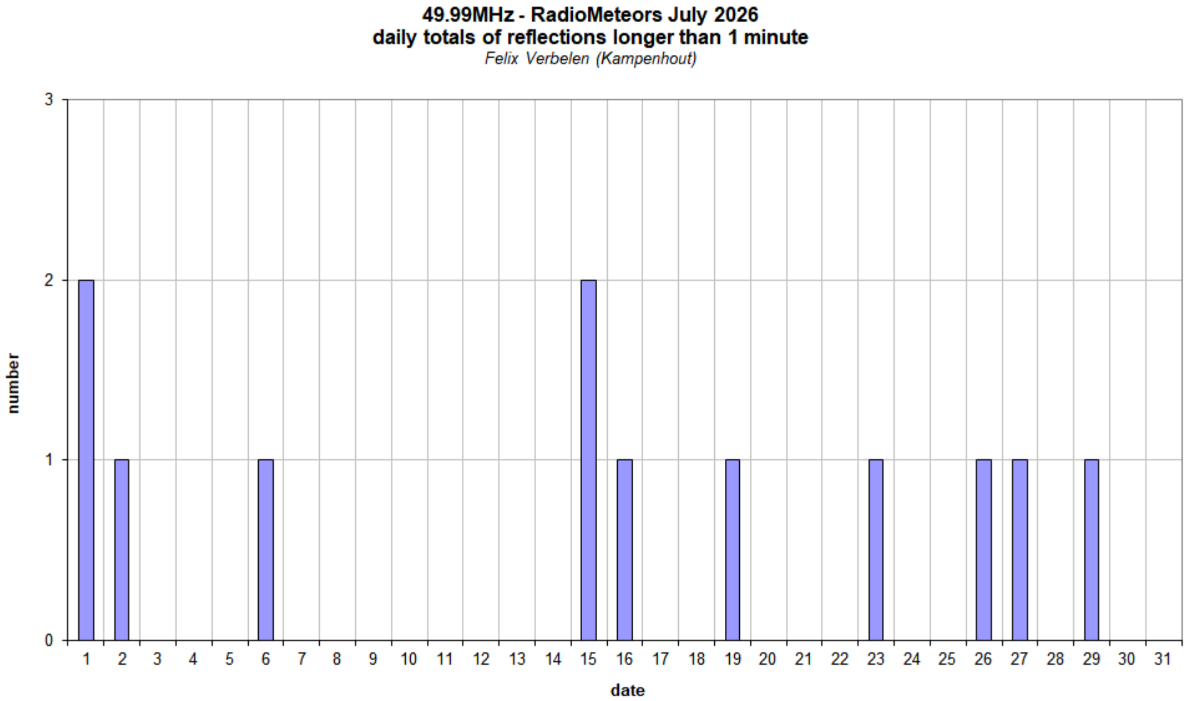

Figure 2 – The daily totals of overdense reflections longer than 10 seconds and longer than 1 minute, as observed here at Kampenhout (BE) on the frequency of our VVS-beacon (49.99 MHz) during July 2026.

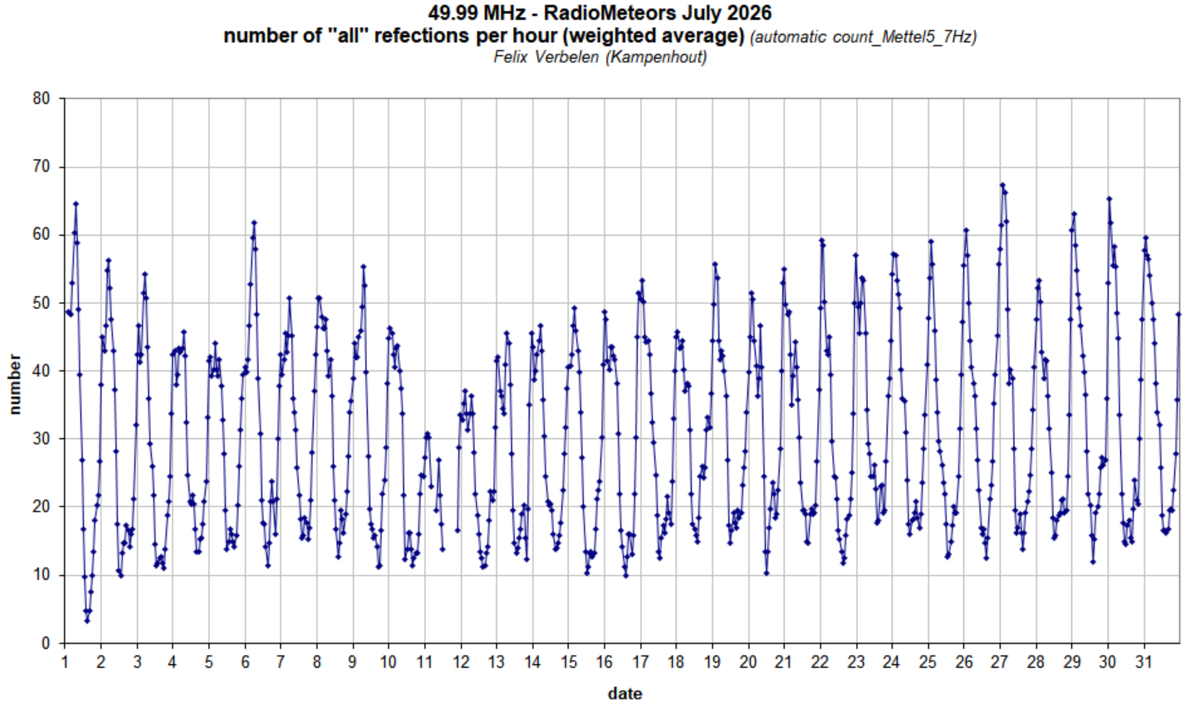

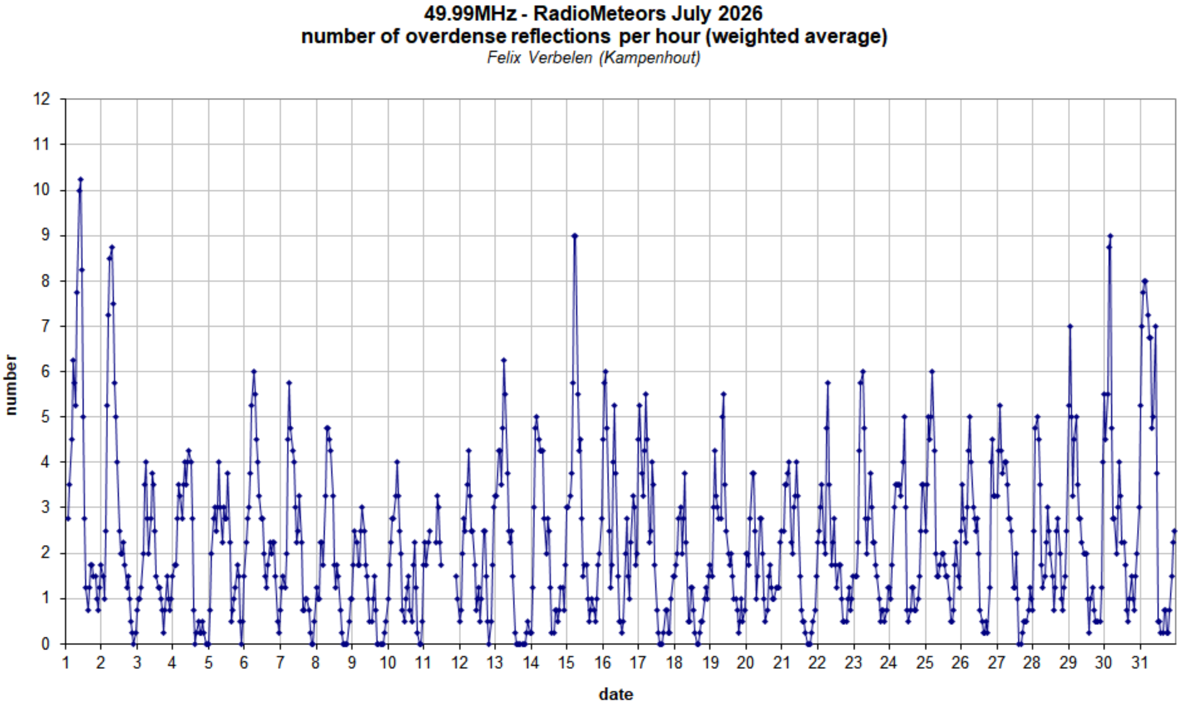

Figure 3 – The hourly numbers of "all" reflections counted automatically, and of manually counted "overdense" reflections, as observed here at Kampenhout (BE) on the frequency of our VVS-beacon (49.99 MHz) during July 2026.

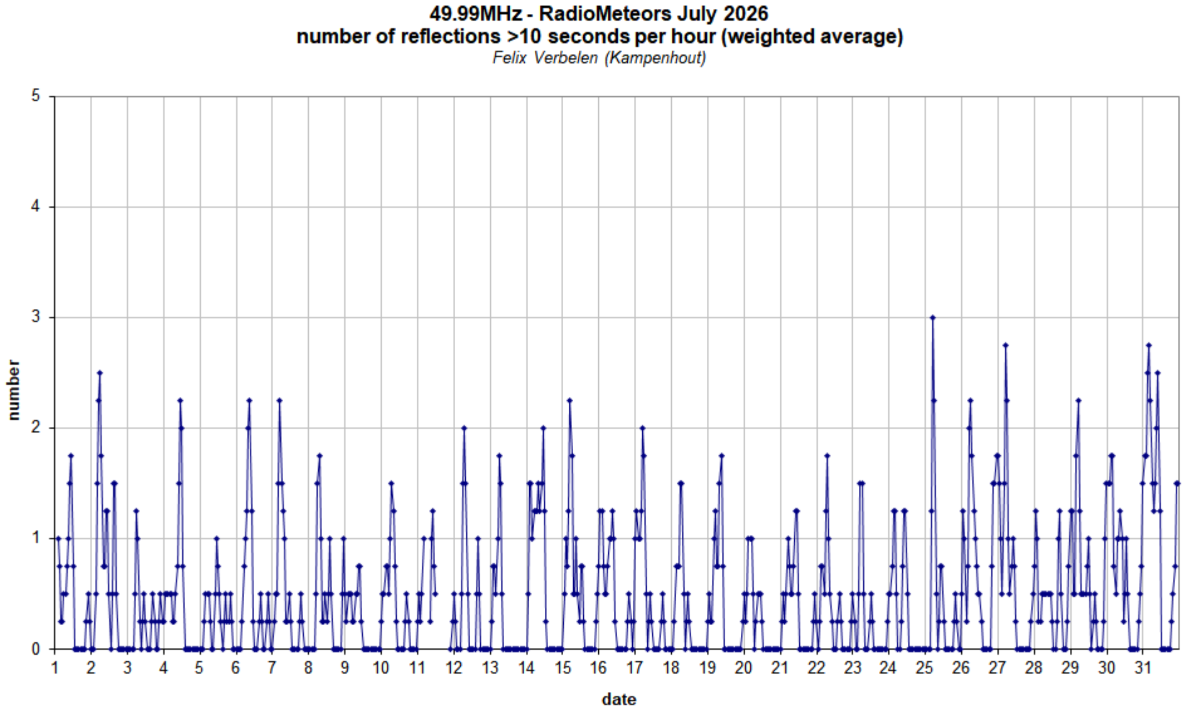

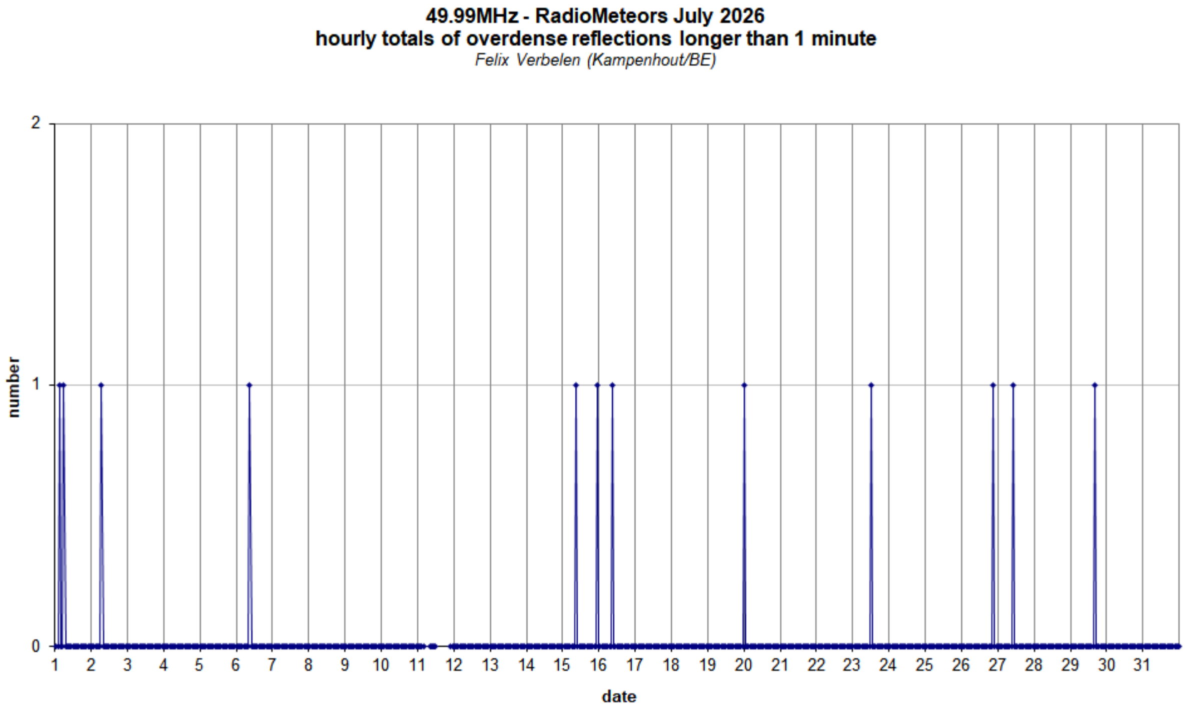

Figure 4 – The hourly numbers of overdense reflections longer than 10 seconds and longer than 1 minute, as observed here at Kampenhout (BE) on the frequency of our VVS-beacon (49.99 MHz) during July 2026.

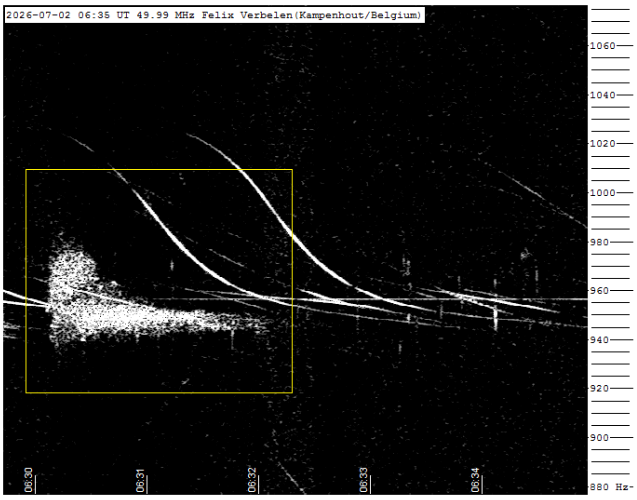

Figure 5 – Meteor echo July 2, 06^{h}35^{m} UT.

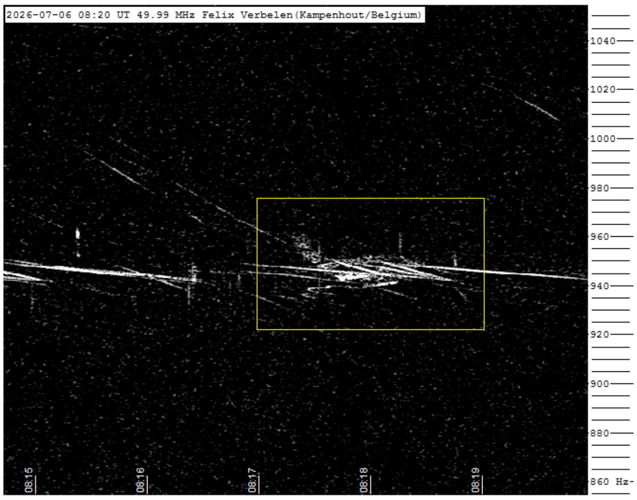

Figure 6 – Meteor echo July 6, 08^{h}20^{m} UT.

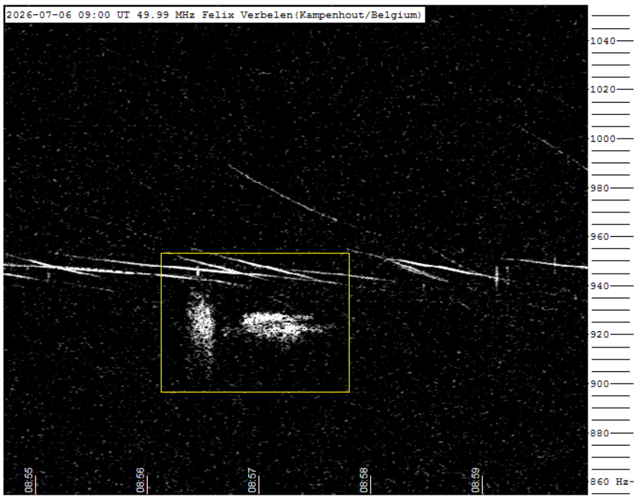

Figure 7 – Meteor echo July 6, 09^{h}00^{m} UT.

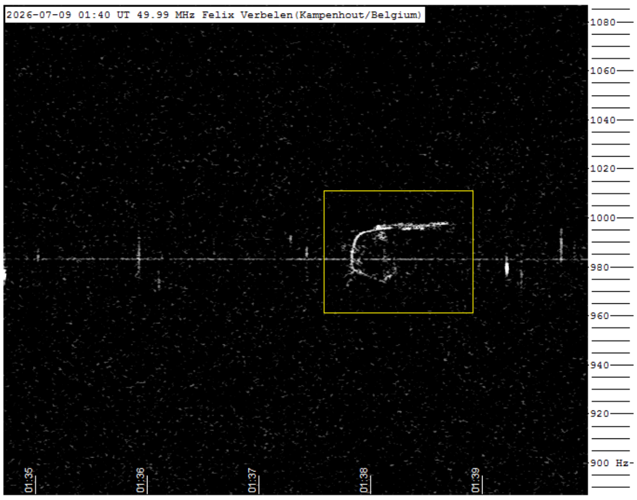

Figure 8 – Meteor echo July 9, 01^{h}40^{m} UT.

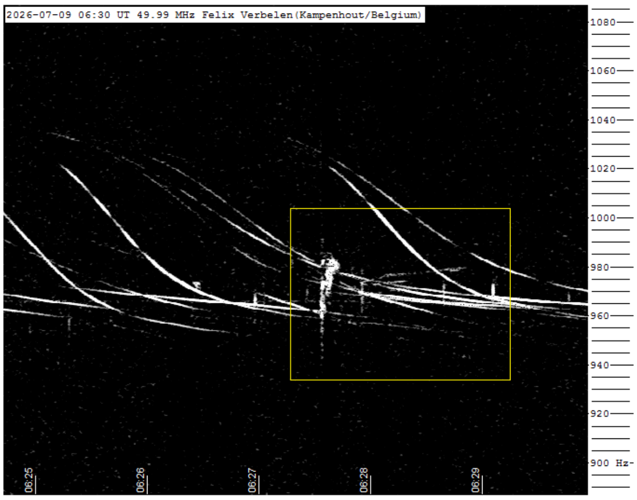

Figure 9 – Meteor echo July 9, 06^{h}30^{m} UT.

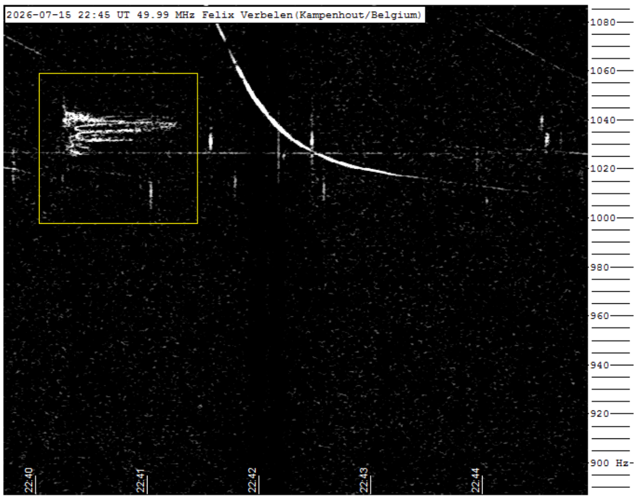

Figure 10 – Meteor echo July 15, 22^{h}45^{m} UT.

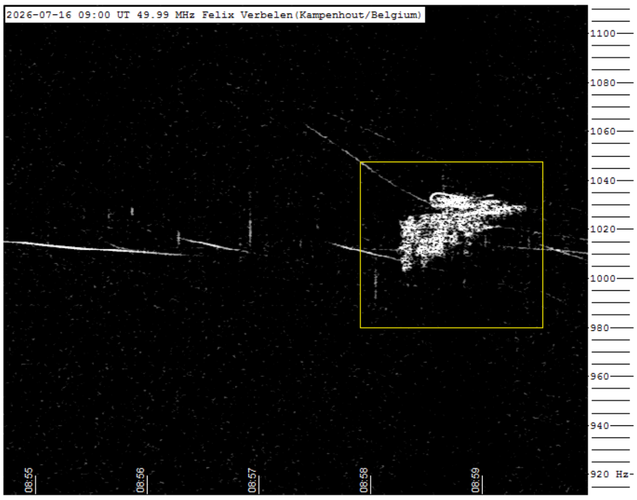

Figure 11 – Meteor echo July 16, 09^h00^m UT.

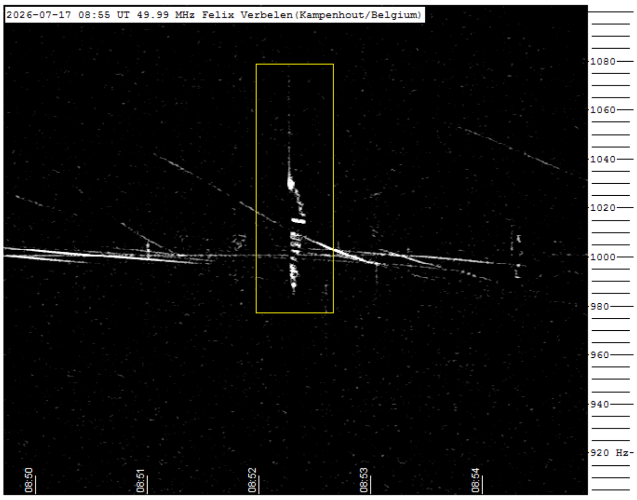

Figure 12 – Meteor echo July 17, 08^h55^m UT.

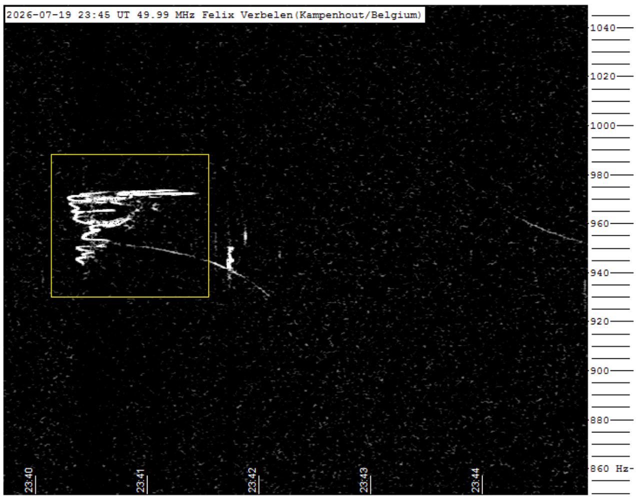

Figure 13 – Meteor echo July 19, 23^h45^m UT.

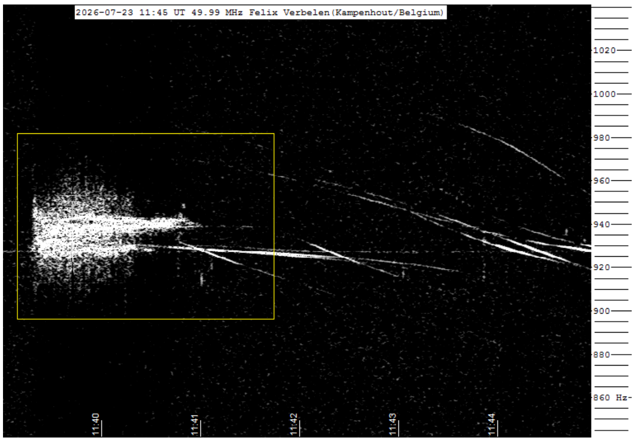

Figure 14 – Meteor echo July 23, 11^h45^m UT.

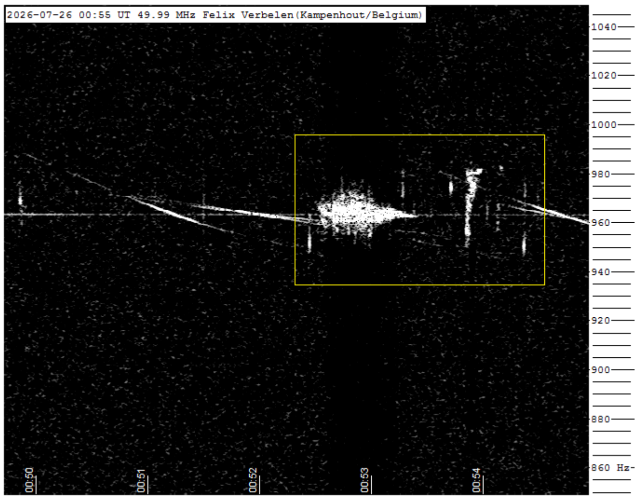

Figure 15 – Meteor echo July 26, 00^h55^m UT.

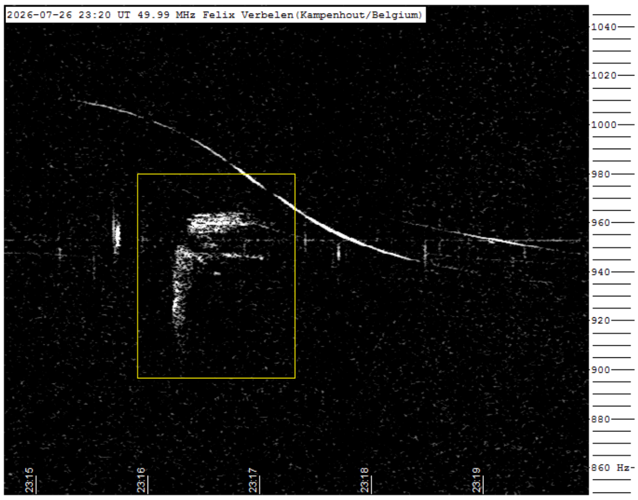

Figure 16 – Meteor echo July 26, 23^h20^m UT.

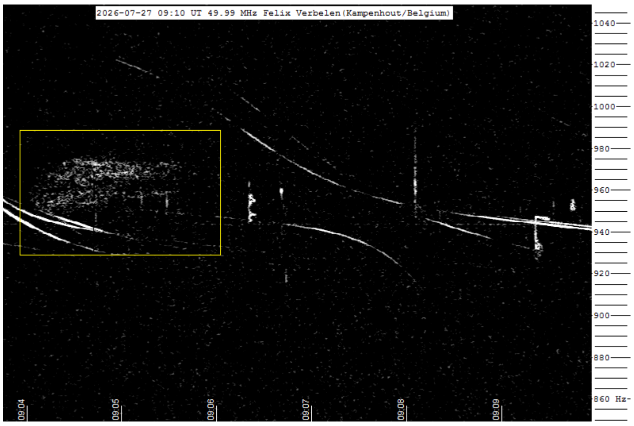

Figure 17 – Meteor echo July 27, 09^{h}10^{m} UT.

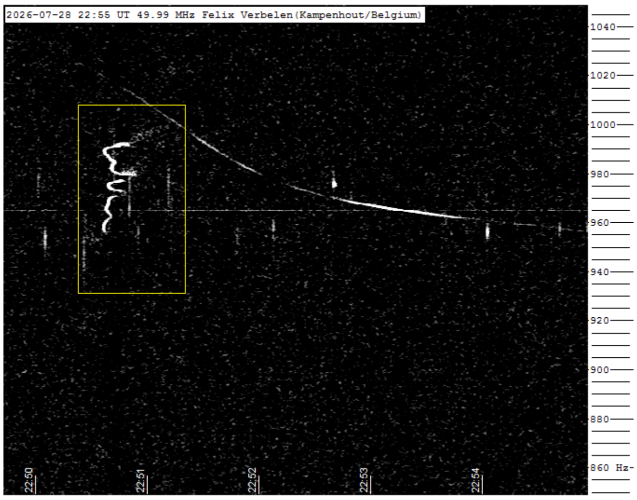

Figure 18 – Meteor echo July 28, 22^{h}55^{m} UT.

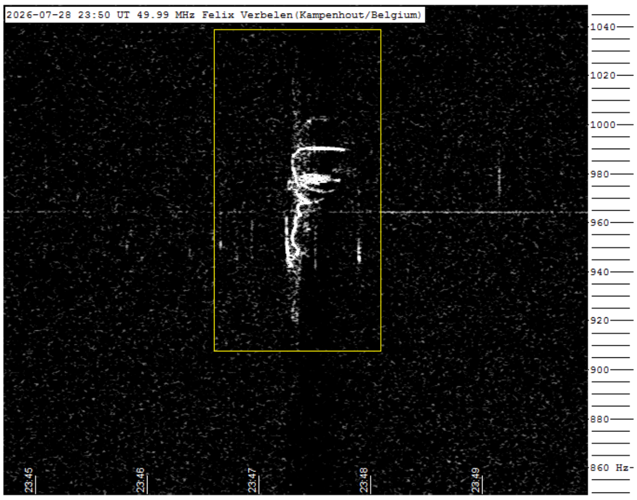

Figure 19 – Meteor echo July 28, 23^{h}50^{m} UT.

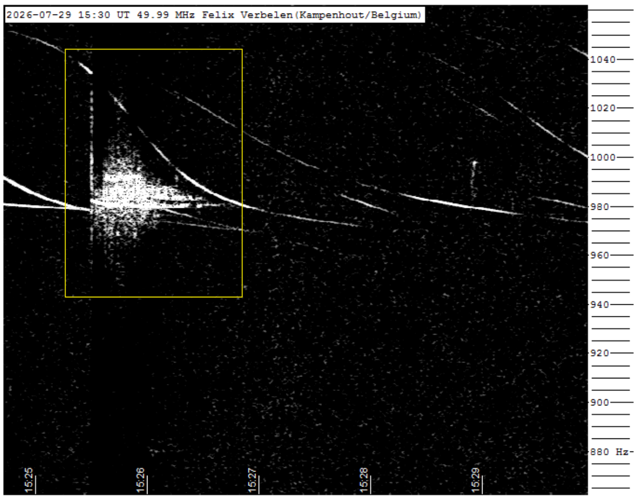

Figure 20 – Meteor echo July 29, 15^{h}30^{m} UT.

Figure 21 – Meteor echo July 31, 22^{h}30^{m} UT.

Analysis of the 21 April 2012 southeastern Brazil fireball

Alberto Silva Betzler[1,2]

[1] **Instituto de Física, Universidade Federal da Bahia, Salvador, Bahia, Brazil**
a_betzler@yahoo.com

[2] **Centro de Ciência e Tecnologia em Energia e Sustentabilidade,
Universidade Federal do Recôncavo da Bahia, Feira de Santana, Bahia, Brazil**

A very bright, fragmenting meteor was widely observed over southeastern Brazil at about 02^h30^m UT on 21 April 2012. Two publicly available videos, recorded in Belo Horizonte and Campos dos Goytacazes, were reduced using terrestrial landmarks to estimate horizontal coordinates. The Fireball software developed by Albino Carbognani was used to calculate a nominal atmospheric trajectory, velocity, and heliocentric orbit. The solution yielded a minimum altitude of 74.5 km, an apparent J2000 radiant near Right Ascension 83 degrees and Declination +47 degrees, and orbital elements q = 1.005 AU, e = 1.190, i = 28.51 degrees, Ω = 31.22 degrees, and ω = 180.45 degrees. The nominal orbit was compared with 1757 complete, non-removed solutions in the IAU Meteor Data Center Shower Database updated on 25 June 2026. The April Lyrids are excluded by an approximately 99.2-degree separation between the apparent event radiant and the cataloged Lyrid radiant, together with D_{SH} = 1.095. The smallest D_{SH} found for any cataloged solution was 0.586, and the smallest value for an established shower was 0.785. The nominal solution therefore has no plausible shower association. However, the elevation measured from Belo Horizonte changed by only about 0.7 degrees, an amount comparable to the expected uncertainty of the landmark-based reduction, and the timing was not independently calibrated; the speed and hyperbolic eccentricity are therefore poorly constrained. The event is best described as having no identified shower association, or as apparently sporadic; an interstellar origin and a confirmed Earth-grazing passage are not established by the available data.

Keywords - fireball; meteoroid orbit; Earth-grazing meteor; Southworth-Hawkins criterion; meteor showers; Brazil.

1 Introduction

Bright fireballs are increasingly documented by surveillance cameras, mobile phones, and other non-scientific imaging systems. When the recording sites and image geometry can be reconstructed, publicly available footage can provide useful constraints on the atmospheric trajectory and, in favorable cases, on the pre-atmospheric orbit. Such reconstructions are nevertheless sensitive to camera calibration, timing accuracy, convergence geometry, and the measured angular extent of the luminous path (Ceplecha, 1987; Zuluaga et al., 2013).

At approximately 02^h30^m UT on 21 April 2012, a bright meteor was reported from the Brazilian states of Bahia, Espírito Santo, Minas Gerais, and Rio de Janeiro (*Figure 1*). Witnesses described flares and the separation of the object into three or four fragments. The event occurred near the annual maximum of the April Lyrids, and an association with that shower was therefore informally suggested.

This article revisits and consolidates the original reconstruction presented by Betzler (2015), compares the complete nominal orbit with the current IAU Meteor Data Center Shower Database, and distinguishes between conclusions supported by the available observational data and those that remain provisional because of uncertainties in the measurements and reconstruction.

Figure 1 – Reported observer locations for the 21 April 2012 fireball. The original map was compiled from comments associated with a publicly available YouTube video recorded in Belo Horizonte. The marker "A" indicates the city of Belo Horizonte. Base map: Google Maps.

2 Observational material

2.1 Available records

A web search identified four YouTube videos of the fireball, recorded in Belo Horizonte, Campos dos Goytacazes, Ipatinga, and the Greater Vitória metropolitan area, all in southeastern Brazil. The two records used in the reduction were the videos at Belo Horizonte[18] and Campos dos Goytacazes[19]. The exact recording sites could be reconstructed only for the Belo Horizonte and Campos dos Goytacazes videos (*Figure 2*).

Those two videos therefore formed the basis of the trajectory and orbit calculation. Both appear to have been made with mobile-phone cameras, and neither contains stars or planets bright enough for a conventional astrometric plate solution.

The recording sites were estimated by matching buildings, utility poles, walls, and street geometry visible in the videos with ground imagery. The initial and final meteor directions were then estimated as azimuth and elevation angles from the terrestrial reference features. This landmark-based method resembles the approach later applied to public footage of the Chelyabinsk event (Zuluaga et al., 2013), but its precision is inherently lower than that of calibrated meteor-camera observations.

Figure 2 – Observational material used in the original reduction: (a) meteor frame from Campos dos Goytacazes; (b) estimated Campos recording site; (c) meteor frame from Belo Horizonte; and (d) estimated Belo Horizonte recording site. Arrows identify the meteor. Site imagery: Google Street View.

2.2 Angular and timing assumptions

The local horizontal coordinates, station locations, and adopted timing were processed with Fireball, developed by Albino Carbognani (unpublished software), to calculate the nominal atmospheric trajectory, velocity, and heliocentric orbital elements. The reported apparent radiant was obtained by extending the reconstructed atmospheric trajectory backward; the true/geocentric radiant was not preserved. The records were treated as simultaneous at approximately 23^h30^m local time on 20 April (02^h30^m UT on 21 April) because reliable frame-level timing was unavailable.

The apparent transit lasted about 2s in the Belo Horizonte video and about 11s in the Campos video (*Figure 3*). The elevation measured from Belo Horizonte changed by only about 0.7 degrees. Because the change is comparable to the expected uncertainty of a landmark-based reduction and frame-level timing was not independently calibrated, the velocity and orbital solution are poorly constrained.

3 Nominal trajectory and orbit

3.1 Atmospheric solution

The atmospheric trajectory was obtained by intersecting the observation planes defined by the estimated sight lines from the two stations, following the general geometric approach used for multi-station fireball reductions (Ceplecha, 1987). The nominal ground track runs approximately southwest to northeast and is consistent with reports that the meteor passed near the zenith from parts of eastern Minas Gerais (*Figure 4a* and *Table 1*). The calculated minimum altitude was 74.52 km.

[18] https://www.youtube.com/watch?v=d4aHh0ibJik

[19] https://www.youtube.com/watch?v=3yNR118wbmg

A minimum altitude near 75 km is compatible with a shallow, high-altitude passage. It does not by itself demonstrate that the meteoroid emerged from the atmosphere. A confirmed Earth-grazing classification requires a sufficiently constrained trajectory through and beyond the point of closest approach, including a reliable velocity history. The present records provide only a provisional indication of such a geometry.

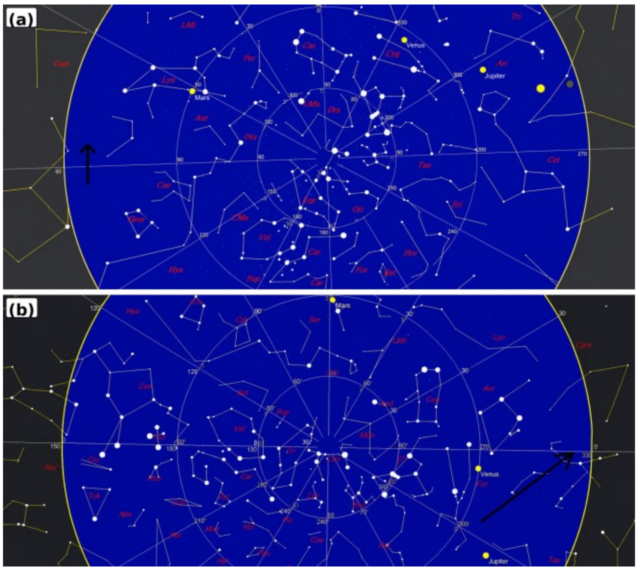

Figure 3 – Approximate apparent tracks in horizontal coordinates for (a) Belo Horizonte and (b) Campos dos Goytacazes. The transit times adopted in the original reduction were 2s and 11s, respectively.

Table 1 – Nominal parameters from the original reduction.

Parameter	Nominal value	Unit
Minimum altitude	74.52	km
Apparent RA (J2000)	83.0	deg
Apparent Dec. (J2000)	+47.0	deg
Perihelion distance, q	1.005	AU
Eccentricity, e	1.190	-
Inclination, i	28.510	deg
Ascending node, Ω	31.220	deg
Argument of perihelion, ω	180.450	deg
True anomaly, ν	359.550	deg
Heliocentric speed (~1 AU)	44.0	km/s
Perihelion epoch, T	2456038.907	JD

3.2 Heliocentric solution

The nominal heliocentric solution has q = 1.005 AU, e = 1.190, i = 28.510 degrees, Ω = 31.220 degrees, and ω = 180.450 degrees. Its nominal heliocentric speed near 1 AU is 44.0 km/s, compared with a solar escape speed of about 42.1 km/s at that distance (*Figure 4b*). Taken literally, these values describe an unbound orbit. However, the excess above the escape speed is only about 1.9 km/s, while the input speed is derived from uncalibrated video measurements with uncertain timing. The hyperbolic classification is therefore highly sensitive to small systematic and timing errors.

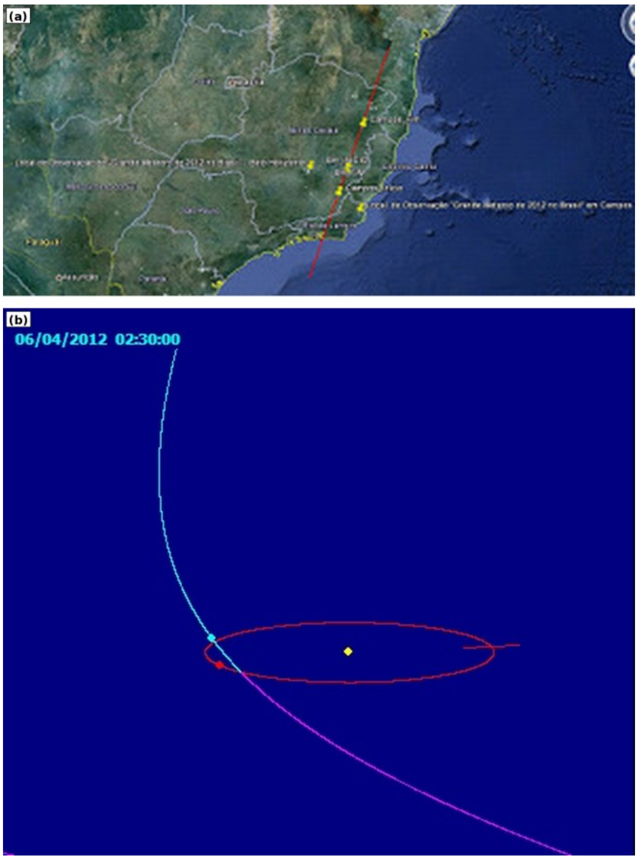

Figure 4 – Nominal reconstruction: (a) projected atmospheric ground track, with the two recording sites and video endpoints marked; the continuation toward Bahia is arbitrary; (b) heliocentric orbit plot for the meteoroid and Earth, shown 15 days before the encounter. At that plotted epoch, the nominal separation was 2.93 × 10^7 km, or about 76 mean Earth–Moon distances. Ground-track base map: Google Earth.

Figure 5 – Apparent J2000 radiant of the 21 April 2012 meteor, marked by a cross in Auriga. The cataloged April Lyrid radiant lies far outside this field, in Lyra. Diagram generated with The Night Sky Atlas.

4 Meteor-shower association

4.1 Radiant comparison with the April Lyrids

The apparent J2000 radiant is near RA = 5h32min (83 degrees), Dec. = +47 degrees, in Auriga (*Figure 5*). The April Lyrid solution yielding the smallest nominal D_{SH} in the current IAU MDC catalog has a geocentric radiant near RA = 272.0 degrees, Dec. = +33.4 degrees. The great-circle separation between these tabulated directions is 99.2 degrees. Although the two radiant types are not identical, the correction from an apparent to a geocentric radiant is far too small to bridge a discrepancy of this magnitude. Daily radiant drift likewise cannot bridge it. The coincidence between the event date and the Lyrid maximum is therefore not evidence of membership.

4.2 Southworth-Hawkins comparison

A radiant comparison is sufficient to reject the April Lyrids, but a general search for related showers requires the full orbit. The Southworth-Hawkins dissimilarity criterion was calculated from the nominal orbit and each cataloged shower solution (Southworth and Hawkins, 1963):

$$D_{SH}^2 = (q_1 - q_2)^2 + (e_1 - e_2)^2 + \left(2\sin\frac{I}{2}\right)^2 + \left((e_1 + e_2)\cdot\sin\frac{\Pi}{2}\right)^2$$

Here I is the angle between the orbital planes and Π is the difference between the directions of perihelion. There is no universal D_{SH} cutoff: an appropriate threshold depends on the data set, shower inclination, measurement uncertainty, and local sporadic background (Galligan, 2001; Moorhead, 2016; Roggemans et al., 2026).). Nevertheless, values approaching 0.6 or larger are far beyond the ranges normally used to assign individual meteors to streams.

The comparison used the IAU MDC all-showers file streamfulldata2026.txt, updated on 25 June 2026 and accessed on 14 July 2026 (*Table 2*). Records with negative MDC status flags, or lacking any of q, e, i, Ω, or ω, were excluded. The remaining set contained 1757 complete solutions representing 863 shower codes; 503 solutions represented 113 established showers. The MDC status system and validation procedures are described by Jopek and Kaňuchová (2017), Jenniskens et al. (2020), and Hajduková et al. (2023).

Table 2 – Smallest nominal D_{SH} values in the IAU MDC comparison.

Reference solution	D_{SH}	Key difference
April Lyrids (6/LYR; established)	1.095	Apparent/catalog separation: 99.2 deg
May lambda-Draconids (532/MLD; working)	0.586	Radiant RA 155 deg, Dec. +73 deg; later activity
Southern delta-Cancrids (97/SCC; established)	0.785	Different radiant and season

The smallest dissimilarity in the entire non-removed catalog is D_{SH} = 0.586 for one solution of the May lambda-Draconids. That shower has a substantially different radiant and reaches its nominal activity near solar longitude 52 degrees, about three weeks after the Brazilian event. Among established showers, the minimum is D_{SH} = 0.785 for a Southern delta-Cancrid solution active in a completely different season. These are not plausible associations. The nominal orbit therefore does not resemble any shower currently listed in the MDC.

5 Uncertainty and interpretation

5.1 The hyperbolic orbit is not secure

The nominal eccentricity should not be interpreted as evidence for an interstellar meteoroid. The orbital energy depends strongly on the pre-atmospheric speed, and small velocity errors near the parabolic limit can change a bound orbit into an apparently hyperbolic one. Hyperbolic solutions are common in low-precision meteor data and frequently disappear when observational uncertainties are modeled (Hajduková et al., 2014). Recent analyses likewise emphasize that the confidence level of a hyperbolic orbit must be evaluated from the complete uncertainty distribution rather than from the nominal eccentricity alone (Barghini et al., 2025).

For the present event, no formal covariance matrix is available. The measured elevation change from Belo Horizonte was only about 0.7 degrees, comparable to the expected reduction uncertainty, and the timing and frame rates were not independently calibrated. The reported e = 1.190 and 44.0 km/s heliocentric speed are therefore nominal Fireball outputs, not statistically secure physical determinations.

5.2 What can be stated reliably

Three conclusions have different levels of robustness. First, the event was not an April Lyrid: its apparent radiant is grossly inconsistent with the cataloged shower radiant, and its nominal orbit is also grossly inconsistent with the shower. Second, the nominal orbit has no plausible association with any non-removed IAU MDC shower solution. Third, the broader label "sporadic" remains provisional because the orbit itself has large, unquantified uncertainties. The most defensible wording is "a meteor with no identified shower association", with "apparently sporadic" as a concise alternative.

The possible Earth-grazing geometry is also provisional. The calculated minimum altitude and shallow path are compatible with a meteoroid that traversed the upper atmosphere and returned to space, as in the well-documented 1972 daylight fireball (Ceplecha, 1994). The available data, however, do not constrain the outbound trajectory and post-encounter speed well enough to demonstrate survival and escape. Similarly, a pre-atmospheric mass cannot be derived because the videos lack a reliable photometric calibration.

6 Conclusions

The 21 April 2012 southeastern Brazil fireball was reconstructed from two public, non-astrometric videos. The nominal solution gives a minimum altitude of 74.5 km, an apparent radiant in Auriga, and a formally hyperbolic orbit. A new comparison with the IAU MDC Shower Database shows that the April Lyrids are decisively excluded: the cataloged Lyrid radiant is 99.2 degrees from the apparent event radiant, and the closest Lyrid solution has D_{SH} = 1.095. No other cataloged shower is a plausible match; the minimum D_{SH} is 0.586 for a working-list solution, and the minimum among established showers is 0.785.

These results support the classifications "no identified shower association" and "apparently sporadic." They do not establish an interstellar origin because the small measured elevation change and uncertain timing leave the velocity and orbital energy poorly constrained. Nor do they prove atmospheric escape, although the nominal geometry is compatible with an Earth-grazing passage. A definitive reanalysis requires the original videos, exact sites, verified timing and frame rates, improved camera geometry, and Monte Carlo propagation of angular and temporal uncertainties.

Acknowledgment

The author thanks the observers who shared the 2012 videos, Ernesto Pinheiro Borges for supervising the doctoral work, and Albino Carbognani for developing Fireball.

References

Barghini D., Ďurišová S., Koten P., Bertaina M. E., Gardiol D. and Hajduková M. (2025). "The Kresáks' diagram: Hyperbolic meteoroid orbits and their confidence level". *Astronomy & Astrophysics*, **701**, A135.

Betzler A. S. (2015). Aplicações da Mecânica Estatística Não Extensiva na Astrofísica de Pequenos Corpos do Sistema Solar. PhD thesis, Universidade Federal da Bahia, Salvador, Brazil.

Ceplecha Z. (1987). "Geometric, dynamic, orbital and photometric data on meteoroids from photographic fireball networks". *Bulletin of the Astronomical Institutes of Czechoslovakia*, **38**, 222–234.

Ceplecha Z. (1994). "Earth-grazing daylight fireball of August 10, 1972". *Astronomy & Astrophysics*, **283**, 287–288.

Galligan D. P. (2001). "Performance of the D-criteria in recovery of meteoroid stream orbits in a radar data set". *Monthly Notices of the Royal Astronomical Society*, **327**, 623–628.

Hajduková M. Jr., Kornoš L. and Tóth J. (2014). "Hyperbolic orbits in the EDMOND". In Jopek T. J., Rietmeijer F. J. M., Watanabe J. and Williams I. P. (eds.), *Meteoroids 2013*, Adam Mickiewicz University Press, Poznań, 289–295.

Hajduková M., Rudawska R., Jopek T. J., Koseki M., Kokhirova G. and Neslušan L. (2023). "Modification of the Shower Database of the IAU Meteor Data Center". *Astronomy & Astrophysics*, **671**, A155.

Jenniskens P., Jopek T. J., Janches D., Hajduková M., Kokhirova G. I. and Rudawska R. (2020). "On removing showers from the IAU Working List of Meteor Showers". *Planetary and Space Science*, **182**, 104821.

Jopek T. J. and Kaňuchová Z. (2017). "IAU Meteor Data Center - the shower database: A status report". *Planetary and Space Science*, **143**, 3–6.

Moorhead A. V. (2016). "Performance of D-criteria in isolating meteor showers from the sporadic background in an optical data set". *Monthly Notices of the Royal Astronomical Society*, **455**, 4329–4338.

Roggemans P., Vida D., Šegon D. and Scott J. M. (2026). "Meteoroid orbit shower identification method and its application in meteor shower case studies". *eMetN Meteor Journal*, **11**, 189–204.

Southworth R. B. and Hawkins G. S. (1963). "Statistics of meteor streams". *Smithsonian Contributions to Astrophysics*, **7**, 261–285.

Zuluaga J. I., Ferrin I. and Geens S. (2013). "The orbit of the Chelyabinsk event impactor as reconstructed from amateur and public footage". arXiv:1303.1796.

Asteroids Comets Meteors Conference Impressions 6–10 July 2026, Poznan, Poland

Paul Roggemans and Adriana Roggemans

Pijnboomstraat 25, 2800 Mechelen, Belgium
Paul.roggemans@gmail.com

A summary report on the 2026 ACM conference in Poznan, Poland is presented with an overview of the meteor related lectures.

1 Introduction

The Asteroids, Comets, Meteors conferences started in 1983 organized by the Uppsala Astronomical Observatory (Astronomiska observatoriet i Uppsala) at the nearby University of Uppsala in June 20–22, 1983. The aim of the conference was to bring scientists together who study small bodies in order to improve the interaction between the different domains of minor planets, comets and meteors. The meeting proved successful and Asteroids, comets, meteors II was organized June 3–6, 1985 in Uppsala, Sweden. When the third ACM conference was organized in Uppsala June 12–16, 1989, the number of attendants had increased to 158. While the first ACM meetings involved mainly scientists from European countries, the 1989 ACM had 41 participants from America, Australia and Japan. The 4th ACM was organized at the Northern Arizona University, Flagstaff, USA, June 24–28, 1991. Until then, the ACM conference published its own Proceedings. The 5th ACM took place in Belgirate, Italy, June 14–18, 1993, with 323 participants from 38 countries. Proceedings were published as the 160th Symposium of the International Astronomical Union. The 6th International Conference on Asteroids, Comets, Meteors (ACM 1996) took place in Versailles, France, July 8–12, 1996 and conference papers were published in Planetary and Space Science (Vol. 46, No. 8, 1998). The number of participants exceeded 500 and from then on the conference was organized every three years, July 26–30, 1999 at Cornell University in Ithaca, New York, USA, July 29–August 2, 2002 in Berlin, Germany, August 7–12, 2005, in Búzios, Rio de Janeiro, Brazil, July 14–18, 2008, Baltimore, Maryland, USA, July 18–22, 2011, in Niigata, Japan, June 30–July 4, 2014, in Helsinki, Finland and April 11–15, 2017, in Montevideo, Uruguay. The planned ACM 2020 had to be postponed due to Covid and was finally held June 18–23, 2023 at Flagstaff, Arizona, USA as the 14th ACM conference.

The 2026 ACM was the 15th meeting since the start of these conferences in 1983 and took place in Poznan, Poland at the Poznań University of Technology, July 6–10. More than 600 participants had registered from 48 countries.

2 The 15th ACM

Traditionally meteors represent the smallest bodies among small bodies and have far less contributions than the asteroids or comet sessions. Nevertheless, most meteor researchers were present at the conference. Most of them had attended the Meteoroids conference 2013 in Poznan which was organized 13 years earlier by the Adam Mickiewicz University and the 15th ACM in Poznan was a good reason to revisit Poznan after the good memories of the 2013 event in the same city.

The authors arrived on Sunday 5th of July and already at the check-in at our hotel we met with several ACM participants. Poznan had changed a lot since 2013. Sunday evening had a first socializing activity as an ice-breaking walking dinner. Most science conferences are characterized by typical cheap student catering but the Sunday evening informal reception at the 15th ACM exceeded all expectations, fine food with accompanying drinks presented in multiple large buffets created a jovial, collegial atmosphere to meet with friends.

The conference itself was opened Monday morning with a welcome ceremony by *Jacek Bogusławski*, Member of the Executive Board of the Wielkopolska Region, *Prof. dr hab. Teofil Jesionowski*, Rector of Poznań University of Technology and *Prof. dr hab. Michał Banaszak*, Vice-Rector of Adam Mickiewicz University, Poznań. After the welcome addresses a first series of invited speakers were introduced in a plenary session. Because of the large number of presentations, the lectures were programmed in parallel sessions and in this report, we only highlight the meteor related talks. Of course, the lectures and posters represent the main content of a conference, but the coffee breaks, generous lunch breaks and free evenings offered plenty of time for informal contacts.

3 Meteors at the 2026 ACM

To avoid duplication, we refer for details about each talk to the ACM Abstract Book[20]. Most presentations refer to work published elsewhere and can be consulted via the listed references. The complete lecture program can be consulted here[21]. The posters are listed here[22]. The meteor related lectures can be summarized as follows:

Monday, July 6
Chairs: *Maria Gritsevich & Nick Moskovitz*

- *Hadrien Devillepoix* (*Figure 1*): "Discovery and Characterization of a Meteorite Strewn Field from a Small Asteroid Impact Using Orbital Sensors, Radar, and Drones".
- *Jiří Borovička*: "Analysis of the Iron Meteorite Fall of April 17, 2026".
- *Pavel Koten*: "Croatian Meteor Cluster as a Result of the Catastrophic Disruption of a Parent Meteoroid".
- *Peter Brown* (*Figure 2*): "From Iron Meteoroids to I-type Micrometeorites : A Meteor Perspective".
- *Julie Brisset*: "Sub-Micron Mineral and Organic Mapping in Primitive Solar System Materials".
- *Veronika Pazderová*: "Transferring Laboratory Emission Diagnostics to Meteor Spectra: Application to the AMOS Spectral Catalogue".
- *Shinsuke Abe*: "Comparison of Sodium Variations in the 2017-2025 Geminid Meteor Shower with the Parent Body Phaethon".
- *Iona Clemente*: "Cross-Validation of Infrasound Detections and Fireball Observations from the Global Fireball Observatory".
- *Maximilian Vovk*: "Sporadic Meteoroids Density, Structure, and Composition Beyond Orbital Class".

Tuesday, July 7
Chairs: *Jérémie Vaubaillon & Regina Rudawsk*a

- *Peter Jenniskens*: "Review of Asteroids, Meteors and Meteorite Type Links".
- *Margaret Campbell-Brown*: "Spectral Observations of Meteors and Luminous Efficiency".
- *Patrick Shober* (*Figure 3*): "Detecting Asteroidal Activity Using Meteor Observations: How to Find a "Rock-Comet'"".
- *Tomáš Vörös*: "Deconstructing mm-sized Meteoroids: Indication of Heterogeneity from the Physical Properties of Gross Fragments".
- *Tam Do*: "Dynamical Origins of Earth-Impacting Millimetre-Sized Sporadic Meteoroids".
- *Dario Eickhoff*: "Bayesian Acoustic-seismic Characterization of the March 8, 2026 Koblenz Meteoroid".
- *Ryo Ishimaru*: "ASTERISC: A CubeSat Mission to Observe Beta Meteoroids with a New Large-Area Film Dust Sensor".
- *Gabriel Borderes-Motta*: "Simulating the Alpha Capricornid Meteor Shower: A Dynamical Study Based on the Proposed Parent Bodies".
- *Tomáš Henych*: "Geminids are Initially Cracked by Atmospheric Thermal Stress".

Wednesday, July 8
Chairs: *Regina Rudawska & Miroslav Brož*

- *Martin Čuľák*: "Telescopic meteors observed by AMOS and ATLAS in Hawaii".
- *Dale Giancono*: "High-Speed Observations of Lunar Impact Flashes".
- *Jérémie Vaubaillon* (*Figure 4*): "When the Leonids Meteor Storms are Back".
- *Apostolos Christou*: "2020 BX_14: A New Fragment of the Alpha Capricornids Parent Comet".
- *Simon Anghel* (*Figure 5*): "Breaking the Threshold Barrier in Orbital Similarity Metrics".
- *Hervé Lamy*: "Computing the Velocity of a Meteor Using the Phase of the Fourier Transform: Application to BRAMS Data".
- *Maria Gritsevich*: "Bulk Density Estimation Using α-β Inversion of Fireball Trajectories".
- *Thomas Stevenson*: "Ballistic-Strength Survival Limits for Metallic, Siliceous and Carbonaceous Meteoroids".
- *Kosuke Watanabe*: "Spectroscopic Study of Rocket Debris During Atmospheric Re-entry".

Friday, July 10 Plenary session, invited speaker
Chair: *Gonzalo Tancredi.*

Denis Vida (*Figure 7*): "The Renaissance of Meteor Physics: New Optical and Radar Perspectives".

4 Informal contacts

If there is something that distinguishes the ACM conferences from others, it is the time allocated for informal contacts with long lunch breaks, coffee breaks, cultural events, a luxurious banquet and excursions. The 15th ACM in Poznan impressed its participants with lavish buffets from Monday to Thursday and coffee breaks with rich dessert buffets, all taken care off with great care.

On Tuesday evening a performance with the Amadeus Chamber Orchestra & MozART group concert took place in the beautiful theatre of the Adam Mickiewicz University. Anyone who might think that classic music could be boring would have been surprised by the very original interpretation and performance of Mozart's compositions that we will remember as a most unique concert. Guided

[20] https://share.ppnt.poznan.pl/index.php/s/QNCyAPcAnpdMLDK

[21] https://acm2026.eu/conf-data/ACM2026/files/Program/ACM2026_program_new_final3.pdf

[22] https://acm2026.eu/conf-data/ACM2026/files/Program/Poster_sessions_ver10.pdf

city tours were offered during the free evenings. Thursday evening, the ACM banquet proved to be another catering highlight with plenty of tasteful food and drinks. After the banquet, a live rock group entertained the audience and got many "minor bodies" on the dance floor (*Figure 6*). The latest IAU minor planet names were announced with many nominees being present among the participants followed by the announcement of the 16th ACM which will be held in Macau, China in 2029.

The last plenary session Friday 10 July included the only meteor researcher who was invited as speaker, *Denis Vida*, who gave an up-to-date presentation: "The Renaissance of Meteor Physics: New Optical and Radar Perspectives".

The ACM 2026 ended with a number of excursions and the authors had chosen for the visit to the birth place of Nicolaus Copernicus in the well-preserved medieval city of Toruń in Poland. The guided tour brought us to the Nicolaus parents' house that survived revolutions as well as the German and Soviet evil destructions during WWII.

Acknowledgment

The ACM 2026 organizers delivered a perfectly organized conference and saved neither effort nor time to make it an unforgettable successful event. Thanks a lot, to all people involved in making this possible.

Figure 1 – Maria Gritsevich and Hadrien Devillepoix.

Figure 2 – Peter Brown and Maria Gritsevich.

Figure 3 – Regina Rudawska, Jérémie Vaubaillon and Patrick Shober.

Figure 4 – Miroslav Brož, Regina Rudawska and Jérémie Vaubaillon.

Figure 5 – Miroslav Brož, Regina Rudawska and Simon Anghel.

Figure 6 – The live concert after the Thursday evening banquet.

Figure 7 – Invited speaker Denis Vida and plenary session chairman Gonzalo Tancredi.

eMetN METEOR JOURNAL

Since 2016 the mission of eMetN Meteor Journal is to offer meteor news to a global audience and to provide a swift exchange of information in all fields of active amateur meteor work. eMetN Meteor Journal is freely available without any fees. eMetN Meteor Journal is independent from any country, society, observatory or institute. Articles are abstracted and archived with ADS Abstract Service: https://ui.adsabs.harvard.edu/search/q=eMetN

You are welcome to contribute to eMetN Meteor Journal on a regular or casual basis, if you wish to. Anyone can become an author or editor, for more info read: https://www.emeteornews.net/writing-content-for-emeteornews/

Articles for eMetN Meteor Journal should be submitted to: paul.roggemans@gmail.com

Contact: info@emeteornews.net

Contributors:

- Aitov A.
- Barbieri L.
- Betzler A.S.
- Campbell-Burns P.
- Greaves J.
- Kalina M.
- Koseki M.
- Latini A.
- Maglione M.
- Miskotte K.
- Rivato W.
- Roggemans A.
- Roggemans P.
- Scott J.M.
- Šegon D.
- Verbelen F.
- Vida D.
- Wood J.

Online publication https://www.emeteornews.net and https://www.emetn.net
ISSN 3041-4261, publisher: Paul Roggemans, Pijnboomstraat 25, 2800 Mechelen, Belgium